Synergetic Effects of Polymer-Surfactant Mixtures on Solid-Liquid Interfaces

DISSERTATION

Zur Erlangung des Doktorgrades
Der Naturwissenschaften
Der Naturwissenschaftlichen Fakultät IV
Chemie und Pharmazie
Der Universität Regensburg

vorgelegt von
Diplom-Biophysiker Denys Zimin
aus Kiev
im Dezember 2003

Gutachter: Prof Dr. Werner Kunz; Prof. Dr. Georg Schmeer

Die Arbeit wurde angeleitet von:		Prof. Dr. W. Kunz
Promotionsgesuch eingereicht am:		07.01.2004
Prüfungsausschuss:	Vorsitzender	Prof. Dr. A. Pfitzner
	1. Prüfer	Prof. Dr. W. Kunz
	2. Prüfer	Prof. Dr. G. Schmeer
	3. Prüfer	Prof. Dr. M. Liefländer
Das Kolloquium fand statt am:		30.01.2004

ACKNOWLEDGMENTS

БЛАГОДАРНОСТИ

DANKSAGUNGEN

Моей жене Тане. Без тебя я никогда бы этого не завершил...

Meinen ersten und größten Dank möchte ich an meinen Doktorvater, Herrn Prof. Dr. Werner Kunz aussprechen. Ohne seine Hilfe wäre diese Dissertation überhaupt nicht entstanden.

Ich möchte mich auch bei meinem Gutachter Herrn Prof. D. Georg Schmeer für wertvolle Hinweise und die Idee von „Übergang vom Chaos zur Ordnung“ bedanken. Weiterhin bedanke ich mich bei allen Kollegen und Mitarbeitern des Instituts für Physikalische und Theoretische Chemie, besonders bei Dr. Edith Schnell für die Einführung und Begleitung in der wunderschönen Welt der Rastersondenmikroskopie sowie für ihre stetige Hilfsbereitschaft, bei Dr. Didier Touraud für wertvolle und sachliche Diskussionen, bei Dr. Josef Duschl, Dr. Michael Eberwein, Diplom-Chemikerin Ŝarka Fernandes, Diplom-Chemikern Christian Blattner und John DeRoche sowie bei Frau Barbara Widera für ihre Hilfe, stete Ermunterungen und Diskussionen.

Зоря, тебе спасибо, что всегда настаивала на простой истине – ученье свет, а неученье тьма.

My last, but in no case least, acknowledgments go to the colleagues from the Department of Applied Mathematics of the Research School of Physical Sciences and Engineering in the Australian National University in Canberra, especially to Foundation Professor Barry Ninham and Professor Stephen Hyde, Head of the Department who invited me to Canberra, to Dr. Vincent Craig and Dr. Tim Senden for their constant help, brilliant ideas and valuable discussions, to Anthony Hyde for wonderful devices, without which no work was possible.

Danke! Спасибо! Thanks!

TABLE OF CONTENTS

ABSTRACT

Despite the existing scientific and commercial interest in surfactant-polymer systems, there is still not enough connection between the understanding of the polymer-surfactant interactions in solution and at solid-liquid interfaces. In this work, the surfactant-polymer system SDS-JR400 with different component ratios was studied in the bulk solution using DLS and during adsorption at solid-liquid interfaces using AFM.

DLS measurements delivered data concerning the size and uniformity of micelle-like clusters formed in the bulk solution. Soft-contact AFM imaging was used to visualize the structure of the adsorbed layer, the acquirement of the force-distance curves together with the special “scratching” treatment brought information about the mechanical properties of the layer.

The adsorption from the mixed solutions in the concentration range from below CAC to above PSP was cooperative at native mica, hydrophobized mica and hydrophobized silica surface. The surfactant-rich mixtures showed the less and the polymer-rich mixtures – the most pronounced adsorption at all surfaces. In all cases of adsorption from mixtures the adsorbed layer was structured showing a presence of polymer-surfactant aggregates. A correlation between light scattering data concerning sturcturizing and particle size, on the one hand, and AFM images, on the other hand, was observed. A resemblance between images of mixture samples of the same or similar composition, but acquired on different surfaces, was found. It turned out that the influence of surface properties is of less importance for adsorption, compared to the influence of the mixture composition in bulk. It should be remarked that this conclusion can only be drawn, when surfactant and polymer are mixed prior to adsorption. A dependence between the surface charge and hydrophobicity, on the one hand, and the strength of adsorption, on the other hand, was visualized: SDS-JR400 mixtures of the same composition demonstrated different properties of the adsorbed layer after adsorption at native mica, hydrophobized mica and hydrophobized silica. The data obtained during “washing-off” experiments including a subsequent substitution of mixtures in the bulk phase with increasing surfactant/polymer ratio demonstrated that the composition and structure of the adsorbed layer follow the same changes that occur in the bulk phase: SDS penetrates the adsorbed layer and causes changes in its properties.

PUBLICATIONS

Usage of the "Zond-3" analyzer for measurement of isoelectric potentials on the biomembranes of native erythrocytes and lymphocytes. Yu.A. Gryzunov, D.L.Zimin. Proceedings of the IVth all-union conference "Luminescent analysis and equipment in medicine and biology", p. 21; Moscow, 1992.

The influence of physical exercises on the total amount of LDL and VLDL in capillary plasma and serum. G.P. Arutyunov, Yu.A. Gryzunov, A.A. Marfunina, D.V. Dmitriev, D.L.Zimin. Proceedings of the IVth all-union conference "Luminescent analysis and equipment in medicine and biology", p. 47; Moscow, 1992.

Fluorescent beads coated with polyaniline. A novel nanomaterial for optical sensing of pH. Pringsheim, Erika; Zimin, Denis; Wolfbeis, Otto S. *Advanced Materials* (**2001**), 13(11), 819-822.

Vapor Pressure Measurements of Liquid Solutions at Different Temperatures: Description of a Novel Apparatus and New Precise Reference Data. Karamat Nasirzadeh, Denys Zimin, Roland Neueder, and Werner Kunz* Submitted to *Journal of Chemical & Engineering Data*

Investigation and characterisation of electrodes modified by artificial receptors to creatinine. T. Delaney, V. Mirsky, D. Zimin, M.Rahm, O. Wolfbeis, to be published in *Electroanalysis*

Adsorption pattern of mixtures of trimethylammonium-modified hydroxyethylcellulose and sodium dodecyl sulphate at solid-liquid interfaces. D. Zimin, V. Craig, and W. Kunz; Submitted to *Langmuir*

Adsorption pattern of mixtures of trimethylammonium-modified hydroxyethylcellulose and sodium dodecyl sulphate at solid-liquid interfaces. D. Zimin, V. Craig, and W. Kunz; Poster presentation at XVII Conference of European Colloid and Interface Society, 21-26 September 2003, Florence, Italy.

LIST OF USED ABBREVIATIONS AND SYMBOLS

Substances

C_{14}TAB	tetradecyltrimethylammonium bromide
C_{16}TAB	hexadecyltrimethylammonium bromide
DDAPS	dodecyldimethylammoniopropanesulfonate
EHEC	ethyl hydroxyethylcellulose
HEC	hydroxyethylcellulose
HM-EHEC	hydrophobically modified ethyl hydroxyethylcellulose
HOPG	highly oriented pyrrolithic graphite
JR400	Cellulose, 2-hydroxyethyl 2-[2-hydroxy-3-(trimethylammonio)propoxy]ethyl 2-hydroxy-3-(trimethylammonio)propyl ether, chloride
LM200	hydrophobically modified JR400 polymer
PAA	polyacrilic acid
PAAm	polyacrylamide
PCMA	poly{(propionyloxy)ethyl}trimethylammonium chloride
PEI	polyethyleneimine
PMA	polymetacrylic acid
POE	polyoxyethylene
PP	polypropylene
PVAl	polyvinyl alcohol
PVC	polyvinyl chloride
PVP	polyvinylpyrrolidone
RNA	ribonucleic acid
SDS	sodium dodecyl sulphate
TMCS	trimethylchlorosilane
Triton X-400	alkyaryl polyether alcohol

Descriptions

CAC	critical aggregation (or association) concentration
CMC	critical micellar concentration
CPP	critical packing parameter

DLVO	Derjaguin, Landau, Verwey and Overbeek
DS	degree of substitution
MW	molecular weight
PSP	polymer saturation point
PSPD	position-sensitive photodiode
SFA	surface forces apparatus
SG	substitution grade

Methods

AFM	atomic force microscopy and atomic force microscope
CFM	chemical force microscopy
DLS	dynamic light scattering
FFM	frictional force microscopy
FT-IR/ATR	Fourier transform infrared spectroscopy/ attenuated total internal reflection spectroscopy
LFM	lateral force microscopy
MFM	magnetic force microscopy
NFTM	near-field thermal microscopy
NMR	nuclear magnetic resonance
NSOM	near-field scanning optical microscopy
PCS	photon correlation spectroscopy
SEM	scanning electron microscopy
SPM	scanning probe microscopy
SPR	surface plasmon resonance
STM	scanning tunnelling microscopy
TAM	tunnelling acoustic microscopy
TEM	transmission electron microscopy

Symbols

N	surfactant aggregation number
a_0	the effective surfactant headgroup area
v	the volume of the surfactant hydrocarbon chain

l_c	the critical surfactant chain length
δ	polymer solubility parameter
ΔH_{vap}	enthalpy of vapourization
V_m	molar volume
R_g	radius of gyration
β	degree of binding
K	binding constant
k_B	Boltzmann constant
D	diffusion coefficient
η	shear viscosity of solvent

CHAPTER 1. INTRODUCTION

Surfactants and polymers find application in nearly every field of human activity, their interactions are of importance for many industrial processes, and investigations in the mechanisms of these interactions may be useful in fundamental sciences as well as in many industrial applications.

The application of surfactants is essential in detergency and emulsion technology in the chemical industry, medicine and personal care, in oil recovery and mineral separation in the oil and mining industries [68]. The behaviour of surfactants at solid-liquid interfaces attracts attention due to their role in colloid stabilization and wetting processes that are important in most of the applications mentioned above. There exists still a considerable need in better understanding of the mechanisms of this behaviour.

Polymers consist of numerous molecular units or monomers. Both natural (polysaccharides, polynucleotides or other biopolymers, such as natural caoutchouc) and synthetic (polyvinyl acetate, nylon) polymers are used in nearly any technical or industrial application. For their use, especially for the use of soluble polymers, the understanding of the interfacial behaviour (adsorption and desorption, interaction with other components) is of critical importance.

The branches where polymers and surfactants find their application intersect frequently with one another (personal care, cosmetics and pharmaceuticals, paints and inks, detergents, flotation). On the one hand, in practical applications, the addition of every component has its own purpose. However, interactions between polymers and surfactants occur and have influence on the effectiveness of both components. On the other hand, a fundamental interest in the mechanisms of these intermolecular interactions and hydrophobic aggregation phenomena is a reason of the great research activity in this field. Many applications of surfactant-polymer systems are connected with their interaction with liquid-air and solid-liquid interfaces. This has been described in several reviews in this area. The special attention of the reviewers was attracted by applied systems, like mineral processing and solid suspensions, detergency, and personal care and cosmetics [17, 44, 136]. For the latter application field, the system comprising sodium dodecyl sulphate (SDS) and the cationic polymer JR400 (cationically modified hydroxyethyl cellulose ether) is of special importance due to the broad use of the both components.

In the huge amount of studies performed on polymer-surfactant systems, a great majority deals with the interactions in bulk, and much less investigations had been made on liquid-air and solid-liquid interfaces. If any, investigations considered a broad range of concentrations, focusing on the area around and above the cmc of the surfactant. This concerns the specific SDS-JR400 system, too. Therefore, little detailed information is available regarding the interactions of this system with different surfaces. This is especially true for low concentrations, sufficiently below the cmc of the surfactant.

1.1 AIM OF THIS THESIS

The aim of this work is to provide a better understanding of the interaction between SDS and JR400 at the solid-liquid interface, compared with the composition in bulk. The work is focused on the area of high dilutions. Specifically, this work will make an attempt to distinguish between the roles of the mixture composition in bulk, on the one hand, and of the surface properties, on the other hand, in the general adsorption pattern. The structure and properties of the adsorbed layer is studied with Atomic Force Microscopy (AFM), and the properties in bulk with Dynamic Light Scattering (DLS).

1.2 OUTLINE OF THIS THESIS

A theoretical overview and background information are presented in the Chapter 2: a summary of scientific data concerning the structure and properties of polymers and surfactants both in solution and at interfaces is given. The SDS surfactant and the JR400 Polymer are described. The modern view of polymer-surfactant interactions is presented, with an emphasis on the interactions between ionic polymers and surfactants bearing opposite charges. The history of investigations of polymer-surfactant systems is stated, with a deepened view into the SDS-JR400 system. General description of solid-liquid interfaces is given, and the surfaces used in this work are described.

A description of the research methods and preparation procedures used in this work is given in the Chapter 3. The method of atomic force microscopy, ways and details of data acquisition (imaging, “scratching”, force-distance curves) used in the work are examined in details.

Only one polymer-surfactant system was chosen for study in this work. A summary of data collected while investigating the SDS-JR400 system in bulk and at solid-liquid interfaces is given in the Chapter 4. The SDS-JR400 system is described in bulk and after and during adsorption at negatively charged mica and silica, both hydrophilic and hydrophobized. In this chapter these results are also examined from the point of view of theory and compared to the literature data.

Chapter 5 contains a general summary of conclusion drawn from the results given in Chapter 4.

CHAPTER 2. THEORY AND BACKGROUND

Two substances that belong to different classes of chemical compounds are used in this work. They interact in the bulk as well as at interfaces. Their adsorption at different types of surfaces will be described in this thesis.

This chapter provides background information concerning the substances and interfaces and their interaction. The first two sections deal with surfactants and polymers, respectively. A summary of classification, research history, structure and properties in the bulk and at interfaces is provided, followed by a description of an individual substance used in the work. The third section gives a look at polymer-surfactant interactions with a more detailed view at patterns significant for this work. The final section gives a theoretical overview of solid-liquid interfaces in context of polymer-surfactant interactions and describes specific properties of interfaces that come to use in this work.

2.1 SURFACTANTS

Surfactants occur naturally, like phospholipids, in biological systems or can be made synthetically. Their broad application is caused by their ability to modify surface properties of liquids, like surface tension and, therefore, wettability. They are used as dispersants, surface modifiers, emulsifiers or to aid solubility both in industry and chemical formulations. The following section provides a general description of surfactants, their behaviour in solution and at interfaces.

2.1.1 General structure and properties

Surfactants are called so due to sufficient surface activity, i.e., the ability to lower the surface tension of a solution. Generally, a surfactant molecule consists of two parts

having different properties: a “headgroup” with a strong affinity for the solvent and a longer “tail” with less affinity for the solvent. In the case of an aqueous solution, we can refer to hydrophilic and hydrophobic parts of the molecule, respectively. The whole molecule is thus amphiphilic. A schematic representation of a surfactant molecule is given in Figure 2.1.

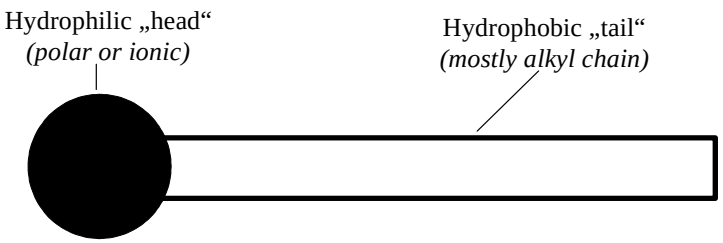

Figure 2.1 – Schematic illustration of a surfactant molecule in aqueous solution

According to the properties of the hydrophilic headgroup, surfactants may be classified as ionic and non-ionic [74]. Among ionic surfactants, one can distinguish cationic, anionic and zwitterionic surfactants. Examples for every group are given in Table 2.1.1.

Table 2.1.1 Surfactants classification and examples

Surfactant type		Headgroup charge	Example	
Ionic	Cationic	+	**C_{14}TAB**	$C_{14}H_{29}N^{+}(CH_3)_3Br^{-}$
	Anionic	-	**SDS**	$C_{12}H_{25}SO_4^{-}Na^{+}$
Zwitterionic		+ and -	**DDAPS**	$C_{12}H_{25}NH_4^{+}(CH_2)_3SO_3^{-}$
Non-ionic		no charge	**$C_{10}E_8$**	$C_{10}H_{21}[OCH2CH2]_8OH$
			Dodecyl sulphil ethanol	$C_{12}H_{25}SOCH_2CH_2OH$

Polymeric [53] and dimeric or gemini [51, 52] surfactants have been synthesized and used in research. Generally, these are also molecules with intermitting hydrophilic and hydrophobic groups. A schematic illustration of gemini surfactants is given in Figure 2.2.

A B

Figure 2.2 – Schematic illustration of an asymmetric (A) and symmetric (B) gemini surfactant. Reproduced from [54].

Surfactants are often soluble in water due to favourable hydrophilic interaction between the polar headgroup and water. A typical ionic surfactant behaves in water as any other strong electrolyte: the counterion dissociates from the surfactant ion.

The dual nature of a surfactant molecule predefines their unique interaction with water: as mentioned above, the polar headgroup ensures a certain solubility; but the hydrophobic tails, in opposition to the former, have a very entropically unfavourable interaction pattern with water, usually referred to as the hydrophobic effect: the hydrophobic tails cause a more ordered structure of water. This results in an entropy decrease. This property naturally leads to a formation of a more energetically favourable interaction patterns, where the hydrophobic tails aggregate, or they are “hidden” or removed from the solution. As a consequence structures such as micelles occur or the surfactant molecules concentrate at interfaces, respectively.

2.1.2 Surfactant behaviour at liquid-air interfaces and in bulk solution

At a water-air interface, or generally, on a border between a polar and an unpolar phase (e.g., at a water-oil or water-vapour interface), the thermodynamic favourability causes an orientated location of surfactant molecules: the polar (ionic or non-ionic) headgroup is in the aqueous phase and the tail is directed out of water, as shown in Figure 2.3.

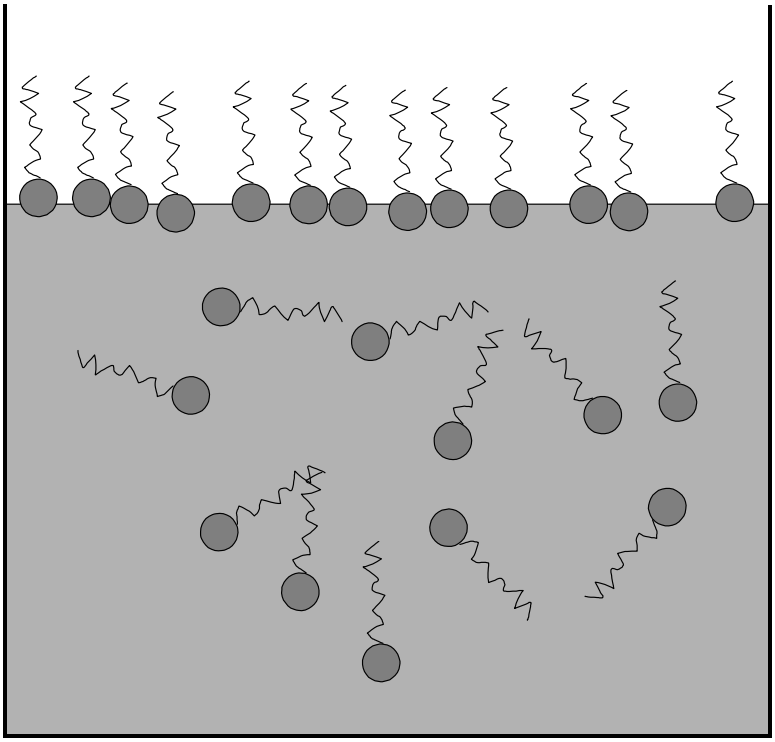

Figure 2.3 – Surfactants accumulation at air-water interface with energetically favourable orientation of molecules.

The accumulation of surfactants at the air-water interface lowers the polarity difference between air and water, and, therefore, lowers the surface tension as well, in accordance with the Rebinder rule [56]. The surface activity of the surfactant (derivative of the surface tension in the surfactant concentration with the reverse sign) depends on the length of its unpolar "tail" – the hydrocarbon group. According to the Duclaux-Traube's rule (1891), every –CH2– group of the hydrocarbon chain increases the surface activity of the surfactant 3 to 3,5 times. The surface tension of water (72 mJm^{-2} at 293 K [56]) can be reduced to 30 – 35 mJm^{-2} by adding a surfactant with a sufficiently long hydrocarbon chain [68]. In summary, the dual, amphiphilic nature of a surfactant causes it to concentrate at the air-water interface with a specific orientation, thus reducing the system free energy and the surface tension.

The second way to achieve an energetically favourable state is the interaction of the surfactant molecules with one another in the bulk solution.

At concentration increase, the saturation of the air-water interface occurs. The molecule migration into the surface layer brings less and less energetic “profit”. The natural way to reduce the hydrocarbon-water interactions is such an arrangement of the surfactant molecules in the bulk solutions, that the hydrophobic “tails” of the surfactant molecules are as close to one another as possible. As a logical result of such arrangement, a special kind of molecule aggregate emerges called micelle. A surfactant micelle is schematically represented in Figure 2.4.

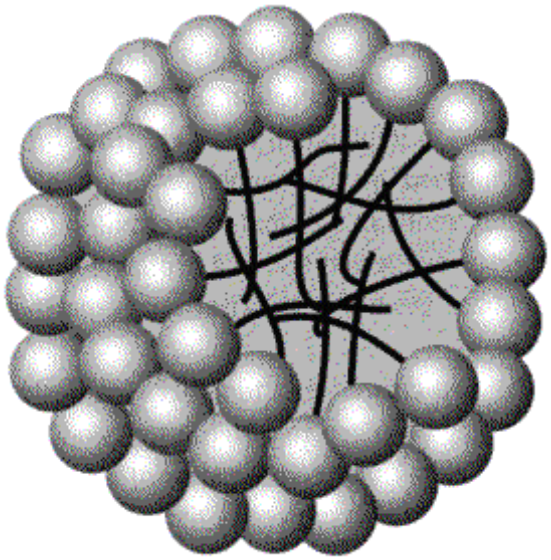

Figure 2.4 – Schematic representation of a spherical surfactant micelle. Reproduced from [http://www.upol.cz/resources/kafch/micelles_cz.htm].

A micelle is a complex of surfactant molecules with hydrophilic headgroups directed in the bulk solution and hydrophobic tails – in the inner space of the micelle. Inside the micelle, therefore, practically no water molecules are present, and thus no energetically unfavourable hydrocarbon-water interactions occur.

Generally, there exist spherical, rod-like, and lamellar micelles. In this order they emerge, or re-form, with increasing concentrations. Evidence for disc-shaped micelles has also been obtained [68].

At the final stage of the concentration increase, the surfactant solution turns into gel. The micelle forms are schematically illustrated in Figure 2.4. In this work, due to the low concentrations, at which the investigations have been performed, only spherical micelles will be discussed.

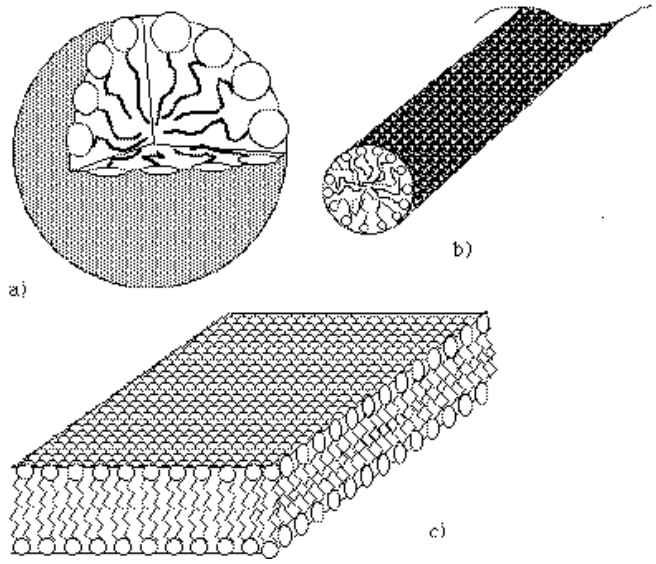

Figure 2.5. – Schematic illustration of possible micelle forms: a) spherical micelle, b) rod-like micelle, and c) lamellar micellisation. Reproduced from [http://perso.curie.fr/Albrecht.Ott/micellescylindriques/amphiphile-Title.html]

Generally the micelle radius is between 1-100 nm, obviously depending on the length of the hydrocarbon chain and on the size of the hydrophilic headgroup. One more important property of a micelle is the aggregation number N – the number of surfactant molecules comprising the micelle. It is characteristic for an individual surfactant at given temperature. The geometric considerations hereto will be discussed later in this section. The micelles of charged surfactant molecules are surrounded with the double electric layer; they contribute to the conductivity of the solution.

The formation of ordered micelles is not only an energetically favourable process: in a micelle, an ordered position of surfactant molecules leads to a loss of freedom, and (more important, especially for ionic surfactants) the location of loaded headgroups close to one another on the micelle surface causes the electrostatic repulsive force to contribute unfavourably to the energy of micellisation. The micellisation process, therefore, is a reversible chemical process that depends on a balance of favourable and opposing factors. Like for any reversible process, there exists an equilibrium condition for micellisation between micelles and saturated surface that is characterized by the critical micelle concentration (CMC). The CMC in aqueous solution is characteristic for a surfactant at a given temperature and electrolyte concentration. Micelles can only form when the temperature is above the Krafft point. The Krafft point is the temperature (more precisely, narrow temperature range) above which the solubility of a surfactant rises sharply (IUPAC).

The CMC is to define as a concentration at which exactly 50% of the surfactant molecules in the bulk solution are aggregated to micelles [56]. Since a transition from single molecules to larger aggregates in the solvent takes place at CMC, it is expectable that many properties of the solution would change at this point. And really, sharp changes are experienced by the concentrational dependence of a large number of properties.

This concerns properties relying on the size (and, therefore, mobility) and number of particles in solution, i.e., colligative properties. Most significant are abrupt changes of surface tension, turbidity and light scattering (optical density), electric conductivity and osmotic pressure.

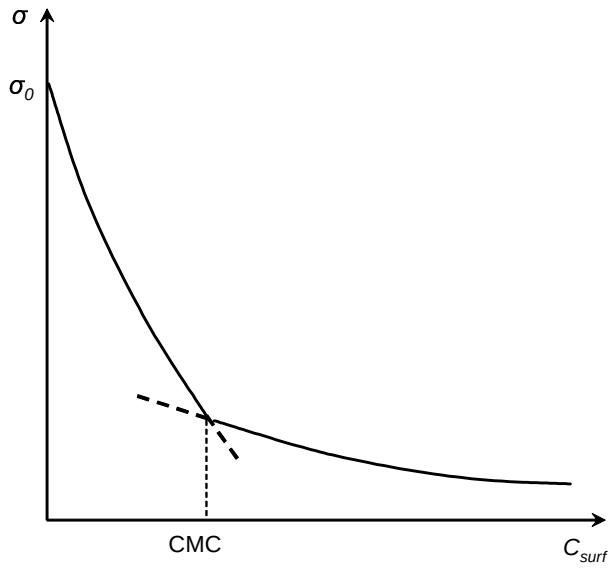

Figure 2.6. – Typical change in surface tension for a surfactant with increasing concentration

These changes can be used for the experimental location of the CMC. For example, the typical change in surface tension for a surfactant with increasing concentration is shown in Figure 2.6. The deceleration in the surface tension decrease observed in the illustration can be explained in terms of surface saturation mentioned above: at further increase of the surfactant concentration above the CMC, most of “new” surfactant molecules coming in the solution, participate in the formation of micelles, and not in the migration to the water-air interface contributing to the reduction of the surface tension. As shown by Corkill et al. [69], above the CMC. the surfactant monomer concentration remains constant while the total concentration increases. Changes in other properties of

the surfactant solution are generally to attribute to the abrupt increase of the size of the dissolved particles and to the decrease of their number and mobility (significant for electric conductivity, since micelles, and not single molecules become main charge carriers in the system).

The nature of micelles is dynamic, and surfactant molecules are in continuous motion. There is constant interchange between micelles and solution. The lifetime of a surfactant molecule in a micelle is of the order of 10^{-7} seconds [70, 71], and the half-life for micellar formation or breakdown is usually in the region of 10^{-3} to 1 seconds [72, 73].

Geometric considerations

Size and properties of surfactant micelles and, therefore, the properties of the surfactant solution at given concentration, depend very strongly on the geometric characteristics of molecules of a specific surfactant. There exists a theory of micellar structure, based upon the geometry of various aggregate shapes and the space occupied by surfactant headgroup and tail [61-63] It allows prediction of micellar shape using three geometric parameters that play the most important role:

***a_0* – the effective headgroup area:**

this is the minimum physical size of the headgroup representing a balance between the opposing forces – mutual headgroup repulsion (especially for charged headgroups) and hydrophobic attraction;

***v* – the volume of the hydrocarbon chain(s),** and

***l_c* – the critical chain length:**

this is the maximum length that the chain(s) can have in a “stretched” state.

Taking into account the bond lengths and the group volumes, we can use for a saturated hydrocarbon chain with “n” carbon atoms [60],

$$l_c \leq l_{max} \approx (0.154 + 0.1265n)\ \text{nm}$$

and,

$$v \approx (27.4 + 26.9n) \times 10^{-3}\ \text{nm}^3$$

The following mathematical expression incorporating these three terms defines the dimensionless critical packing parameter (CPP):

$$CPP = \frac{v}{a_0 l_c}$$

The CPP value defines the micellar form. The critical values can be derived from simple geometric arguments. For example, a spherical micelle of radius R has mean aggregation number *n* that can be expressed as

$$n = \frac{4\pi R^2}{a_0}, \quad \text{and} \quad n = \frac{4\pi R^3}{3v}$$

What means that,

$$R = \frac{3v}{a_0}$$

Therefore, since R≤ l_c, a spherical micelle can assemble when

$$\frac{v}{a_0 l_c} < \frac{1}{3}$$

This parameter (CPP) is a numerical description of monomer shape. Its value of 1/3 for spherical micelles indicates that mostly surfactants with relatively small hydrocarbon chain volumes and large effective headgroup areas tend to form spherical micelles. If the CPP value is between 1/3 and 1/2, i.e., with smaller headgroups and larger “tails”, rod-like micelles assemble, and if CPP exceeds 1/2 bilayers can form.

Solution conditions, like electrolyte concentrations, ionic strength, and pH have a significant influence on size and shape of surfactant aggregates and on CMC as well [136]. This can be explained by, for example, screening of electrostatic repulsion between the ionic headgroups by the added electrolyte: the repulsion between them is reduced which means that the effective headgroup area is decreased, and, therefore, CPP

increases. An example for such an influence is a transition of spherical CTAB micelles to rod-like form in the presence of 80 mM KBr [64].

2.1.3 Surfactant adsorption at solid/liquid interfaces, dependence on mutual charge relations and hydrophobicity

2.1.3.1 General considerations

This work is devoted mostly to interactions between surfactants and polymers, and it studies adsorption of their mixtures. Only a simple overview will be presented concerning adsorption of pure surfactants. It will give a general “framework” understanding of pattern and mechanisms of surfactant adsorption at solid-liquid interfaces.

At a solid-liquid interface, surfactants readily adsorb from solution. This adsorption can be driven by nearly all kinds of intermolecular interactions: hydrophobic and hydrophilic, electrostatic and other. Whether adsorption takes place or not; its mechanisms, and the final structure and properties of the adsorbed layer, – all these issues are generally dependent on the properties of the surfactant and that of the surface, as well as on the concentration of the surfactant in bulk. The main surface properties having an influence on the adsorption of surfactants are the following: surface structure, surface hydrophobicity, and surface charge, especially the sign of the charge and the surface charge density [68]. These properties can vary in a very broad range; the condition of the surface, and in some cases the condition of surfactant, can depend critically on the solution properties (temperature, pH). A unified general approach to understanding the adsorption process is hardly available under such circumstances [75]. Therefore, only a brief review of adsorption patterns and results of investigations on the isolated surfactant adsorption at solid-liquid interfaces is presented in this section.

Only aqueous solutions are considered here, and most of the solid surfaces bear an electric charge when in contact with water [75]. It is therefore useful to discuss the surfactant adsorption at charged surfaces in the first place. What concerns uncharged surfaces, the only fundamentally and practically important kind of them is graphite. The adsorption process and properties of the adsorbed layer at uncharged surfaces will be in

further mentioned separately for cases when this process differs significantly from that on the charged surfaces.

One of the most important factors governing the adsorption of ionic surfactants is the electrical interaction between ion and surface. It is obvious that only interactions between oppositely charged items (surfactant and surface) can be considered here because no adsorption e.g. of a cationic surfactant at a positively charged surface is possible if no other mechanisms are involved or no other components are present in solution.

Probably the most important feature of solid-liquid interfaces of this kind is the electrical double layer formed by the loaded surface and ions in water close to the surface. If a surfactant is present in solution it contributes sufficiently to the formation of the layer. Depending on the solvation grade, the centers of the ions (or ionic groups) lay in the inner Helmholtz plane or in the outer Helmholtz plane (Stern plane). In the former case, the surfactants are “specifically” adsorbed, i.e. electrical interactions play a minor role in the formation of the adsorbed layer. In the latter case, the adsorption is of no specific character, which means, mostly of electrical nature. This is the situation that we discuss here. In this case, the surfactant molecules are oriented with their polar (in this case, ionic) heads directed to the surface.

The second important mechanism of surfactant adsorption at solid-liquid interfaces is by hydrophobic interaction. This mechanism participates in the formation of the adsorbed layer in a case when the surface itself is hydrophobic, and this mechanism plays the leading, or the only, role when the surface bears no electric charge at all. The part of the surfactant molecule directed to the surface is in this case its hydrophobic tail that bears no electric charge as well.

So we can see that the dual nature of the surfactant molecule can lead to the formation of adsorbed layer caused by nearly every combination of electrostatic and hydrophilic/hydrophobic properties, both of the particular surface and the particular surfactant molecule. The variety of adsorption patterns emerges that depends on contribution of different kinds of interaction in every particular case. This variety will be partially presented downwards.

2.1.3.2 Measurements of surfactant adsorption

The usual method to quantitatively describe surfactant adsorption at a solid-liquid interface is the measurement of the surface excess concentration, **Γ**, which is defined as excess of surfactant concentration at the interface compared with the bulk equilibrium concentration. A result of such experiment is usually an adsorption isotherm that provides a quantitative picture of the adsorbed layer without any regards to the layer structure.

A generalized adsorption isotherm for a surfactant and surface of opposite charge looks generally as presented schematically in Figure 2.7.

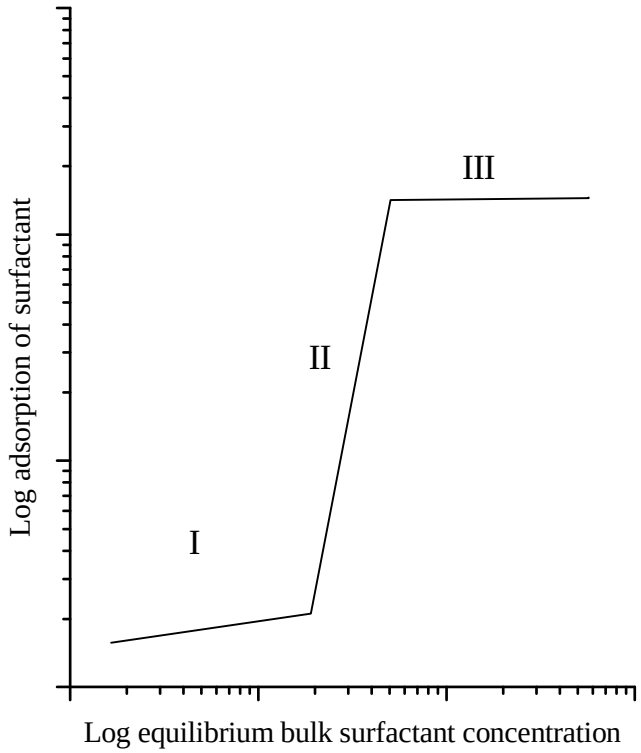

Figure 2.7 – Typical simplified adsorption isotherm for a surfactant adsorbing to an oppositely charged surface [137]

In Region I (where C << CMC), individual surfactant molecules adsorb via ion exchange until the surface charge is neutralized. It is clear that for surfaces bearing no

charge, the isotherm looks different, having no Region I. An example for such isotherm (in linear scale) is presented in Figure 2.8 (reproduced from [82]). At such surfaces, the adsorption process starts from the Region II.

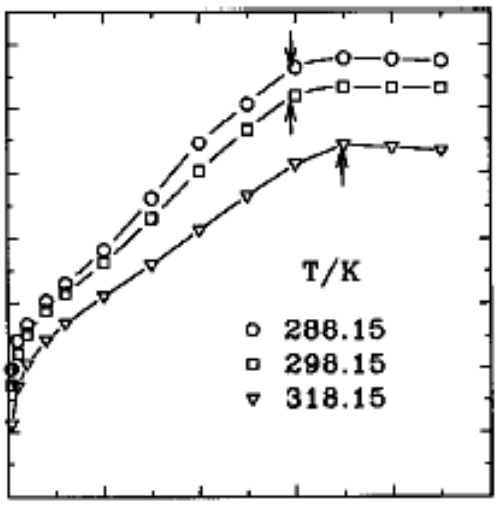

Figure 2.8 – Cumulative adsorption isotherms of aqueous solutions of C12TAB on graphite. Reproduced from [82].

As (in case of charged surfaces) the surface charge is neutralized, and the surface is covered with a kind of monolayer of surfactant molecules with their tails directed to solution, adsorption proceeds further in Region II (C< CMC). Here it is driven mostly by hydrophobic interaction: a tail-to-tail association of surfactant molecules in solution and those already adsorbed at the surface takes place. This association causes a rapid increase in adsorption. The surface charge in this region becomes eventually reversed.

As the surfactant concentration experiences further increase, the isotherm reaches its plateau in the point where surfactant concentration becomes equal to CMC. The isotherm Region III where C > CMC shows no more adsorption increase. The adsorbed surfactant layer is saturated in this region, and this condition is considered to be a very stable state.

The adsorbed surfactant layer was studied in early decades mostly quantitatively. The equilibrium adsorbed layer was assumed to have no lateral structure. The conformation of the layer (film) was considered to be similar to bilayers. The qualitative studies of the film performed since middle 80es have allowed the further characterization of its properties and, in some cases, direct visualization of the adsorbed layer. Due to the use of specialized techniques such as neutron reflection [65],

ellipsometry [85], optical reflectometry [50], fluorescent spectroscopy [86], FT-IR/ATR [87], NMR [88], SPR [83, 84] and Scanning Probe Microscopy (to be discussed in the Chapter 3), a rich array of structures formed by surfactant aggregates adsorbed at solid-liquid interfaces has been revealed. The Atomic Force Microscopy (the variation of the Scanning Probe Microscopy) has made direct in-situ imaging of these structures possible.

Manne et al. imaged the structures formed by surfactant C_{16}TAB adsorbed to graphite surface with the AFM in 1994 [89]. The reported structures have been hemi cylinders that were ordered parallel to one another and obviously templated by the crystal structure of substrate (graphite). Since then, a great amount of works has been published reporting a wide variety of surfactant structures adsorbed at solid-liquid interfaces of various kinds at concentrations above the CMC [117, 66, 67, 91, 92, 119]. This variety, from the point of view of general properties and important environment features influencing adsorption, is summarized and briefly described in the following subsections.

2.1.3.3 Substrate

Surfactant adsorption at solid-liquid interfaces is strongly influenced by substrate properties. The main substrate properties influencing the adsorption pattern are surface charge and surface hydrophobicity, as it was noted above.

If adsorption takes place at hydrophilic surfaces where the electrostatic interaction prevails over the hydrophobic one, spherical and cylindrical aggregates (often referred to as (adsorbed) micelles or micelle-like structures) defines the picture of the saturated adsorbed layer. Laterally homogeneous adsorbed layers (bilayers) were also reported [120, 114, 54]. In all these structures, surfactant molecules closest to the solid surface are oriented to it with their polar or ionic heads. A cross-section view of cylindrical or spherical aggregates typical for such adsorption is schematically presented in Figure 2.9 a).

a) b)

Figure 2.9 – Schematic representation of cross-section views of structures formed by adsorbed surfactants above the CMC: a) at hydrophilic surfaces, b) at hydrophobic surfaces.

When hydrophobic surfaces are in use as adsorption substrate the adsorption process is lead by the hydrophobic interaction that prevails over the electrostatic one. This causes formation of the adsorption layer where surfactant molecules are oriented with their heads to solution and these are the hydrophobic tails which contact with the solid surface. The most frequent structures of which usually such adsorbed layer consists are hemispheres and hemicylinders. A cross-section view of hemicylindrical or hemispherical aggregates typical for adsorption driven by hydrophobic interaction is schematically presented in Figure 2.9 b). Laterally homogeneous monolayers of surfactant molecules can also form.

Hemicylindrical structures have to be mentioned separately since they were actually the first kind of surfactant adsorption structures observed by the AFM [89]. Hemicylinders are also remarkable because they are reported to be formed both at hydrophobic [89, 119, 66] and at hydrophilic (gold [84, 115] and mercury [106]) surfaces. This can be probably explained in different cases by specific activity of sulphur or by electric potential applied to the surface [84].

It is to mention that the formation of saturated adsorption layers at solid-liquid interfaces possesses some similarity to the process of surfactant micellar aggregation in bulk: we can consider the hydrophobic interface plane as a symmetry plane for the aggregates and can discover structures very similar to those formed by micellisation in bulk solution and described in the section 2.1.2 (see Figure 2.5). Presumed that the inner space of a micelle is hydrophobic, we can easily see this resemblance: a hydrophobic solid-liquid interface naturally belongs to the inner space of a micelle and thus divides it to two hemimicelles only one of which can be observed. A hydrophilic surface, in

contrary, belongs to the water environment of micelles, and therefore, to their outer space, which causes formation of “complete” micelle-like structures. Generally, we can say that solid-liquid interfaces ***induce*** self-aggregation of surfactant molecules.

Another important feature is the substrate structure: depending on whether the substrate is crystalline or amorphous, the adsorbed layer can be templated by the (lattice) structure of the underlying solid surface. Examples of such templating were collected especially during AFM investigations of adsorbed layers [117, 118]. These results are supported by electronic microscopy and surface plasmon resonance studies [83,84]. In particular, position and length of hemicylindrical and cylindrical micelle-like structures of the adsorbed layer are likely to be strongly influenced by the structure of the underlying substrate. This was observed, for example, on gold and highly oriented pyrrolithic graphite (HOPG) [117].

A particular case has been observed especially on mercury and gold surfaces when the surface potential is changed [84]. Such changes lead in experiments to transformations of (hemi)cylindrical aggregates to a condensed monolayer and back again. This can be explained by the charge screening on the surfactant aggregates what caused their “melting”.

2.1.3.4 Influence of solution conditions

Generally, solution conditions able to influence the structure of adsorbed layer are the concentration of surfactant itself and the presence of various additives. The influence of counter- and coions as well as that of the solution temperature can be also significant.

A higher surfactant concentration causes the increase of packing density of the adsorbed surfactant structures: the spacings between them become smaller [119]. An increase of aggregates’ period (i.e., both aggregates size and spacing) was also reported. Similarly, electrolyte addition results in a decrease of interaggregate spacing, since the repulsive electrostatic forces between the surface micelles are screened. Non-polar additives, like dodecanol [124] can lower the curvature of aggregates due to the hydrophobic interactions with the surfactant.

The influence of solid-liquid interfaces usually decreases the Krafft temperature sufficiently: the structures observed below and above the bulk Krafft point are similar [120].

To summarize briefly, surfactants form different structures when adsorbed at solid-liquid interfaces at concentrations above the CMC. On hydrophobic surfaces, the structures are hemispherical and hemicylindrical micelle-like clusters (hemimicelles) or monolayers. Hydrophilic surfaces make adsorbed surfactant molecules to form spherical or cylindrical micelle-like structures or bilayers. The most typical structures are presented in Figure 2.10. The behaviour of surfactant at interfaces demonstrates a qualitative similarity with their bulk properties. The interfaces can be considered as a part of environment and their influence can be discussed in terms of environment properties.

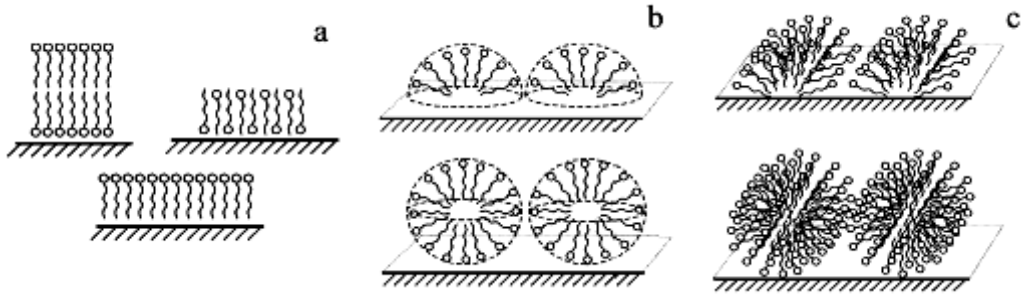

Figure 2.10 – Examples of different types of structures, which may form due to the adsorption of surfactants on solid surfaces: (a) bilayers and monolayer; (b) spherical hemimicelles and micelles; (c) cylindrical hemimicelles and micelles. Reproduced from [84].

2.1.4 Sodium dodecyl sulphate – an anionic surfactant

Sodium dodecyl sulphate $C_{12}H_{25}NaO_4S$ (SDS) is probably the most commonly used anionic surfactant in the world. It finds a very broad application in nearly every branch. Its annual production in the world reaches millions of tons [55]. SDS is normally the most significant component of many important personal care products like shampoos, shower gels, cleaners etc.

The first scientific description of SDS is given by Hartley [76]. Due to the very broad application mentioned, it is not surprising that the number of scientific publications concerning this substance grows rapidly during last 60 years. This nearly exponential growth seems to be so illustrative for the question of practical importance of investigations on this substance that it is presented in Figure 2.11.

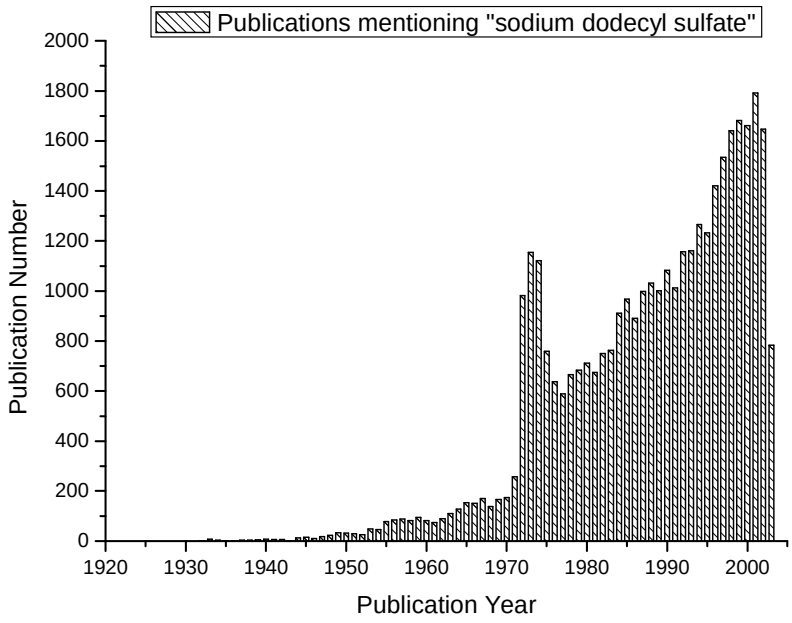

Figure 2.11 – Increase of publications amount concerning sodium dodecyl sulphate according to the scientific search system Science Finder Scholar

The rapid increase of publications number in early 70s, when personal care products mentioned above came into daily life is of a special interest.

SDS is used in this work as a typical anionic surfactant. SDS is an alkyl ether sulphate. Its molar mass is 288.38 g/mol. The chemical structure of SDS is presented in Figure 2.12.

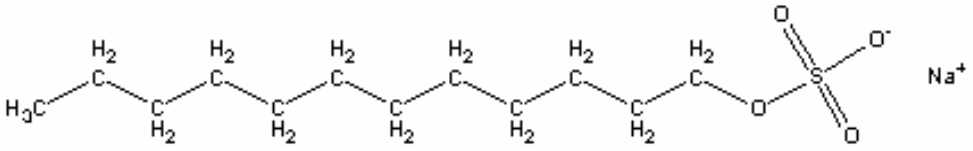

Figure 2.12 – Structural formula of sodium dodecyl sulphate

At room temperature, SDS is highly soluble in water (up to 150 g/L). It dissociates in water as every strong electrolyte. The pH values of a 10 g/L solution of SDS are between 6 and 9 [Merck Product data, 113760]. The micellisation behaviour of this surfactant has been studied very precisely in last decades. According to the different literature data, the critical micellisation concentration of SDS is about 8.3 mM at 25oC [79, 77].

The mean aggregation number N, also according to slightly varying literature data obviously depending on the precision of individual method, is between 67 and 76 at room temperature when measured close to the cmc[77, 78]. Micelles radius of SDS at 25 ^{o}C is about 2.5 nm [80].

As a typical and easily commercially available anionic surfactant, SDS is used in investigations of surfactant adsorption at solid-liquid interfaces since 1957 [81].

2.2 POLYMERS

Polymers occur in nature, like starch or RNA, or can be produced synthetically, like polyethylene. Polymers are macromolecules; they consist of many repeating units called monomers. Polymer properties generally differ significantly from those of monomers. Polymers can consist of monomer units of the same type (homopolymers), like polyacrilic acid or of two or more unit types (heteropolymer or copolymer), like proteins, which consist of 20 amino acid types. The structure of the polymer molecule can be linear, branched (dendritic) or cross-linked. In the latter case the polymer forms a three-dimensional network. The overall properties of the polymer vary according to the type of monomers, the structure of the polymer and its resulting molecular weight.

Depending on the nature of monomers, polymer molecules can carry charges. Uncharged polymers are referred to as neutral or non-ionic ones and those carrying charge – as polyelectrolytes. They will be discussed in the following sections.

2.2.1 Polymer solubility, polyelectrolytes

Water is the only solvent used here. The general aspects of polymer solubilisation in water and their behaviour in aqueous solution are briefly overviewed in this section.

Most polymers, like e.g. PP, PVC, are insoluble in water. Polymers that are water-soluble have wide applications in water treatment processes, emulsion stabilization, especially in emulsion paints, cosmetics, pharmaceutical formulations etc.

Dissolution of a polymer consists of two stages. The first one is the water uptake by the dry polymer and leads to a formation of a swollen gel, and during the second one the gel breaks down to form a true solution. The main property defining the solubilisation process is the affinity of the polymer to the solvent. Since water is a polar solvent it dissolves polar or ionic polymers. This affinity can be expressed as a comparison of attractive forces between solvent molecules and polymer segments, on the one hand, and inside the pairs "segment – segment" and "solvent molecule – solvent molecule", on the other hand. In order to form a solution, the force between segments and solvent molecules has to exceed the sum of those inside the "pairs". If the affinity of solvent to polymer is low, the solvent can be described as "poor", and if there is a high affinity – as "good".The temperature at which the force between the segments is equal to the sum is referred to as theta, θ, temperature. The size of the polymer molecule is here uninfluenced by the solvent effects; that is, the polymer molecule behaves like being in its "own liquid".

Quantitatively, the solubility of a polymer in the given solvent is characterized by the solubility parameter δ, depending on the enthalpy of vapourization, ΔH_{vap}, normalized with the molar volume, V_m.

$$\delta^2 = \frac{\Delta H_{vap}}{V_m}$$

To enable polymer solubilisation in the given solvent, the solubility parameter of the polymer has to be equal or close to this of the solvent. The main components contributing to the solubility parameter are dispersion forces, polar forces and hydrogen bonding. The latter, namely its strength, is one of the main reasons, why no satisfactory thermodynamic theory has been given for aqueous polymer solutions.

Polymers can aggregate in the solution, in extreme cases undergoing phase separation. This property of water-soluble polymers is used to characterize their solubility quantitatively in another way then with the help of the solubility parameter. In this method the measure of the polymer solubility is the so-called "cloud point". This point is the temperature where the precipitation of 1 % aqueous solution of the polymer occurs.

2.2.1.1 Polymer conformations in solution

Polymer molecules are relatively flexible due to the ability of their backbone to rotate freely around single bonds along the polymer chain. In a dilute solution, this flexibility causes constant motion of the polymer molecule and its interchange between one conformation and another. Some information about the polymer conformation can be acquired when measuring its hydrodynamic radius by light scattering (details to the method see Section 3.2.2.). In this case, the radius of gyration denoted as R_g or $\bar{s}^2$ can be measured. This is a part of a concept considering the average shape coiled polymer molecule as spherical with the origin in its centre of gravity.

The polymer molecule form can vary from completely coiled conformation, where the polymer chain possesses the minimal possible hydrodynamic volume, up to completely extended one. The size of a fully extended polymer chain is called its contour length.

The prevailing conformation type is defined by many factors and conditions, like solvent properties, polymer concentration, temperature, pH value and electrolyte concentration, and polymer affinity to solvent as well. With increasing affinity between polymer segments and solvent molecules, the preferred conformation changes from coiled to extended, as presented in Figure 2.13.

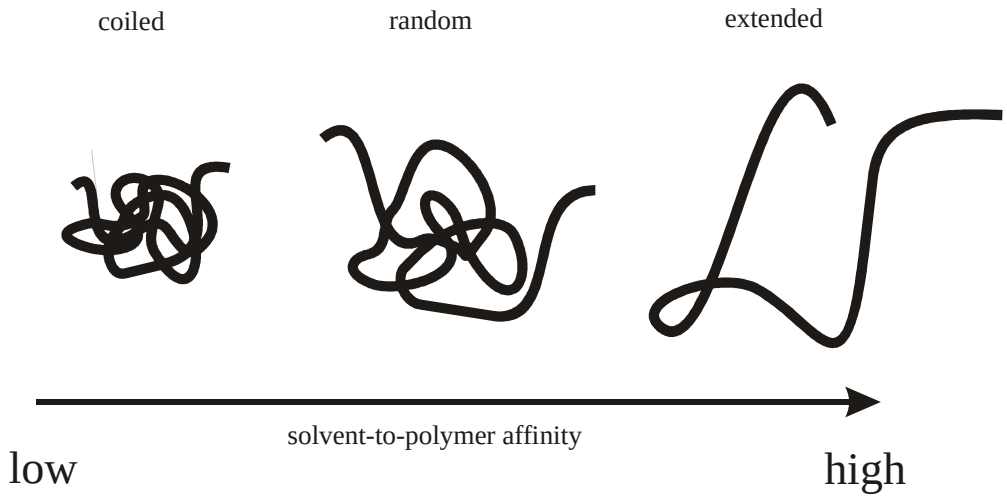

Figure 2.13 – Schematic illustration of polymer conformations in solution.

2.2.1.2 Various classes of water-soluble polymers

Among non-ionic water-soluble polymers, following classes can be mentioned: first of all, polymers with an oxygen or nitrogen in the backbone. These are in the first line polyoxyethylene (POE) and polyethyleneimine (PEI), respectively. The latter polymer is usually branched and contains normally ¼ of quaternary amine groups. Secondly, a presence of an acrylic group causes polymer solubility in water. Here polyacrilic acid (PAA) and polymetacrylic acid (PMA) can be mentioned. PAA and POE form a complex in aqueous solution due to the hydrogen bonds emerging between the hydrogens in the PAA and oxygens in the POE. Another water-soluble polymer in this class is polyacrylamide (PAAm). It is very hydrophilic, has a high affinity to surfaces due to cationization at lower pH values and is therefore used as a flocculent. Thirdly, it is a vinyl group that also makes a polymer water-soluble. The most important examples in this group are polyvinyl alcohol (PVAl) and polyvinylpyrrolidone (PVP). These both polymers are very important in the practical applications, especially PVP having a weak basic character and thus interacting with anionic surfactants (e.g. SDS) in aqueous solutions. Such solutions are used in pharmacy, cosmetics and medicine. The SDS – PVP system has been also widely used in the fundamental research of polymer-surfactant interactions both in bulk solutions and at interfaces [116, 104]. All the classes of water-soluble polymers listed above are of synthetic origin.

The fourth and final class includes polymers occurring in nature and their derivatives. These are polysaccharides and cellulose derivatives. Polysaccharides can be linear or branched; they are made up of sugar-based units. Such of them like dextran, gum arabic and agar are widely used in food industry as gelants.

The derivatives of cellulose are of special importance for this work, since the JR400 Polymer used here belongs to this class. Most commonly, cellulose can be made water-soluble using the three hydroxyl groups of β-anhydroglycose unit, which constitutes the cellulose chain, as derivatization starting points. The extent of their reaction is referred to as the degree of substitution (DS) and is defined as the average number of hydroxyls that have reacted; the DS can thus vary between 0 and 3. (It is important to distinguish between the DS and the substitution grade (SG), an average number of functional groups per monomer unit. The SG plays an important role at further functional modifications of cellulose derivatives and will be mentioned later).

This reaction is the way how the cellulose derivatives, which are most significant for research and application, are manufactured. These are carboxymethylcellulose, hydroxyethylcellulose (HEC), and ethyl hydroxyethylcellulose (EHEC). The first substance is the product of the cellulose hydroxyls reaction with monochloroacetate, giving a sodium salt of the carboxylic acid. It is acidic, displays almost no surface activity and is used in detergents preventing re-deposition of removed pollutions. HEC is manufactured by the reaction of alkali-swollen cellulose with ethylene oxide. It is used as thickener, binder, etc. The addition of ethylene chloride to freshly produced HEC leads to EHEC manufacturing. This polymer is very versatile depending on the DS and molar substitution (MS – the molar ratio of ethylene oxide to cellulose hydroxyl groups for HEC). EHEC and its further derivatives, like hydrophobically modified EHEC (HM-EHEC) or JR400 Polymer are most frequently used in research and diverse formulations together with polymers in cosmetics and pharmacy.

Among the classes of water-soluble polymers listed above, one can note polymers containing charged groups, like PAA or carboxymethylcellulose, or polymers able to carry charged groups after functionalization, like EHEC and its derivative JR400. They, as mentioned above, are called polyelectrolytes. Polyelectrolytes play an important role among water-soluble polymers; they have many applications and are used technically as flocculation aids, thickeners, dispersants, etc. The charged groups are usually carboxylate or sulphate groups or protonated amines.

It can be distinguished between strong and weak polyelectrolytes. The charge of the strong ones is almost independent on pH. The weak polyelectrolytes carry weakly ionisable groups, and their charge depends strongly on the solution pH.

This work considers the strong cationic polyelectrolyte JR400; its charge is caused by protonated aminogroups.

2.2.2 Adsorption of polymers at solid-liquid interfaces

The adsorption of polymers is used in many technical applications, such as treatment of surfaces, flocculation processes, dispersion of particles, etc [136]. The point of polymer adsorption in these applications is to modify the surface properties. A short description of the basics of polymer adsorption is given in this section.

Polymer adsorption can be driven by different forces. These are similar to interactions driving the adsorption of surfactants discussed above. The most significant generalized reason for polymer adsorption is energetic favourability that originates from the competition of interactions between polymer segments and solvent molecules with one another and among themselves, similar to that described in Section 2.2.1. In case of polymer adsorption at solid-liquid interfaces, one new item, namely the solid surface, participates in this competition. For example, interaction of segments of a cationic polymer with an anionic surface is generally stronger than that between polymer segments with one another or with solvent molecules. Another important contribution is usually made by the affinity between the solvent molecules and polymer segments. If this is poor then the effective polymer-surface interaction can become attractive, "helping" the polymer molecule to minimize the contact with the solvent. It is obvious, therefore, that the polymer adsorption has to increase dramatically with polymer concentration increase. This increase frequently foregoes precipitation.

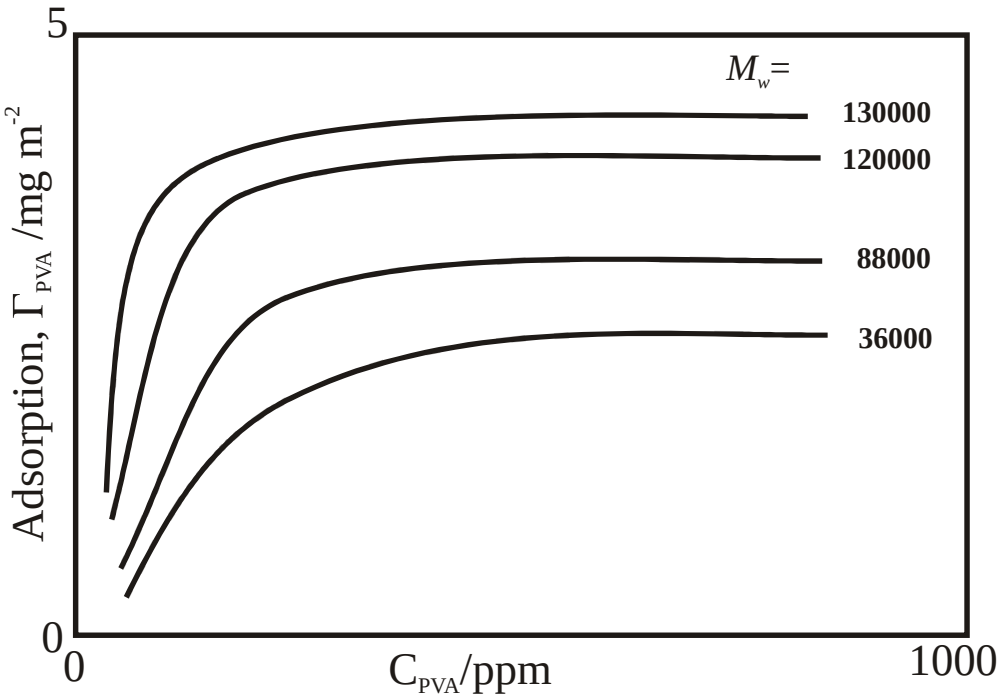

Figure 2.14 –Isotherms of the adsorption of polyvinyl alcohol (PVA) of different molecular weights on a polystyrene surface. Redrawn from [136]

Polymer adsorption at solid surfaces, similar to that of surfactants, is usually measured with help of surface excess measurements. A typical adsorption isotherm shows the steep rise in adsorption at low polymer concentrations and saturation at higher ones where the isotherm reaches its plateau. This kind of adsorption is referred to

as positive adsorption. If a surface shows no net attraction on the polymer segments, so-called negative adsorption commonly referred to as depletion, can occur [93].

Polymers with higher molecular weight adsorb more intensively than low molecular weight species. This is illustrated schematically in Figure 2.14. This figure shows at the same time typical forms of the adsorption isotherm. This molecular weight dependence can vary for different polymers and surfaces. The most significant here is whether the polymer chain adsorbs with its end to the surface or lies flat on it. In reality, most polymer systems tend to adsorb in coiled or random conformation, so that the adsorbed amount is proportional to M^{α}, where α is a constant varying in the range 0.3 – 0.5. The dependence of polymer adsorption on the conformation of the polymer molecule is logically bound, in turn, with the fact that adsorption depends strongly on the solvent properties, as mentioned above. Polymer chains adsorbed at a solid surface are usually presented as in Figure 2.15, to have a "tail-loop-train" conformation. Tails are non-adsorbed chain ends, segment length in direct contact with the surface are called trains, and loops are "free" segments between the trains, that is, segments that are not in contact with the surface. To understand many properties of adsorbed polymer layers, the total segment concentration profile as a function of the distance from the surface, is commonly used [94].

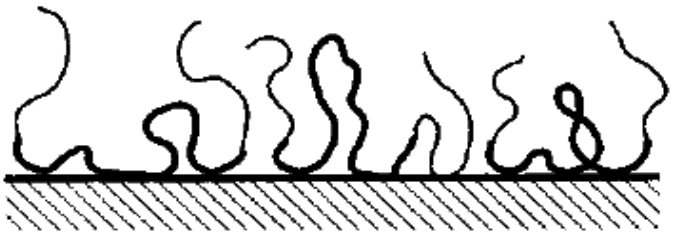

Figure 2.15 – Schematic illustration of the adsorption of polymer chains at solid-liquid interfaces. Reproduced from [83]

A logical consequence of the adsorption dependence on the molecular weight is that, from mixed systems, polymers with higher molecular weight adsorb preferentially at the expense of the low molecular weight species [136].

For polyelectrolytes, the adsorption is predominantly influenced by the electrostatic interactions between the polymer and the surface, but non-electrostatic effects can also play an important role. For electrostatic interactions, the adsorption exerts a strong

dependence on the pH value. The second important factor influencing the adsorption is the concentration of added salt. As the pH factor varies, the surface and the polyelectrolyte can acquire the charges of the same sign or opposite charges. For both of these cases, the adsorption driving forces and mechanisms, as well as the role of the added electrolyte, are different. They can be explained in terms of thermodynamics [136].

In the first case, i.e., when the polymer and the surface have the same charge, the driving force of adsorption stems from attractive van der Waals interactions between the polymer chain and the surface. Here, the addition of salt can increase the adsorption. A possible explanation for this effect is that in the salt-free solution the local counterions concentration will increase during adsorption process since they are needed to maintain electrical neutrality. This local increase lowers the adsorption entropy, thus increasing the system free energy. Upon addition of salt, this effect caused by the "own" counterions of the polyelectrolyte, is diminished due to the increasing salt concentration in the whole solution volume, not only close to the surface. The second explanation suggests a shielding of the repulsive forces between the polymer and the surface by the added salt, therefore causing a higher adsorption of the polymer. Divalent cations demonstrate more shielding efficiency [105].

The second case, where the polymer and the surface have opposite charges, the driving force of the adsorption is not as obvious as it could seem at first sight. Indeed, the first factor driving the adsorption in this system is the electrostatic attraction between the polyelectrolyte and the surface. There exists, however, one more reason that makes the polyelectrolyte adsorption to the opposite charged surface practically irreversible: this is the presence of counterions: while adsorption proceeds, counterions are released from both the polymer and the surface into the bulk solution. This increases the entropy of the system, which brings the system into a lower free energy state. Therefore, the addition of salt in this case will decrease the adsorption of the polyelectrolyte, since the energetic effect of the released counterions will be less when compared to a salt-free system. In addition, the added salt will shield the attractive electrostatic forces between the polymer and the substrate and also compete with the polymer for the adsorption sites at the solid surface.

Polyelectrolytes can modify the behaviour of charged colloids when added to the system. The interactions between two surfaces bearing the same charge that is, in turn, opposite to the charge of the polyelectrolyte get dramatically changed upon

polyelectrolyte addition: polyelectrolytes adsorb to the surfaces of the particles and can, depending on the amount added, change their normally repulsive interaction pattern to the attractive one. The factor playing an important role here is so-called bridging, i.e., connection of the surfaces at short separation distances by the polymer chains adsorbed on the both surfaces. The flexibility of the polymer chains is here crucial, since it allows connection of two surfaces if the molecule is adsorbed to both of them. This phenomenon is referred to as bridging and is of importance in practical applications, like e.g. flocculation.

The adsorption of practically all polymer classes at the solid surfaces can be considered as irreversible at normal circumstances; this can be also explained with the help of considerations concerning the slow dynamics in polymer systems as well as length and flexibility of the polymer chains: in order to desorb a polymer molecule from the surface, all its segments have to desorb simultaneously. This is less probable, especially for the polymers with high degree of polymerisation. This property can be used for modification of the surface properties, e.g. hydrophilization of the surface. If any factors influencing adsorption are introduced into the system, for example surfactants, the adsorption at solid surfaces can become energetically unfavourable, and thus the polymer can desorb. A special attention will be devoted to this process in the section considering interactions between polymers and surfactants.

The method for determining the polymer adsorption and creating adsorption isotherms described at the beginning of this section belongs to indirect methods where the adsorbed amount can be calculated from the equilibrium bulk concentration of the polymer. Any technique that can measure solution concentration can be used here, like e.g. spectroscopic methods. Direct methods, in contrary, can determine the amount of the polymer in contact with the surface. The techniques such as neutron and optical reflectometry, ellipsometry, surface plasmon resonance can be used for these measurements.

To determine the structure of an adsorbed polymer layer, various types of microscopy techniques have been used. These include Scanning Electron Microscopy (SEM) and Transmission Electron Microscopy (TEM), and since 1994 [107, 108] Scanning Probe Microscopy techniques such as STM and AFM. More detailed discussion of the application of these methods is provided in the Section 3.3.

AFM investigations of the adsorbed layer structure have been performed on proteins [108] and polyacrilic acid [109] at graphite and mica, respectively. They have shown

the adsorption proceeding from nucleation sides to a homogeneous coverage. The roughness of the adsorbed layer changed in cycles indicating the attachment of subsequent polymer layers, while the layer “stickiness” increased gradually.

The Surface Forces Apparatus (SFA) has been extensively used for the study of the forces between polymer-coated surfaces [110-113, 16]. These invesitgations much contributed to the understanding of the “bridging” process described above in this section.

2.2.3 JR 400 Polymer

The cationic polymer JR400 is a chloride salt of the N,N,N-trimethylammonium derivative of hydroxyethylcellulose (**CA Index Name:** Cellulose, 2-hydroxyethyl 2-[2-hydroxy-3-(trimethylammonio)propoxy]ethyl 2-hydroxy-3-(trimethylammonio)propyl ether, chloride) of molecular weight around 500000. The structure of a monomer unit bearing the trimethylammonium group is represented in Figure 2.16.

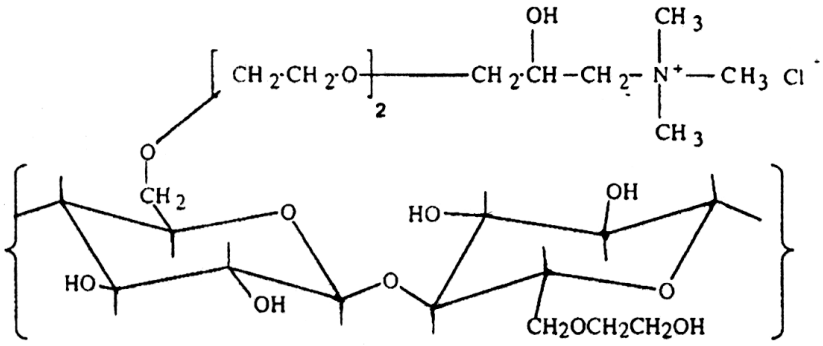

Figure 2.16 – The structure of a functionalized monomer unit of the JR400 Polymer. Reproduced from [10]

The substance is also known under different names such as Amerchol JR 400; Catinal LC 100; Celquat SC 230M; JR 125; JR 30M; Leogard P; LR 300M; LR 400; Polyquaternium 10; Quaternium 19; UCARE Polymer JR. This wide variety of identifiers illustrates the variability of the polymer structure and some properties and the

fact that the polymer is used by a plenty of research organisations and industrial companies.

The polymer finds extensive application in health and body care, in first line, as an emulsion stabilizer [125, 14]. The JR400 Polymer was first reported in 1974 [121]. The first publication series in 1975 by Goddard described the most interesting properties of the polymer, its importance in body care applications, and its interactions with surfactants [126, 127]. These features will be discussed in the next section.

There is some inconsistency in the literature data concerning charge density and mean chain length of the polymer. According to Chronakis and Alexandridis [10], an aqueous solution of 1 wt % polymer bears a charge concentration of 10 mM and a mean contour length between charges of about 20 Å. This result suggests an average relative molecular weight of 1000 per charge. On the other hand, Goddard [8] uses the value of 670 per charge, a value that is confirmed by an electrophoretic mobility study. These data can obviously vary depending on the substitution grade of the polymer. This is, according to different sources, between 3 and 20 %, i.e., 3 to 20 of every 100 monomer units of hydroxyethylcellulose bear a trimethylammonium group [8, 128]. The wide variety of the identifiers mentioned above is an indirect confirmation of this.

In the present paper, the average polymer molecular weight of 670 per charge is presumed. In accordance with this assumption, we use the ratio 1/2.3 w/w between the JR400 Polymer and SDS, as an estimation of the stoichiometrical equality between the polymer and the surfactant charges.

2.3 POLYMER-SURFACTANT INTERACTIONS

When considering previously described application areas of surfactants, on the one hand, and polymers, on the other hand, we find out that these areas “intersect” in many branches. Both polymers and surfactants occur in such diverse products as paints, foods, detergents, cosmetics, formulations of drugs and pesticides. Since they occur together in the same formulation, the question arises, whether they interact with one another and if yes, then which influence does this interaction have on the formulation.

In this section a review of polymer-surfactant systems both in bulk and at interfaces will be presented. Special attention will be given to the interactions of compounds that have been used in this work.

2.3.1 General aspects of polymer-surfactant interactions in solution

Usually, polymers and surfactants are employed to achieve different effects – emulsification, flocculation, colloidal stability, rheology control and other – but in some cases a synergistic effect of polymers and surfactants is expected, that is, an effect caused by their interaction.

Nowadays, a wide consensus exists that polymer-surfactant interactions in the bulk are the result of a fine balance between hydrophobic, hydrophilic and electrostatic interactions [3, 4].

The particular pattern of interaction between a polymer and a surfactant in aqueous solution is generally determined by the following factors: sign and value of the charge of every component, hydrophobicity or hydrophility of the polymer molecule or its parts, substitution grade for a functionalized polymer, length and rigidity of both polymer backbone and the carbohydrate chain (hydrophobic tail) of the surfactant. The first and probably the most important issue is here the relation between charges beared by the surfactant and the polymer. Possible cases of polymer-surfactant systems are presented in the Table 2.2. In this Chapter they will be referred to as they are denoted in this table.

Table 2.2 – The types of possible combinations of polymers and surfactants in solutions.

Polymer / Surfactant	Cationic	Anionic	Neutral
Cationic	S^+P^+	S^+P^-	S^+P^0
Anionic	S^-P^+	S^-P^-	S^-P^0
Neutral	S^0P^+	S^0P^-	S^0P^0

As mentioned above, this is the electrostatic interaction that plays generally the most important role in the polymer-surfactant system. Same charge systems will not therefore be discussed in details. The combinations highlighted in the Table 2.2 (ionic surfactant

– non-ionic polymer and systems with oppositely charged components) are now the most well studied ones and find the broadest application. The SDS and JR400 Polymer build a $S^{-}P^{+}$ system that is highlighted extra.

According to the classification proposed by Lindman and Thalberg [122] for polymer-surfactant interactions in solution, also of importance is the concentration region where the study is performed since different aspects of the polymer-surfactant interaction are studied at different concentrations. High concentrations are useful for studying practical applications, and fundamental studies dealing with interaction mechanisms, adsorption behaviour and possible complexes formation are performed primarily in low concentration ranges. In this work the surfactant-polymer system of the type S-P+ was studied at very low concentrations.

2.3.1.1 How do surfactants and polymers interact?

Generally, water-soluble polymers, as well as solid-liquid interfaces (section 2.1.3.3), induce surfactant aggregation. Micelle-like structures, or clusters, tend to form along the polymer molecule and around it. A long, flexible polymer chain possessing alternating hydrophobic and hydrophilic parts, when placed in a surfactant solution, offers various interaction opportunities for surfactant molecules. On the one hand, hydrophilic groups of non-ionic polymers can interact with ionic headgroups of the surfactant by ion-dipole association, and those of ionic polymers – by electrostatic attraction. On the other hand, hydrophobic parts of the polymer provide an energetically favourable environment for interaction with hydrophobic tails of the surfactant. All these mechanisms result in the association patterns where the electrical charge is screened, and less hydrophobic segments are exposed to water i.e. a state that is energetically favourable.

2.3.1.1.1 Characteristic points

These interactions manifest in changes of colligative properties of a surfactant solution. If the polymer is added to surfactant solution, it modifies these properties so that abrupt changes of them which are usually characteristic for the critical micellar

concentration (section 2.1.2) occur at sufficiently lower concentrations. The changes in the surface tension are most illustrative; they are depicted in Figure 2.17.

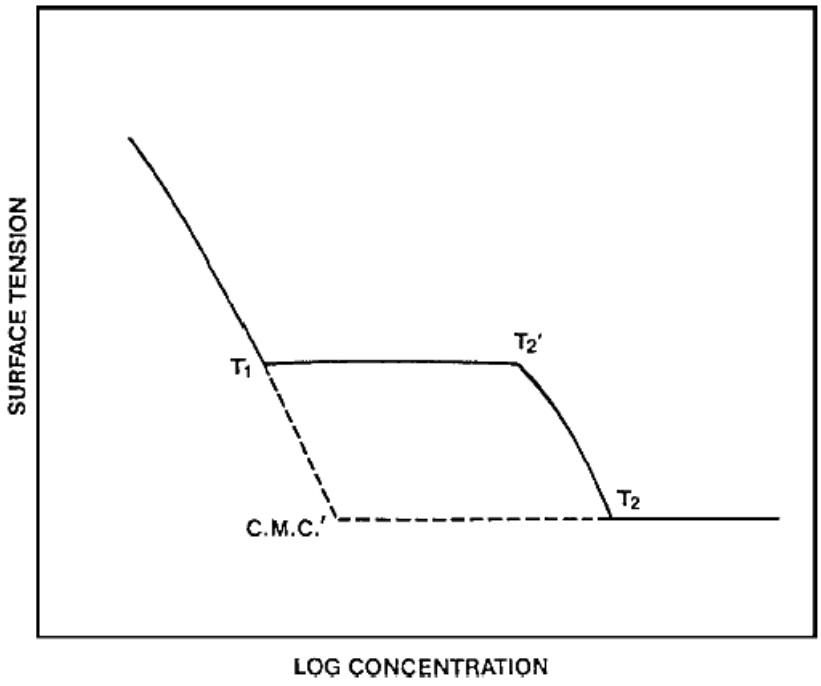

Figure 2.17 – Idealized surface tension / log concentration plot of a surfactant in the presence of a complexing polymer. Reproduced from [123]. The solid line represents the surface tension in presence of the polymer, the dotted line – in absence of the polymer. $\mathbf{T_1}$ is the critical aggregation concentration (CAC); $\mathbf{T_2'}$ – concentration of saturation of the polymer molecule with the surfactant; $\mathbf{T_2}$ – "total saturation concentration"; **C.M.C.'** (CMC') – the critical micellar concentration of the same surfactant without polymer addition.

The critical aggregation (or association) concentration (CAC) often referred to as $\mathbf{T_1}$ is the concentration of the onset of surfactant binding to the polymer molecule. This can be detected also by other techniques such as binding isotherms, conductivity measurements or fluorescence quenching. The exact value of the CAC shows some dependence on the technique used. The processes taking place in solution while the surfactant concentration increases are schematically illustrated in Figure 2.18.

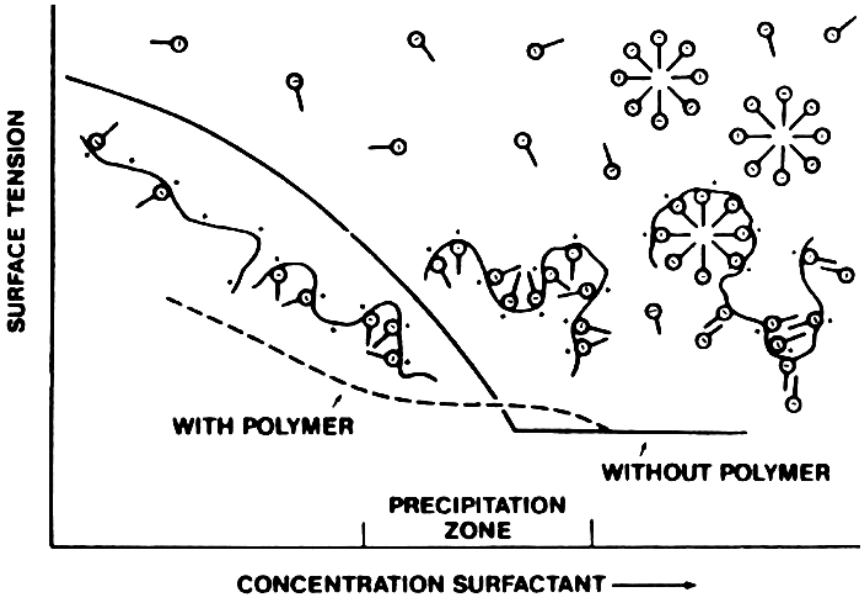

Figure 2.18. – Schematic illustration of an interaction process between a polymer and a surfactant in bulk solution. Sizes of polymer and surfactant molecules are not drawn in scale. The precipitation zone denoted concerns in the first line the interactions between oppositely charged polymers and surfactants. Reproduced from [17].

We see that the CAC should be understood as the surfactant concentration (at given polymer concentration) where a complex between the surfactant and the polymer starts to form, independent of whether the single surfactant molecules or surfactant aggregates first interact with the polymer. At further increase of the surfactant concentration, the "new" surfactant molecule associate favourably with the polymer until the $\mathbf{T_2'}$ is reached – the concentration at which the polymer molecule becomes saturated with the surfactant. It is sometimes denoted as the polymer saturation point (PSP). The mechanisms of this association are discussed in the next section. As the surfactant concentration still increases, the $\mathbf{T_2}$ – "total saturation concentration" is reached. It is easy to see from the Figure 2.17 that this equals the log sum of the difference ($\mathbf{T_2'} - \mathbf{T_1}$) and the **CMC'** – the critical micellar concentration of the same surfactant without polymer addition. The $\mathbf{T_2}$ can be also understood as the "real" or "classical" CMC of the surfactant at the given concentration of the added polymer. The CAC / CMC points are only weakly dependent on the concentration of the added polymer and essentially independent on polymer molecular weight down to very low values [136].

$\mathbf{T_2}$ > **CMC'** – this could be misunderstood as if polymer *rises* the CMC of the surfactant. Nevertheless, the characteristic changes of the colligative properties occur

already at the CAC that is lower than **CMC'** for all kinds of surfactant-polymer systems. Therefore, it is true that the polymer addition effectively "*lowers*" the surfactant CMC. This lowering is indicative of the strength of the interaction between the surfactant. It can be less than one order of magnitude for S^-P^0 or S^+P^0 systems and reaches even several orders of magnitude for S^-P^+ and S^+P^- systems. For example, the system containing SDS and non-ionic polymer polyvinylpyrrolidone (PVP) has the CAC of ~ 2.6 mM, that is, ca. 3 times lower than the CMC of SDS [116]. This relation is nearly constant for the PVP concentrations up to 0,5 wt.%. In contrary, for the JR400 – SDS system (of the kind S^-P^+) studied in this work, Goddard and Hannan [8] found out that already on addition of JR400 Polymer in concentration of only 0,01 wt.%, the CAC of SDS equals ~ 0,1 mM, which is more than 80 times lower than the CMC of SDS. This is illustrative for the stronger binding as a result of the electrostatic attraction between the opposite charges.

2.3.1.1.2 Degree of binding (β)

Another important parameter characterizing polymer-surfactant association is the degree of binding. This can be calculated from binding measurements using techniques like ion-selective electrodes and equilibrium dialysis at low polymer concentrations. The degree of binding is equivalent to the moles of bound surfactant per mole of polymer repeating unit or ionic group, that is, the binding sites of the polymer. When the binding between a surfactant, *S*, and a polymer binding site, *P*, is represented by the equilibrium expression:

$$S + P \overset{K}{\leftrightarrow} PS$$

where *K* is the binding constant, then the degree of binding β for identical and independent binding sites can be expressed in the Langmuir form as:

$$\beta = \frac{KC_s}{1 + KC_s}$$

where C_s is the molar concentration of free surfactant.

2.3.1.2 Interaction models

Since early research, several models have been proposed to describe the interactions between polymers and surfactants. First, a site-binding process was assumed to be the only mechanism of interaction. More recent experimental work revealed a certain level of cooperativity in the binding. That is, the first bound surfactant molecule facilitates the binding of the second, they both aid the binding of the third, and so on.

Depending on the nature of the interacting surfactant-polymer pair, two different kinds of description are in discussion. In cases where either one of the components (in practice it is only the polymer molecule) is non-ionic (S^+P^0 and S^-P^0 systems), the hydrophobic interactions play a leading role. In this case the hydrophobic tails of surfactant molecules are attracted to the hydrophobic polymer backbone. Some early studies [17] suggested a uniform distribution pattern of surfactant molecules along the polymer chain in such systems. This model assumes a formation of a molecular "bottlebrush" consisting of surfactant molecules assembled around the polymer backbone. The ionic headgroups of the aggregated surfactant molecules are, according to this model, directed into the solution. Recent simulations [7] partially supported this model. Figure 2.19 represents schematically the results of one of these simulations including the both typical conformations.

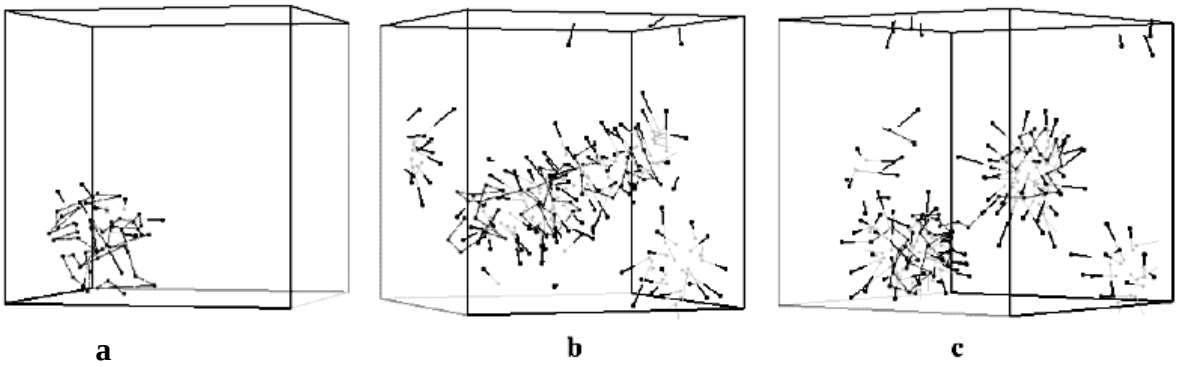

Figure 2.19 – Conformations of polymer-surfactant complexes (mesoscopic simulation with 50 monomer units) with 10 surfactant molecules present (a) and with 100 surfactant molecules present, for which two typical conformations are shown (b, c) Reproduced from [7]

Nevertheless, at the same time this simulation suggested that surfactant molecules "prefer" assembling not only to "bottlebrush" configuration but also to spherical aggregates similar to micelles in the polymer-free solution (Figure 2.19, c).

This trend is the alternative interaction model that has now a great amount of experimental confirmations and is usually called the pearl-necklace model [5- 7]. This involves micelle-like clusters of surfactant assembled on the polymer backbone like beads on a string. The major driving force is here the stabilisation of the interface between the hydrophobic core of the micelles and water. The model is schematically illustrated in Figure 2.20.

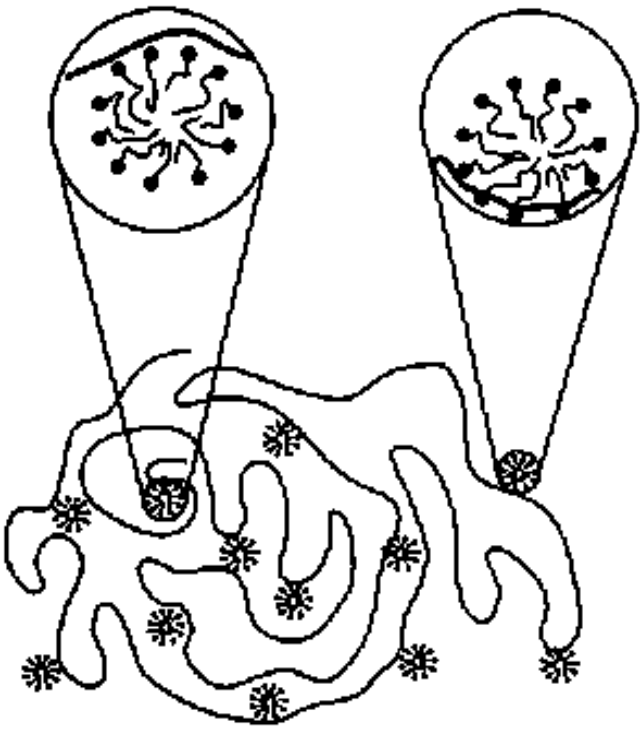

Figure 2.20 – Schematic representation of the pearl-necklace model for polymer-surfactant complexes. Reproduced from [136]

This model seems now to be proved, and well established. It can be explained that after the binding of the surfactant molecule to the binding site on the surfactant, this bound surfactant molecule becomes a centre for forming of a micelle-like cluster. It is to mention that the binding site can be of various nature: a charged group of a polyelectrolyte or a hydrophobic site on the polymer backbone or the side group. We see here exactly that polymer-induced surfactant aggregation that was pointed to at the beginning of this section.

2.3.2 Interactions between ionic polymers and surfactants bearing opposite charges

The interactions in polymer-surfactant systems with oppositely charged components are described here and in the next section, in the first line, in relation to the polymer-surfactant system used in this work, i.e. the system consisting of SDS and JR400 Polymer. Probably the greatest contribution to investigation of this system was made by the group of E.D. Goddard [e.g., 8, 11-14, 17, 123]. From 117 references (excluding patents) in Chemical Abstracts which concern this system, 41 articles, reviews and other publications are written by Goddard.

In the case of ionic polymer and surfactant bearing opposite charges the electrostatic attraction evidently plays the leading role in the interaction. Here, it is the charged head of the surfactant molecule that binds to the charged sites on the polymer molecule. The role of hydrophobic and other forces is noticeable at surfactant rich compositions and in some specific cases like polycomponent systems or behaviour at interfaces [118].

A specific phenomenon characterizing the interactions in the system consisting of oppositely charged polyelectrolyte and surfactant is the formation of insoluble precipitate, which was described in 1970s by Goddard *et al.*, and later by Yamaguchi *et al*., and Shubin for the SDS – JR400 system [8, 9, 11-16] and also by different authors for other systems, including those of S^+P^- type, like polyvinylsulphate/CTAB [130, 131].

The precipitation occurs when a stoichiometrical equality between charges in the mixture is reached, and the polyelectrolyte charge is neutralized. The strength of the electrostatic interaction between the two components causes the precipitation well below the surfactant CMC. When the stoichiometrical ratio between the components is not close to equality, the solution is clear. In a generalized and simplified form this phenomenon is illustrated in Figure 2.21.

Generally, the interaction between the JR400 Polymer and SDS in water solution can be described as follows. At a constant polymer concentration (the horizontal dotted line in Figure 2.21), a subsequent addition of surfactant leads to viscosity changes: Either a rapid increase at higher polymer concentrations (1 wt% and more) or a slight decrease at lower concentrations. The reason for this behaviour variation is explained downwards. This is followed by an increase in turbidity of the solution that ends in precipitate formation and then, upon further surfactant addition, resolubilisation. This

pattern is explained by Goddard [8, 17] in terms of two stages of SDS adsorption on the polymer molecule: the first stage involves mostly electrostatic interactions, where SDS adsorbs to the sites of positive charge on the polymer, the anionic heads of the surfactant molecule being directed to the polymer. As a result, a hydrophobic "layer" consisting of surfactant alkyl tails forms around the polymer molecule at the point of stoichiometrical equilibrium between surfactant and positive charges. This stage corresponds to the conditions of maximum precipitation of the mixture. A further increase of the surfactant concentration leads to the formation of the second "layer" of the surfactant molecules, where surfactant alkyl tails are directed towards the polymer backbone. Since the polar heads of the surfactant are now facing into the solution, the resolubilisation occurs. Hydrophobic attraction is responsible for adsorption during this stage.

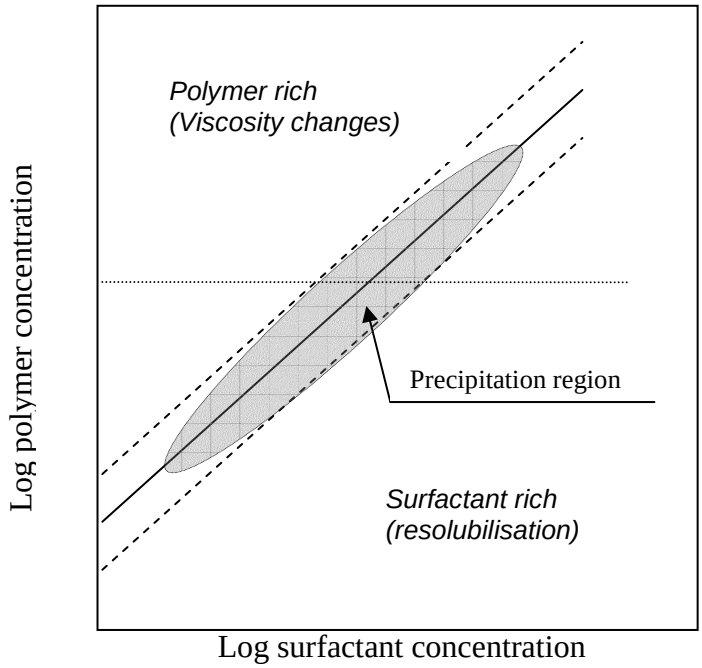

Figure 2.21 – Simplified solubility diagram of the polymer-surfactant system with opposite charges. Notation of viscosity changes concerns the SDS – JR400 system.

As mentioned above, the polymer-surfactant complexes formed at the precipitation concentration are nowadays considered not as a plain layer (bottlebrush pattern) but as micelle-like clusters attached to the polymer backbone. This can illustrate the viscosity changes mentioned above. These changes are now considered to be caused by hydrophobic attraction between polyalkyl tails of bound surfactant molecules. At higher polymer concentrations intermolecular tail-to-tail associations play the leading role, i.e.,

the associations between surfactant bound to the different polymer chains. This causes formation of networks and a sharp viscosity increase. If the polymer concentration is lower, the probability of tail-to-tail associations between the surfactants bound to the same polymer chain is of significance, that is, intramolecular association, and therefore, less interactions between different polymer chains take place than in the surfactant-free solution.. This is schematically illustrated in Figure 2.22.

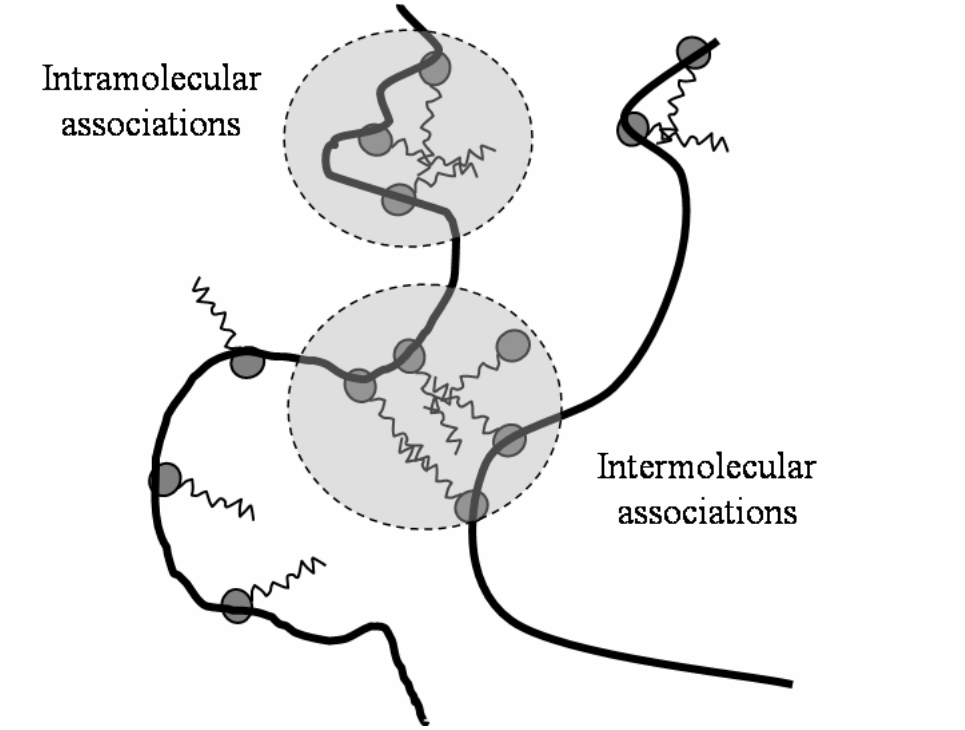

Figure 2.22 – Schematic illustration of intermolecular and intramolecular associations between hydrophobic tails of bound surfactant molecules.

This viscosity pattern has been observed especially for the JR400 Polymer. Other polycations did not reveal such viscosity behaviour. The most probable reason for this is that JR400 is characterized by low flexibility of the polymer backbone, whereas, e.g. acryl amide / β-methacryloxyethyltrimethylammonium chloride copolymer (Reten) has much more flexible polymer chain and thus does not reveal such viscosity changes [90].

2.3.3 Adsorption of polymer-surfactant mixtures of opposite charge at solid-liquid interfaces – cooperative adsorption

The adsorption of polymer-surfactant mixtures at solid surfaces is of significance for their practical application in nearly all branches mentioned before. There exist several reviews in this area [17, 136, 129, 134]. Special attention has been given to applied systems such as personal care and cosmetics, pharmaceuticals, ink chemistry and paints. Previous works point also to the importance of the properties of every component of the polymer-surfactant system, surface properties and solution conditions like pH and electrolyte concentration. Like with polymers and surfactants themselves, all these conditions and properties affect the adsorption behaviour of the mixtures as well.

An important general observation is that the adsorption properties of a polymer-surfactant mixture can differ greatly from those of any of components in absence of another: surfactant and polymer modify the adsorption behaviour of one another. Generally, surfactant-polymer pairs which do not interact in solution, like S^+P^+ or S^-P^-, usually compete for adsorption sites on the surface. They are outside the topic of this work.

Polymer-surfactant systems that do interact in solution like S^+P^0 or S^-P^+, show various adsorption properties if one or both of the components has a strong affinity to the surface. Of special interest are here the systems consisting of oppositely charged polyelectrolyte and surfactant. In contrary to the investigations in the bulk, comparatively little work has been done to study the adsorption of these mixtures at solid-liquid interfaces, especially that of the oppositely charged polymer-surfactant systems. A brief review with some examples is presented here, with an emphasis on the SDS – JR400 system.

Moudgil and Somasundaran studied the adsorption of a cationic polyacrylamide and dodecanesulfonate onto hematite and quartz [126]. They reported differing results, depending on the order of addition and pH. Generally, the presence of the polymer before the surfactant was of more significance than otherwise. For example, the presence of CTAC only weakly affected the adsorption of an anionic polyacrylamide onto hematite [127].

SDS and JR400 Polymer at liquid-air and liquid-solid interfaces has been intensively studied in recent years, sometimes as a part of more extensive investigations concerning interactions between polymers and surfactants at interfaces and including components

bearing different, the same or no charges. The main methods used were radioactive labeling, ellipsometry, surface force measurements, and fluorescence microscopy. These researches are detailed in the following paragraphs.

Arnold and Breuer [18] studied SDS adsorption on alumina surfaces in the presence of JR400 polymer using adsorption measurements with ^{14}C labelling and electrophoresis measurements. Their results suggested that the strong interactions between polymer and surfactant in solution significantly affected the adsorption. Depending on the composition of the mixture, synergistic effects favored or inhibited adsorption. It is interesting to note that in the recent literature this study seems to be the only one where surfactant and polymer bearing opposite charges were mixed prior to adsorption. In all other studies, surfactant was added to the polymer previously adsorbed on the surface. The adsorption from mixtures is extensively studied mostly after AFM entered into wide research practice. This work is detailed below.

Agrillier et al. [19] and Shubin [16] used surface force techniques and showed that the polymers JR400 and LM200 (hydrophobically modified JR400) readily adsorb at negatively charged surfaces and that this adsorption is affected by the concentration of the SDS present in solution: SDS forms a complex with the adsorbed polymer layer. At lower concentrations, the thickening of the adsorbed layer could be detected, and at concentrations higher than the CMC of SDS, the surfactant causes desorption of the complex from the surface. Since this polymer-surfactant system finds widespread applications in health care and cosmetics, Goddard [14] studied the polymer adsorption on hair surface (keratin, bearing a negative charge) and its interaction with SDS using fluorescence microscopy of the fluoresceine-labelled JR400 polymer. It was again found that SDS at low and moderate concentrations entered the adsorbed polymer layer and affected its thickness positively but at concentrations above the CMC the SDS could cause a partial polymer desorption from the surface.

Both on keratin and on silica surface, ***cationic*** surfactants Triton X-400 and CTAB caused rapid and, in some cases, full desorption of the polymers JR 125, JR 400 and JR 30M (products with different MW, in order of increase) [95, 97]. Preadsorbed surfactant prevented here adsorption of the polymer. This is interesting as an example of partially similar phenomena with different mechanisms: introduction of both kinds of surfactants can cause desorption of the polymer, but in the case of the surfactant of the same charge we observe a competition between polymer and surfactant for the binding sites, whereas the processes taking place when the oppositely charged surfactant is added can be

explained in terms of a “competition” between negatively charged surface and negatively charged surfactant for the polycations.

2.3.4 Use of scanning probe microscopy for the study of adsorption at solid-liquid interfaces

The method of scanning probe microscopy (SPM/AFM) is described in details in the Chapter 3.2. It allows a wide variety of possibilities to investigate the surface before, during and after adsorption of any substance on it. One of the great advantages of the method is that the surface can be visualized directly: the adsorbed particles and their sizes can be seen. The properties of the adsorbed layer, such as viscosity, hydration and rigidity, can be investigated as well. The surface forces can be measured in the selected area with high precision. However, the data concerning the layer thickness are not absolute since the spring constant of the cantilever and the feedback parameters of the AFM software “stand” between the really acquired data and the computed mechanical properties of the adsorbed layer. The details are presented in the section devoted to the method description.

In the last 10 years [20, 21] this method and related techniques have been used to study the adsorption of polymer-surfactant systems on solid surfaces [20, 22, 29, 48-50]. Because AFM studies of colloid systems are a rather sophisticated task, significant work was devoted to the development of the technique [21, 23]. A wide range of methods including contact mode, tapping mode [24, 25] and single-molecule force spectroscopy [26] were applied. A so-called soft-contact AFM imaging technique [21, 27] developed by Senden, Biggs *et al*. proved to be the most powerful tool for the investigation of the adsorption of polymer-surfactant mixtures at solid-liquid interfaces. The systems studied with AFM and related metods, like surface forces apparatus (SFA) were of various compositions, including S^+P^+ [50], S^-P^+ [29, 48, 49] and S^-P^0 [28, 31].

Works published in recent years [27-31] deal also with polymers and surfactants mixed prior to the exposure of the surface and adsorption. For example, Dedinate *et al*. [29] compared the adsorption of mixtures of a highly charged cationic polyelectrolyte, poly{(propionyloxy)ethyl}trimethylammonium chloride (PCMA), and SDS using atomic force microscopy, surface force apparatus for experiments on mica and small-

angle neutron scattering for investigations in bulk. The results, as well as the results of some previous studies [48-50], suggest that the adsorption of established polymer-surfactant complexes from the mixture differs significantly from the adsorption of pure polymer followed by surfactant addition. For example, the adsorbed amount is about 7 times less in the former case; the adsorbed layer is more heterogeneous by adsorption from mixtures; the addition of the surfactant to preadsorbed polymer layer causes a sufficient and nearly irreversible swelling f the layer.

An important general observation made during the direct investigations of adsorption of polymer-surfactant systems at solid-liquid interfaces is that the equilibrium establishment in these systems is extremely slow: The appearance and the properties of the adsorbed layer can change even after several days of equilibration. One main reason why equilibrium is reached so slowly is that the polyelectrolyte is bound to the surface by many segments, each of which has a high affinity for the surface. Hence, the mobility of the chain on the surface will be low and likewise the desorption will be slow.

It is important to mention that most studies were performed at relatively high surfactant concentrations, from 1 × CMC [29] up to 5 × CMC [48]. There is not enough information about the adsorption behaviour of polymers-surfactants systems at high dilutions.

2.4 SOLID/LIQUID INTERFACES AND THEIR INFLUENCE ON COLLOID SOLUTIONS

This section will give a brief description of general questions concerning the nature of interfaces, main definitions; forces acting at the interfaces, their properties that are of importance. The surfaces used in this work, together with their structure and properties, are also described in this section.

2.4.1 Interfaces, general aspects

An interface is the boundary region dividing two immiscible phases. There exist liquid-liquid, liquid-gas, solid-gas, solid-solid and solid-liquid interfaces. The properties of substances close to an interface can in many instances differ from those in the bulk of the corresponding phase. On the other hand, materials at interface can greatly affect the bulk physical properties of a system. In colloidal systems like emulsions, foams and solid dispersions this influence is especially important and apparent.

Adsorption is an increase in concentration of solute in the region of the solid-liquid interface, compared to the bulk of the phase. Contrary to *ab*sorption, the solute (or adsorbate) does not permeate the bulk of the substance to which it adsorbs (adsorbent). There exists also negative adsorption (a decrease in the solute concentration close to interface compared to the bulk concentration) called depletion. Whether adsorption or depletion occurs, depends on the net adsorption energy, which is the difference between the free energy of solute/surface, solute/solvent and solvent/surface contacts.

2.4.1.1 Surface charge and hydrophobicity, theories of interactions at solid-liquid interfaces

The most important properties of solid-liquid interfaces that are of significance for this work are discussed in Section 2.1.3. These are surface charge and surface hydrophobicity. The electrical charge carried by many solid surfaces in an aqueous solution can be explained by the high dielectric constant of water, and thus by very common surface dissociation, or by adsorption of a charged species. The charged surface and the counterions balancing the net charge are known as the electrical double layer, for which exists a detailed theoretical description. A hydrophobic surface can be distinguished from the hydrophilic one by the contact angle, θ, of a water droplet on the surface. Hydrophilic surfaces are referred to as “high energy” surfaces and hydrophobic – as “low energy” ones.

In general, the interactions at solid-liquid interfaces and forces important for these interactions are described by the DLVO theory, named after its authors Derjaguin and Landau and Verwey and Overbeek, who independently developed this quantitative theory in 1940s [57, 58]. The DLVO theory considers the electrostatic repulsion and

van der Waals attraction to be the main forces defining the distance between particles in colloidal solution, H; or the distance between a particle and the surface. Since this theory does not describe all surface interactions completely, it has to be supplemented by so-called non-DLVO forces, which include *solvation* forces (for aqueous solutions referred to as *hydration* forces), *oscillatory* or *structural* forces caused by the oscillations of the solvent molecules successions between two solid surfaces separated only by a thin layer of liquid, repulsive *steric* forces due to the loopings of adsorbed polymer extending into the liquid phase. Of special importance are long-range attractive *hydrophobic* forces.

2.4.2 Types of surfaces (used in this work)

In various types of investigations presented in this work, we used two main surfaces: mica and silica wafers. In some experiments the surfaces were used either "as is", i.e. freshly cleaved mica and industrially supplied silica wafer. In other cases, a hydrophobization of surfaces was performed with a sililation process; their properties, therefore, were changed. As a result, the adsorption and desorption processes presented in this work, took place at four different types of surfaces. These are briefly overviewed in the following table.

Table 2.4. – Properties of surfaces used in this work

Surface	"as is"	sililated
Mica	Strongly negatively charged, hydrophilic	Strongly negatively charged, moderately hydrophobic
Silica	Moderately negatively charged, hydrophilic	Moderately negatively charged, strongly hydrophobic

The detailed description of the structure and properties of the surfaces used in this work is given in the following sections of this chapter. The hydrophobization process is described in the section 3.1.2.

2.4.2.1 Mica

Mica is a layered aluminosilicate mineral. Its general molecular formula is

$R_1R_{2\text{-}3}\,[AlSi_3O_{10}](OH, F)_2$. Here R_1 = K, Na; R_2 = Al, Mg, Fe, Li

The main element of the mica crystalline structure consists of three-layer „packages“, each of them includes two tetrahedral layers of $[AlSi_3O_{10}]$. Between these, there is an octahedral layer consisting of R_2 cations. Two of six oxygen atoms in the octahedrons are replaced by the hydroxyl groups (OH) or by fluorine. The K^+ or Na^+ ions with the co-ordination number of 12 bind the „packages“ to a continuous structure. According to the number of the octahedral cations in the formula, one can distinguish between dioctahedral and trioctahedral mica variations: The Al^+ cations occupy two of three octahedrons, and one remains empty, whereas Mg^{2+}, Fe^{2+} cations, as well as Li^+ with Al^+ occupy all the octahedrons. The crystallization of mica occurs in a single-wedge (pseudo-trigonal) system. The relative location of the hexagonal surface cells of the packages is caused by their turns at angles divisible by 60^o around the c axis, together with a shift along the a and b axes of the elementary cell. This defines the occurrence of different modifications (polytypes) of mica that can be distinguished with X-ray spectroscopy. According to the chemical structure variations, it can be distinguished among aluminum and lithium mica types, magnesial-iron, vanadium and chrome mica types.

To the aluminum mica types belongs muscovite used in this work. The chemical formula of muscovite is $KAl_2[AlSi_3O_{10}](OH)_2$, the layer structure of muscovite is seen with a naked eye, and cleavage to very thin plates is possible. The structure of muscovite layer packages is schematically illustrated in Figure 2.23.

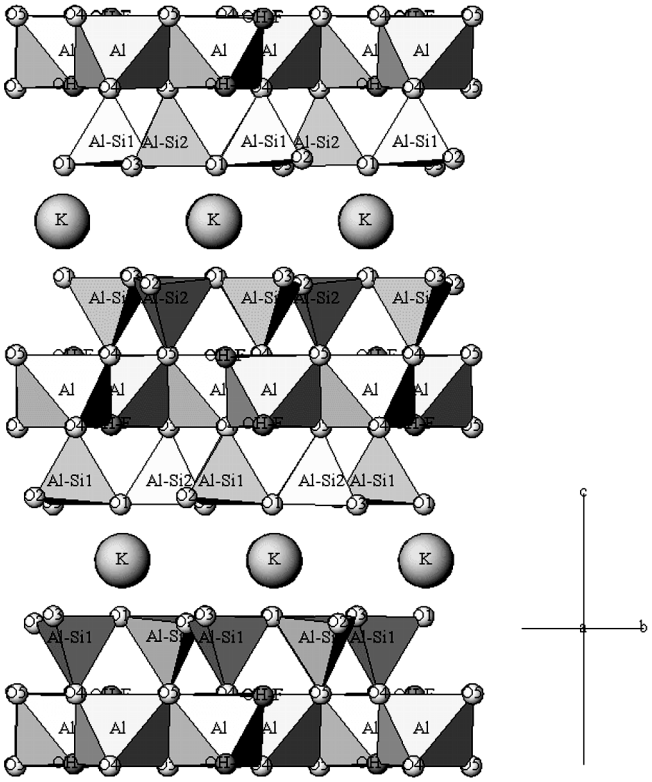

Figure 2.23 – Schematic illustration of the structure of muscovite layer packages. Reproduced from [http://unit.aist.go.jp/greenlife/ii/STRUCIMAGES/Muscovite.gif]

Each layer is strongly negatively charged, about $2.1*10^{14}$ lattice charges/cm^2. The negative charge of the mica lattice stems from the fact that a quarter of the tetravalent Si atoms are substituted by trivalent Al atoms. In the crystal these charges are compensated by mainly K^+ ions. If the mica surface is immersed in an aqueous medium at almost all pH values except strongly acidic, K^+ ions leave the lattice. The charge values mentioned here concern the mica surface itself, i.e., the mica surface immersed in water represents a water-solid interface bearing a strong negative charge.

2.4.2.2 Silica

Silica, the most abundant mineral in earth's crust, can be crystalline (quartz) or amorphous (some kinds of glass). The general chemical formula of silica is SiO_2. The bulk structure of silica consists of siloxane units: tetrahedral lattice where every silicon

atom is bound to for oxygen atoms, and every oxygen atom – to two silicon atoms. Silanol groups –Si–OH constitute the surface of silica. These groups can be hydrated or anhydrous. Hydrogen atoms of anhydrous silanol groups are bound to the oxygen atoms of the neighbour groups with hydrogen bonds. If hydrogen bonds bind water molecules to the silanol groups, such groups are called hydrated. Therefore, the silica surface is hydrophilic under usual circumstances. The surface can be hydrophobized with different methods including polymer deposition by adsorption, spin-coating with non-ionic surfactants [98] or covalent binding of substances carrying non-polar functional groups [32, 33]. The hydrophobization process used in this work is described in the section 3.1.2.

When brought into contact with an aqueous solution, silica acquires a surface electric charge. The charge is mainly generated due to the dissociation of the silanol groups. Depending on the concentration of the potential determining ions, pH, ionic strength and temperature, the sign and magnitude of the charge can vary:

$$–Si–OH + H^+ \leftrightarrow –Si^+ + H_2O \text{ or } –Si–OH_2^+ \qquad \text{(positively charged surface)}$$

$$–Si–OH + OH^- \leftrightarrow –Si–O^- + H_2O \qquad \text{(negatively charged surface)}$$

Since the silanol groups are acidic in nature, silica is generally negatively charged at neutral pH. The isoelectric point of silica is about pH 2 to 3 [96].

CHAPTER 3. EXPERIMENTAL METHODS AND MATERIALS

AFM and DLS have been used to investigate the structure of polymer-surfactant mixtures in the bulk and at solid-liquid interfaces. To visualize the adsorbed structures, “soft-contact” AFM imaging was used. This was complemented by the acquirement of force-distance curves and “scratching”. To compare the sizes of structures of the adsorbed layer with those in bulk, DLS measurements were performed.

The first section of this chapter will describe materials used in this work and details their preparation. The second section will detail the methods of investigations in the bulk solution: the establishment of the ternary phase diagram and the DLS measurements. The final section is devoted to the main method of research: a detailed description of the basics of AFM, and specific techniques used in the investigations will be presented.

3.1 MATERIALS AND PREPARATIVE PROCEDURES

This section will give a description of the substances used in this work and details of their preparation for the experiments. First, the chemicals and dilution/mixture procedures will be presented. The surface types used in this work have been described in the Section 2.4.3. Therefore, mostly the details of surface preparation techniques used in this work will be explained, with a special attention paid to the plasma treatment of surfaces and devices used for this treatment.

3.1.1 Water, Chemicals and Solutions

The purity of all components of the investigated solutions and mixtures, as well as that of surfaces and vessels, is crucial for the relevance of the results of our studies, since any contamination can distort the results by its own participation in the

interactions. Especially at low concentrations of polymer and surfactant, any additional substance even at minimal amount may cause changes in the mixture structure and thus lead to wrong conclusions. Therefore, a special attention was paid to keep the purity of water, chemicals and their mixtures at high level and to avoid their contamination with any external substances.

All water used in this study was deionized water. For the dilution of chemicals and rinsing the fluid cell, only water purified with a passage through a Milli-Q-Plus (Millipore) system of ion exchange and activated carbon cartridges was used. The specific conductivity of water did not exceed 5.6 µS/m. While performing dilutions and measurements, precautions were taken to prevent any water contamination from the laboratory air. No water was kept for use more than 72 hours.

All glassware was soaked for at least 2 hours either in 10 wt% NaOH or in the mixture of KOH and isopropanol, then rinsed with deionized water (minimally 10 times) and finally rinsed with Millipore water. For drying of the glassware and surfaces a specially purified nitrogen flow was used.

Sodium dodecyl sulphate (SDS) from Merck and from ICN was used without further purification. The purity grade of SDS from both manufacturers is >99% a. After first preliminary experiments, it was decided to perform no further special activities to eliminate possible impurities present in the substance delivered from the manufacturer. On the one hand, both recristallisation from ethanol and purifying according to Lunkenheimer [135] seem to have influence on the surfactant properties when studies on liquid-air interfaces are performed. On the other hand, the mentioned preliminary results had shown no difference in the polymer-surfactant interaction pattern, when compared to the literature data [8, 10, 16] where additional purification of SDS was performed.

An aqueous SDS stock solution of 1 wt% concentration was prepared at room temperature and stored at $4^{o}C$ before further dilution and use.

JR 400 Polymer was obtained from Dow Chemicals. A stock solution (preconcentrate) of 1 wt% concentration was prepared at room temperature and then filtered to remove insoluble residues, and then it was diluted to the desirable concentration.

Trimethylchlorosilane from Fluka (> 90% purity) was used without further purification. Trimethylchlorosilane is highly volatile and extremely flammable,

especially at contact with water or with water vapour. All manipulations with this substance were performed only in hood and under exclusion of any contact with water.

3.1.1.1 Samples preparation

All concentrations are expressed in weight %, for the sake of simplicity. As mentioned above in section 2.2.3, the following approximations were used for all concentration calculations: the average molecule weight per charge of JR 400 Polymer was assumed to be 670, the stoichiometric ratio 1:1 between surfactant molecules and polymer charge units (the ratio at the point of electrostatic neutralization) was presumed to be achieved at the weight relation 1/2.3 between w/w solutions of polymer and surfactant, respectively. These assumptions are based on the data of Goddard [8].

All mixtures were made from mixtures and dilutions of a 0.075 wt% solution of JR 400 Polymer and a 0.1 wt% solution of SDS corresponding to ≈ 0.4 of the cmc of the surfactant (later on called “working solutions”). These very high dilutions were needed to avoid the high viscosity that occurs at polymer prevalence at higher concentrations and, on the other hand, to have sufficiently large regions of the ternary phase diagramme exhibiting clear solutions. To avoid precipitation during the mixing process, the mixtures were prepared in the following order: The quantitatively prevalent component (polymer or surfactant) was added, then water and then the minor component (surfactant or polymer, respectively). At compositions for which precipitation could not be excluded the mixtures were stirred while adding the components. All samples were produced at room temperature. Generally, the samples were shaken for about 20 seconds after composition and left at least 10 hours for equilibration. When kept in closed vessels at room temperature, all samples proved to be stable and remain unchanged in their properties during at least 4 weeks.

3.1.2 Surfaces and their preparation

3.1.2.1 Mica (Muscovite)

The 10 * 10 mm² muscovite wafers were cut from natural mica sheets. After this, a cleavage using a sharp preparation needle tip was performed. The freshly cleaved wafers underwent plasma treating as described below. During the whole preparation process, a contact with any foreign objects (tools, fingers, glassware, etc.) was strictly avoided. During pauses and between subsequent preparation procedures the wafers were kept in closed glass vessels to avoid any dust contamination.

3.1.2.2 Silica

Commercially available silica wafers were cut into 10 * 10 mm² pieces and cleaned with Carbon Dioxide snow [34], followed by rinsing with redistilled ethyl alcohol and dried under a stream of clean nitrogen gas. As a rule, the cleaned wafers were set at the AFM scanner immediately after cleaning.

3.1.2.3 Plasma treating – cleaning and hydrophobizing.

The surfaces and AFM cantilevers have been treated in plasma reactor at conditions and times usual for the device. The facilities of the reactor have been used also for making the surfaces hydrophobic.

3.1.2.3.1 Plasma reactor

A plasma reactor custom built in the Department of Applied Mathematics of the Research School of Physical Sciences and Engineering, Canberra, Australia, was used.

This instrument is used to routinely produce clean high-energy surfaces such as silicon wafers, silica, Force Microscopy tips, etc. The sample is placed in a partial vacuum, around 0.1 Torr, composed of argon and water vapour, or air. A high voltage, ~1kV at ~120 kHz, RF signal is capacitively coupled (“electrodelessly”) through a ring

electrode on the exterior of the pyrex cylinder into the low pressure interior by grounding all internal metal (stainless steel) components. The intensity of the treatment is tunable by altering the pressure, composition of the gases and transmitted power. The high voltage generator is the HG-2 model from MKS, ENI® Products Rochester, New York. The layout of the system is presented in Figure 3.1.

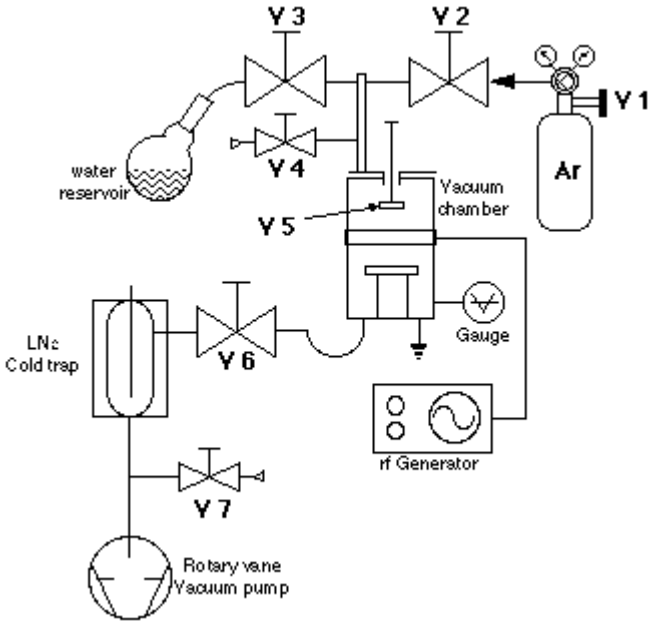

Figure 3.1 – system layout of the plasma treating system.
V1 - 1° & 2° regulator for Oxygen
V2 - fine metering valve
V3 - fine metering valve
V4 - ball valve
V5 - ball valve (Teflon ball)
V6 - Neoprene diaphragm valve
V7 - Neoprene diaphragm valve
V8 - vacuum release valve

In operation the cleaning process continues typically < 1min at 10-20 Watts. For Force Microscopy cantilevers 30 sec at 10 W is sufficient, longer times than one minute may cause damage to the gold coating. The plasma itself is at room temperature, although at plasma powers >50 Watts appreciable sample heating can occur. The actual mechanism of cleaning is predominantly by kinetic activation, although some ionization will occur. As a result, the surface becomes densely hydroxylated, perfect for silanation reactions. Any adventitious carbon is oxidised to volatile species which easily leave the surface. From Force Microscopy there does not appear to be any increase in surface roughness as moderate powers. This has been checked on muscovite mica in the Department of Applied Mathematics.

The advantage of this electrode system is that the risk of contamination from the electrode material is much reduced. The device has a vacuum transference chamber for post cleaning reaction with reactive vapours, such as silanes. The chamber was specifically made from stainless steel and not aluminium alloy because of the ease of sputtering in the latter.

The plunger mechanism allows the user to lower a sample cover assembly under vacuum for clean transferral. The valve in the assembly then allows silanes or other reactive gases to pass over the freshly reacted sample, without exposure to ambient atmosphere. Only stainless steel and pyrex are in contact with the plasma. A scheme of the device is illustrated in Figure 3.2.

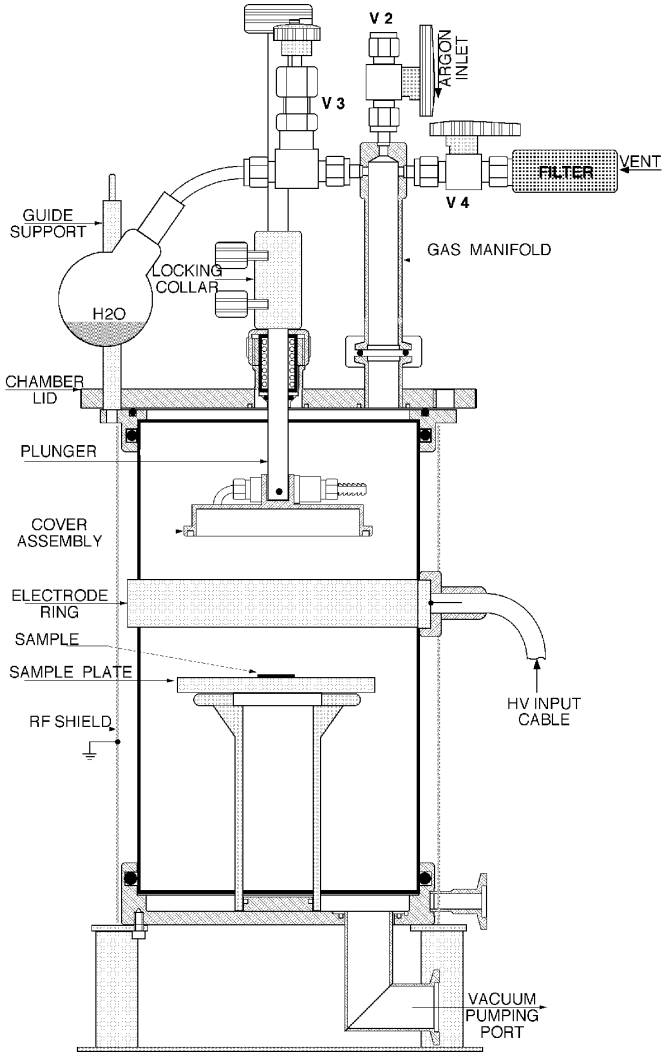

Figure 3.2 – Scheme of the plasma reactor used for preparation of surfaces and cantilevers. Reproduced from http://wwwrsphysse.anu.edu.au/appmaths/plasma.html with great thanks to Mr. Anthony Hyde.

3.1.2.3.2 Hydrophobizing of surfaces

Silicon surfaces were made hydrophobic by coating with a monolayer of trimethylchlorosilane according to the method of Hair [32, 33]. Silicon wafers (10 x 10 mm^2) were cleaned with Carbon Dioxide snow [34], followed by rinsing with redistilled ethyl alcohol and dried under a stream of clean nitrogen gas. Additionally, the wafers were plasma treated as the mica surfaces except that on completion of plasma treatment the samples were stored under vacuum in a transference chamber. This chamber was subsequently connected to a glass vessel containing trimethylchlorosilane (TMCS). Upon opening a valve the TMCS vapour entered the chamber and reacted with the prepared silica surface. The reaction equation [33] was:

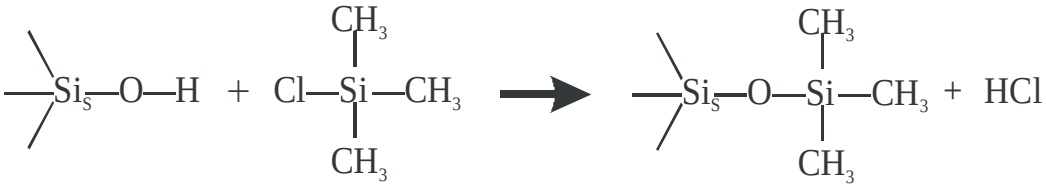

The same procedures have been performed over mica wafers. After exposure to water-vapour plasma, the mica surface becomes reactive to silanation with chlorosilanes in the gas phase. [99].

The degree of surface modification was checked by assessing the inner contact angle of a sessile water droplet. It was 60 – 75° for silica and about 30° for mica. It is important to mention that the contact angle was only assessed with the naked eye, and not measured with the contact angle meter. Due to this, the values given above refer only to the inner contact angle seen with the naked eye.

3.2 INVESTIGATIONS IN THE BULK SOLUTION

3.2.1 Phase diagram establishment

To obtain a general picture of the interaction pattern between SDS and JR400 in bulk solution, a ternary phase diagram was established. The working solutions were

mixed with one another and with pure water at various ratios so that more then 100 different samples could be investigated. The numbers of these samples are used as identification later on. The procedure of the phase diagram establishment was as follows.

All samples underwent a simple visual turbidity test. Evidence of precipitation or turbidity was first checked with the naked eye under back illumination (light shining through the sample). The samples without precipitate or evident turbidity were checked under side lighting and compared with pure water. Clear solutions were attributed to the areas of the diagram indicating pre-precipitation or resolubilisation, depending on the composition of the particular sample. The border of the precipitation area was defined by the compositions where turbidity could only be determined under side lighting. The raster step of composition changes was 10 % at initial screening; at the border of turbidity/precipitation the step decreased subsequently down to 1% of composition variation to achieve the highest precision possible with laboratory devices used. The total number of prepared and evaluated samples was about 110.

3.2.2 Dynamic light scattering measurements

This method is also known as photon correlation spectroscopy (PCS), quasi-elastic light scattering (QELS) or low angle laser light scattering (LALLS). It allows measurement of hydrodynamic radius of particles of various kinds dispersed in solution.

3.2.2.1 Method basics

Particles dispersed in solution can scatter incident light, if the refractive index of the substance differs from that of water. This is true also for colloid solutions and, therefore, for polymer-surfactant mixtures. The theoretical descriptions of light scattering process differ depending on whether the particle size is small or not compared to the wavelength of the incident light, but for the DLS method it is only important that in both cases the light is scattered. i.e., the incident light beam (or, more correctly, photon) changes its direction after interaction with the particle. This scattered light can be registered aside from the initial light direction.

Another feature significant for the DLS method is that the disperse particles or macromolecules suspended in a liquid medium undergo Brownian motion which causes the fluctuations of the local concentration of the particles, resulting in local inhomogeneities of the refractive index. This in turn results in fluctuations of intensity of the scattered light. The speed of the Brownian motion is characteristic, since it depends on the hydrodynamic radius of the particles, or more deeply, on the diffusion coefficient of the particles *D*, with which the mean radius can be obtained from the Stokes-Einstein equation:

$$R = k_B T / 6\pi\eta D$$

where k_B is the Boltzmann constant, T the temperature, and η the shear viscosity of the solvent.

The speed can be measured by collecting data from scattered light from a sample maintained at a precise temperature. The intensity of the scattered light is registered during a pre-defined interval so that a time raw is created. From the raw an autocorrelation function G(τ) is created, often called correlogram. It shows the decay of the correlation between subsequent patterns of the scattered light registered by the detector. This sequence is illustrated schematically in Figure 3.3.

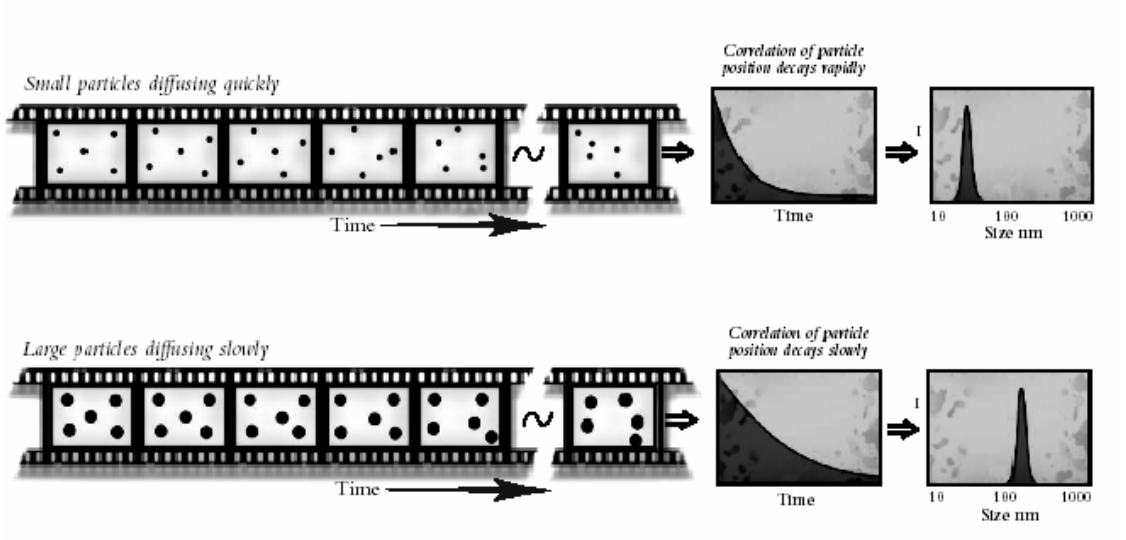

Figure 3.3 – Principles of detection of particle diffusion. Reproduced from Zetasizer family brochure by Malvern Instruments Ltd.. U.K.

The diffusion coefficient of the particles *D* is inversely proportional to the decay time of light scattering fluctuations. Since the hydrodynamic radius *R* is, in turn,

inversely proportional to the diffusion coefficient, we see that the steeper the autocorrelation function (less decay time) then the smaller the particles and vice versa.

3.2.2.2 Instrumentation principles

The calculations and explanations in the previous section are only relevant under the assumption that we deal with the simplest case of spherical monodisperse non-interacting particles in a dust-free fluid. There are some more assumptions that have to be mentioned here.

Older instruments and some existing instruments rely only on the Fraunhofer approximation which assumes:

- The particle is much larger than the wavelength of light employed (ISO13320 defines this as being greater than 40λ i.e. 25μm when a He-Ne laser is used).
- Particles of different sizes scatter with equal efficiencies.
- The particle is opaque and transmits no light.

These assumptions are never correct for many materials and for small material they can give rise to errors approaching 30% especially when the relative refractive index of the material and medium is close to unity. When the particle size approaches the wavelength of light the scattering becomes a complex function with maxima and minima present. The latest instruments (e.g. Mastersizer 2000, Malvern Instruments) use the full Mie theory which completely solves the equations for interaction of light with matter. This allows accurate results over a large size range (0.02 -2000μm typically). The Mie theory assumes the volume of the particle as opposed to Fraunhofer which is a projected area prediction. The "penalty" for this complete accuracy is that the refractive indices for the material and medium need to be known and the absorption part of the refractive index known or guessed.

The instrument used in this work consists generally of:

A laser as a source of coherent intense light of fixed wavelength. He-Ne gas lasers λ=633 nm are the most common as they offer the best stability (especially with respect to temperature) and better signal to noise than the higher wavelength laser diodes.

A suitable detector. Usually this is a slice of photosensitive silicon with a number of discrete detectors. It can be shown that there is an optimum number of detectors (16-32)

– increased numbers do not mean increased resolution. For the photon correlation spectroscopy technique (PCS) used in the range 1nm – 1μm approximately, the intensity of light scattered is so low that a photomultiplier tube, together with a signal correlator is needed to make sense of the information. The registration of the scattered light intensity proceeds at the angle of 90^{o}.

Some means of positioning the sample in the laser beam. Particles in suspension can be measured by recirculating the sample in front of the laser beam. Generally, for suspensions or emulsions, a glass or plastic cuvette is used.

3.2.2.3 Data acquisition and processing

DLS measurements were performed on the Zetasizer 3000 device from Malvern Instruments Ltd, UK, at a wavelength of 633 nm in 1 cm plastic cuvettes. The standard device measurement protocol including sample thermostating at 25°C was followed and the monomodal analysis mode was used. For the light scattering measurements, the samples without evident turbidity or precipitation, including the borderline samples, were selected. Depending on the composition of the mixture, the original device filters “200” or “400” were used. All data acquisitions were repeated 10 to 30 times in order to collect sufficient statistics. All samples were left for equilibration for at least 24 hours before measurements.

3.3 ATOMIC FORCE MICROSCOPY

The atomic force microscope is one of about two dozen types of scanned-proximity probe microscopes (SPM). All of these microscopes work by measuring a local property - such as height, optical absorption, or magnetism - with a probe or "tip" placed very close to the sample. The small probe-sample separation (on the order of the instrument's resolution) makes it possible to take measurements over a small area. To acquire an image the microscope raster-scans the probe over the sample while measuring the local property in question. The resulting image resembles an image on a television screen in that both consist of many rows or lines of information placed one above the other.

The scanning probe microscopy was introduced in laboratory practice in 1980s, after Gerd Binnig and Heinrich Rohrer were awarded half of the 1986 Nobel Laureate in Physics for their design of the scanning tunneling microscope that they reported in 1982 [100].

This section briefly describes principles and variations of the SPM techniques giving special attention to the specific methods used in this work:

- Atomic force microscopy (AFM)
- Soft-contact AFM for investigation of adsorbed layers of colloids
- AFM instruments used in this work
- Modes and techniques used in this work and their details.

3.3.1 Basics of Scanning Probe Microscopy

Scanning probe microscopy covers several related technologies for imaging and measuring surfaces on a fine scale, down to the level of molecules and groups of atoms.

At the other end of the scale, a scan may cover a distance of over 100 micrometers in the x and y directions and 4 micrometers in the z direction. This is an enormous range. It can truly be said that the development of this technology is a major achievement, for it is having profound effects on many areas of science and engineering.

SPM technologies share the concept of scanning an extremely sharp tip (3-50 nm radius of curvature) across the object surface. The tip is mounted on a flexible cantilever, allowing the tip to follow the surface profile.

When the tip moves in proximity to the investigated object, forces of interaction between the tip and the surface influence the movement of the cantilever. These movements are detected by selective sensors. Various interactions can be studied depending on the mechanics of the probe. The principal scheme of the method is represented in Figure 3.4.

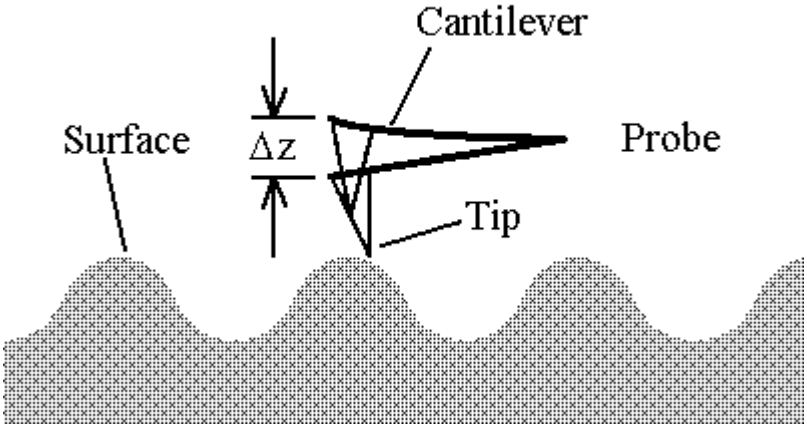

Figure 3.4 – Scanning concept of SPM.
Reproduced from http://www.mobot.org/jwcross/spm/

The interactions between the tip and the surface can be of different kind. According to the properties best corresponding to these interactions, different SPM probe techniques can be used. Some of them are described in the following section, since they are a great part of the methodology or come in use in this work. Other techniques do not concern the topic of this work at all. For the sake of completeness they are listed in the Table 3.1.

Table 3.1 – Other SPM techniques and physical/chemical properties that can be investigated with them.

SPM Technique	Properties
Frictional Force Microscopy (FFM)	Frictional properties
Magnetic Force Microscopy (MFM)	The magnetic field of the surface is imaged
Chemical Force Microscopy (CFM)	Chemical properties (with functionalized tip)
Near-Field Thermal Microscopy (NFTM)	the distribution of thermal conductivity is imaged
Tunnelling Acoustic Microscopy (TAM)	Acoustic properties

3.3.1.1 Probe Techniques

The three most common and significant scanning probe techniques are:

Atomic Force Microscopy (AFM) measures the interaction force between the tip and surface. The tip may be dragged across the surface, or may vibrate as it moves. The interaction force will depend on the nature of the sample, the probe tip and the distance between them. This technique and its different variations have been used in this work.

Scanning Tunnelling Microscopy (STM) measures a weak electrical current flowing between tip and sample as they are held a very distance apart. STM is very significant for electrically conductive materials. As a first approximation, an image of this tunnelling current maps the topography of the sample. More accurately, the tunnelling current corresponds to the electronic density of states at the surface. STMs actually sense the number of filled or unfilled electron states, within an energy range determined by the bias voltage.

Near-Field Scanning Optical Microscopy (NSOM) scans a very small light source very close to the sample. Detection of this light energy forms the image. NSOM can provide resolution below that of the conventional light microscope.

3.3.2 How does an atomic force microscope work

The atomic force microscope (AFM) probes the surface of a sample with a sharp tip, a few microns long and down to less than 10 nm in diameter. The tip is located at the free end of a cantilever that is 100 to 300 μm long. Forces between the tip and the sample surface cause the cantilever to bend, of deflect. A detector measures the cantilever deflection as the tip is scanned over the sample. The measured cantilever deflections allow a computer to generate a three-dimensional map of surface topography. Contrary to STM, AFMs can be used to study insulators and semiconductors as well as electrical conductors.

All AFMs or, more generally, all SPMs consist of the main components presented in Figure 3.5. The principles of detection can be described as follows:

The “heart” of the system is a small, flexible cantilever that bears the sharp probe tip actually sensing the sample.

The general position of the cantilever is defined by a positioning system usually including a small electric motor and a worm transmission.

The sample is fixed on the top of a piezoelectric scanner that bends under the signals of a computer system generally controlling the whole device. Every bending of the scanner means a movement of the sample (or, in rare cases, of the tip).

A laser beam is transmitted to and reflected from the backside of the cantilever for measuring the cantilever position and orientation. The reflected laser beam is detected with a position-sensitive detector (photodiode, PSPD). The output of the PSPD is provided to a computer for processing of the data for providing a topographical image of the surface with high resolution.

Currently used position-sensitive detectors are four-sectional that allows measuring not only longitudinal but torsion bending too, which is important for the lateral force microscopy (LFM).

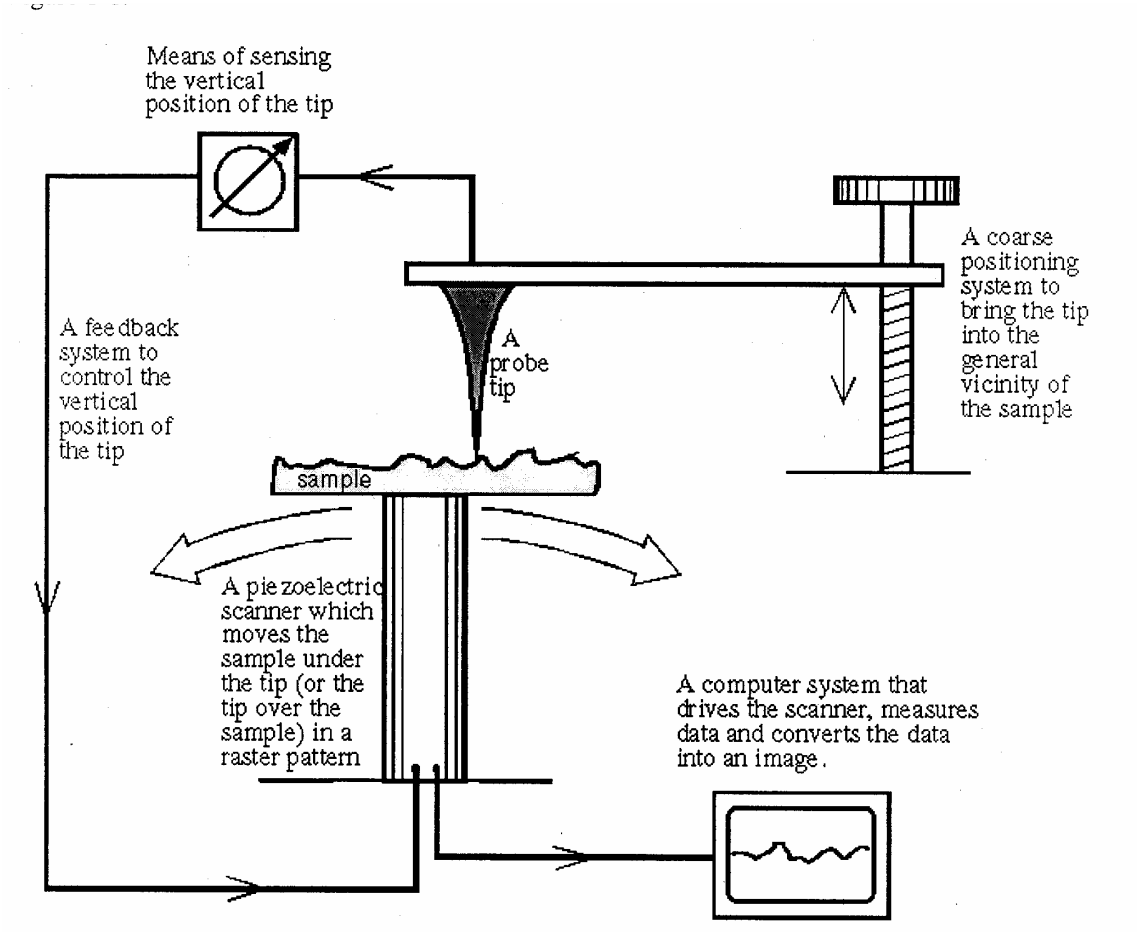

Figure 3.5 – Generalized schematic representation of an AFM. Reproduced from [101]

AFM can operate in several modes which differ according to the force between the tip and surface. They are described in the following section.

3.3.2.1 Method Variations

The application modes of AFM are dependent on the forces acting between the tip and the sample surface. The force most commonly associated with AFM and virtually making the most important contribution to the resulting force is the interatomic van der Waals force. The dependence of the van der Waals force upon the distance between the tip and the sample is illustrated in Figure 3.6.

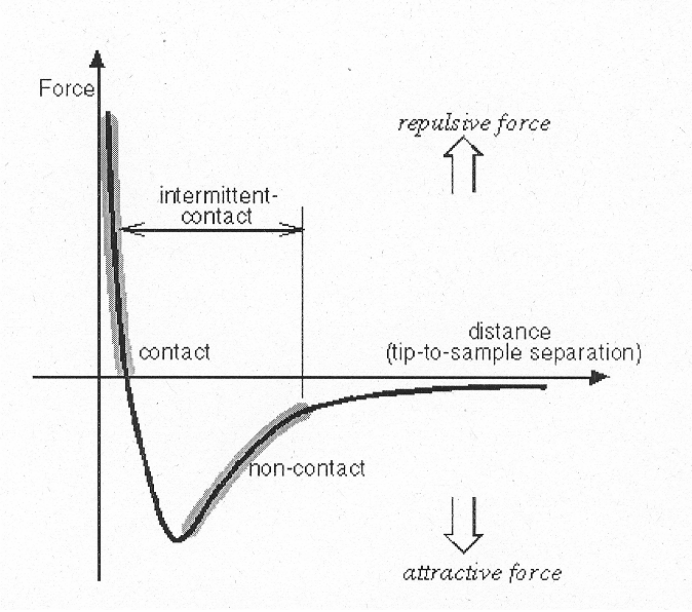

Figure 3.6 – Forces between the tip and the sample and modes of AFM

The most important variations of the AFM with respect to the interaction forces method are presented in the Table 3.2.

Table 3.2 – Operation modes of the atomic force microscopy

Mode of Operation	Force of Interaction
contact mode	strong (repulsive) - constant force or constant distance
non-contact mode	weak (attractive) - vibrating probe
intermittent contact mode	strong (repulsive) - vibrating probe
lateral force mode	frictional forces exert a torque on the scanning cantilever

In contact mode, the tip is usually maintained at a constant force by moving the cantilever up and down as it scans. In non-contact mode or intermittent contact mode (the latter also known as tapping mode^{TM}) the tip is driven up and down by an oscillator.

Especially soft materials may be imaged by a magnetically-driven cantilever (MAC Mode™). In non-contact mode, the bottom-most point of each probe cycle is in the *attractive* region of the force-distance curve. In intermittent contact mode the bottom-most point is in the *repulsive* region. Variations in the measured oscillation amplitude and phase in relation to the driver frequency are indicators of the surface-probe interaction.

To image *frictional force*, the probe is dragged along the surface, resulting in a torque on the cantilever. To image the magnetic field of the surface, a magnetically-susceptible probe is used. In other variations, the electric charge distribution on the surface or the surface capacitance is imaged. For thermal scanning microscopy (TSM) the thermal conductivity of the surface is probed with a resistive tip that acts as a tiny resistance thermometer.

In addition to these modes, many instruments are also designed to plot the phase difference between the measured modes, for example frictional force versus contact profile. This plot is called **phase mode.**

3.3.2.2 Force-distance curves and the soft-contact mode

The atomic force microscope [102] can be used to measure the force between the tip and the sample surface as a function of the distance between them in gas or liquids [103].

The so-called force-distance measurements are suited to characterize the total interaction force of a particle (tip) and a surface in aqueous media. Two examples of graphs characterizing these interactions are illustrated in Figure 3.7.

A cycle of measurements starts at a large tip-sample distance, i.e. without any interaction, so that the cantilever is not deflected. When approaching the sample to the tip, the cantilever deflects in dependence on interaction forces. After tip and sample are in contact, the tip will be retracted. During the whole cycle, the deflection of the cantilever is recorded as a function of sample displacement. The resulting graph can be converted into a force-distance curve, which is independent of the spring constant.

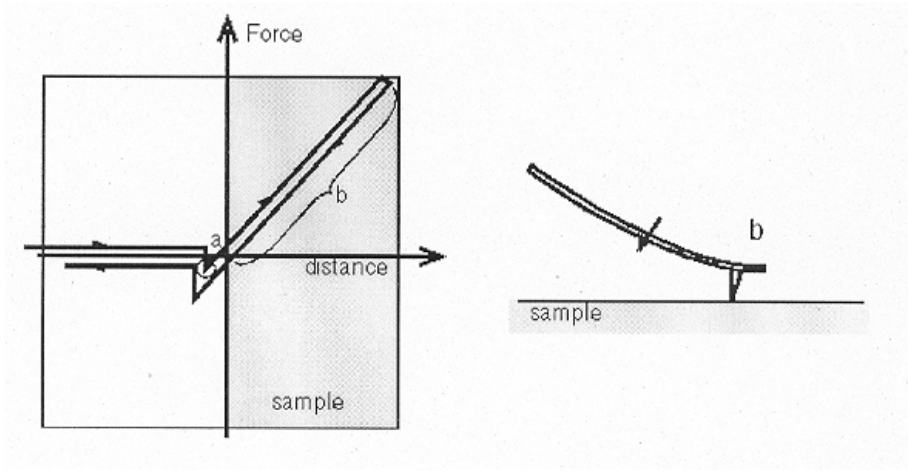

A)

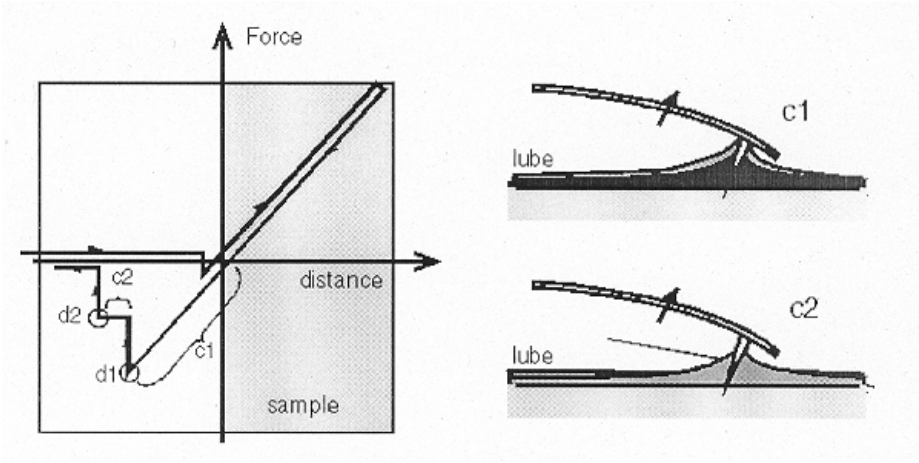

B)

Figure 3.7 – Simplified illustration of force-distance curves at dry sample surface (A) and in case when a liquid layer (or lubricant) is present (B). Arrows on the graph lines indicate the direction of cantilever movement. The ***positive*** direction of the "distance" axis denotes the tip movement ***towards*** the surface. Reproduced from [101].

This AFM feature found extensive application during the last years [21, 46-48]. We will only mention that the force-distance curves bring a lot of information concerning thickness, rigidity, viscosity and other mechanical and adhesive properties of the adsorbed layer.

The variations of AFM can be illustrated by these curves. For example, region **b** in Figure 3.7 (A) is the region of use of contact AFM: the cantilever deflection (or force, according to the Hooke's Law) is directly proportional to the tip-sample separation. Another important feature is that the length of the region c2 shown in the same figure is indicative for the thickness of the liquid layer, or, in our case, for that of the adsorbed layer of polymer-surfactant mixture.

The soft-contact mode by Manne [114] and Senden *et al*. [21, 28] that has been used in this work is a special modification of contact AFM that was developed for soft layers. For adsorbed layers of surfactants and polymers in aqueous solutions, the force-distance curves are a result of interaction (overlap) of two electrical double layers which generates repulsive force. The force gradient then increases as the tip pushes onto the surfactant. The operating force for imaging is set at the steepest part of the force curve, such that during scanning the tip glides across the layer. Changing the interaction force setting allows one to obtain the thickness value of the adsorbed layer.

3.3.2.3 AFM Limitations

An understanding of limits set by any method used is of great significance. AFM, as any other method, is not free from limitations: The properties and types of cantilever and scanner, calibration and feedback parameters, tuning of laser detector – all of these features play an important role when evaluating the relevance of the data acquired. Very often it is difficult, or almost impossible, to distinguish between correct images and artefacts. A short review of possible artefacts and their reasons is given in this section.

The scanner tube of an AFM is a piezoelectric tube made usually of lead zirconium titanate, or PZT. From Figure 3.8 the main principles of scanner operation are seen.

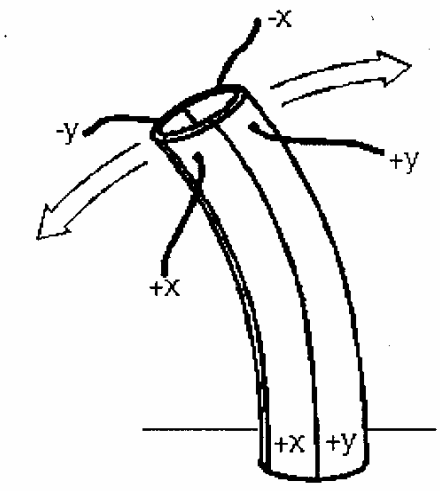

Figure 3.8 – Schematic representation of AFM scanner

It is easy to see that movements in XY plane are, due to the scanner design, not horizontal movements but curves. The data distortion caused by this fact is referred to as cross coupling. Other scanner properties and processes occurring in the scanner are:

intrinsic scanner nonlinearity, hysteresis, creep (two-phase scanner response to strong feedback signals) and scanner aging contribute to nonlinearities in sample imaging [101, 118]. Various means of hardware and software correction, such as optical and capacitive, can be used to eliminate this influence.

Other important sources of artefacts are the tip, the feedback loop and external physical influence. The gains of the feedback loop have to be optimized precisely and maintained during scanning. A non-optimized feedback loop can cause high-frequency oscillations if set too high, or a false flattening of the image if set too low.

The role of form and size of the AFM tip can be critical: a wrongly selected tip can produce images that have almost nothing common with the true structure of the sample surface. There exist a "collection" of tip artefacts. The way how they can emerge is illustrated in Figure 3.9

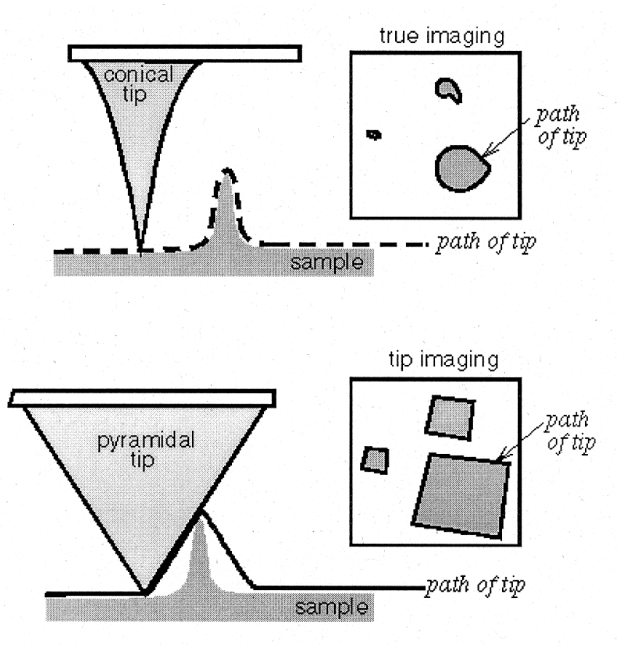

Figure 3.9 – Comparison between true imaging and "tip imaging". The square structures on the bottom image, when presented three-dimensionally, are pyramidal, i.e. they are "tip reflections on the sample surface".

An outside influence can be caused by any external source like strong electromagnetic fields, extreme temperature changes and – most frequently – mechanical vibrations. These can be avoided by a proper positioning of the instrument. The most common way is an instrument suspension on elastic strings, or usage of a very hard and stable pedestal, or a combination of both means.

The ways to prove whether the image is true or an artefact are universal for almost all SPM techniques and include repeat imaging, change of scan direction, scan rotation, scale change and changing of the scan speed [101].

Specifically for investigations of adsorbed layers the AFM technique is good for giving information about the layer structure. Nevertheless, no information about the amount of adsorbed material can be obtained. The results of the layer thickness measurements as well as the force-distance curves are not absolutely precise and will be interpreted mainly qualitatively in this work.

3.3.3 Instrumentation and Operation

The AFM investigations were performed using a Park Scientific Autoprobe CP instrument with the Multitask Head (Institute of Physical and Theoretical Chemistry, University of Regensburg, Regensburg, Germany) and a Digital Instrument Nanoscope MultiMode instrument (Department of Applied Mathematics, Research School of Physical Sciences and Engineering, Australian National University, Canberra, Australia). The devices are represented in Figure 3.10.

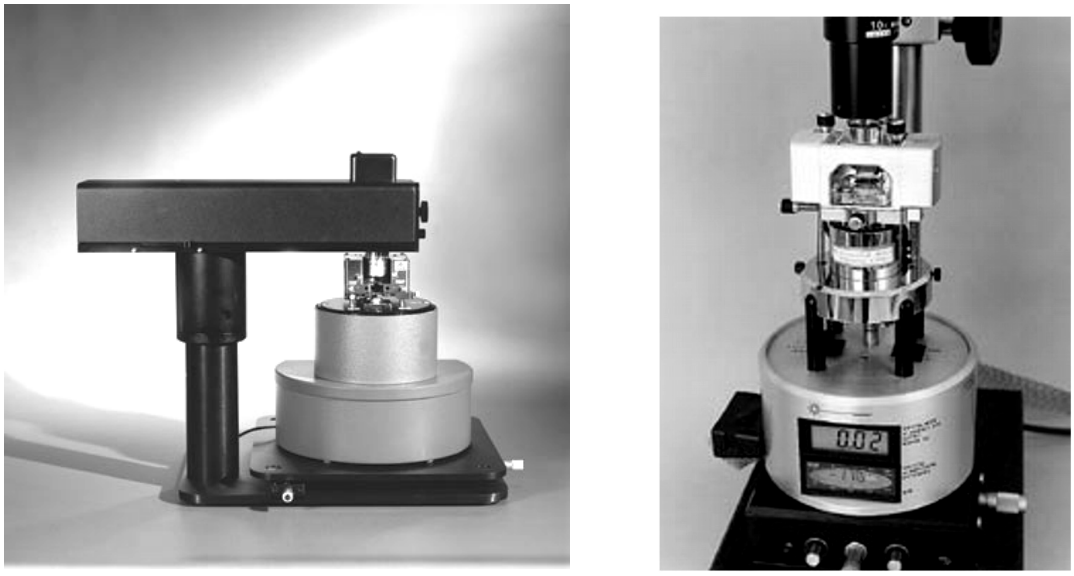

A) B)

Figure 3.10 – AFMs used in this work: A) Autoprobe CP instrument. Illustrated together with the optical microscope and video camera used for control. Reproduced from www.veeco.com. B) DI Nanoscope III instrument. Reproduced from www.eng.yale.edu/environmental/ facilities.html

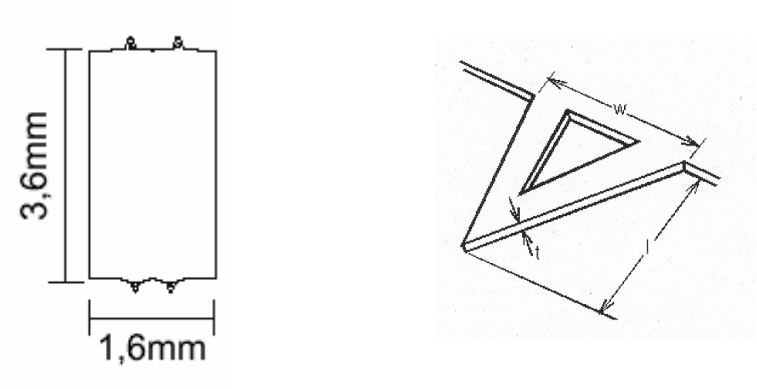

Figure 3.11 – Cantilever chip with 4 cantilevers (left) and standard V-shaped cantilever (right)

The cantilevers from ThermoMicroscopes, Sunnyvale, CA were used on the Autoprobe CP instrument. The length of them was 180 µm and the leg width 25 or 38 µm (C-Ultralevers type A and B, respectively). Nanoscope III instrument used standard silicon nitride V-shaped cantilevers of length 200 µm with a leg width 40 µm (long, fat) (Digital Instruments, Santa Barbara, CA). The tip diameter, according to the manufacturer's data, did not exceed 10 nm, and the spring constant was in all cases below 0.6 $N \cdot m^{-1}$. Cantilever chips and a scheme of a cantilever are presented in Figure 3.11.

New cantilevers have been used for every measurement performed on the Digital Instruments Nanoscope III. Before mounting, the cantilevers underwent plasma treatment identical to the substrate (described above). When working on the Autoprobe CP instrument, each cantilever was used for more than one measurement. Between the measurements, cantilevers mounted on the cartridge, were soaked in a water-isopropyl alcohol mixture, rinsed with deionized water and dried in air. The cantilever integrity and condition was checked before every measurement using a 1µm calibration grating and adjusting feedback software parameters.

A fluid cell constructed and made at the Mechanical Shop of the Faculty of Chemistry and Pharmacy of the University of Regensburg was used during studies on the Park Scientific Autoprobe CP Microscope. Between the measurements, the cell was cleaned using a water-isopropyl alcohol mixture. The standard Contact Mode Fluid Cell was used while working with the Digital Instruments Nanoscope. Cleaning of this cell was performed using Millipore water and redistilled ethyl alcohol followed by drying with a stream of nitrogen gas. The filling of the standard Contact Mode Fluid Cell (Digital Instruments device) was performed by sample injection after mounting the cell

and before cantilever approach. The filling of the custom made fluid cell (Autoprobe CP) was made by adding 2.2 ml of sample into the opened cell before lowering the AFM head.

3.3.3.1 Software

The post-measurement processing of images and curves was performed using ProScan Version 1.6 Image Processing software of Autoprobe CP instrument, NanoScope 4.42 GUI software, and Nanotec WSxM 1.2 software as well as Microcal Origin 4.1 and Microcal Origin 7G software.

3.3.3.2 Imaging

The soft-imaging method of Manne *et al.* and Senden *et al*. [114, 21, 28] was used. The key to this method is fine control of the imaging force in the repulsive regime of the tip-sample interaction, enabling the adsorbed layer to be imaged without damage. Adsorbed aggregates are generally only visible over a narrow range of applied force (<1 nN), with the substrate imaged at higher forces. Generally, the applied force on both instruments can be controlled directly using the operation software of the AFM. In all cases it was below 0.9 nN.

3.3.3.3 "Scratching"

For investigation of the properties of the adsorbed layer of the polymer-surfactant mixtures a special treating of the layer with the cantilever was applied. First, a scan image (typically, 10*10 μm^2 or 5*5 μm^2) of the adsorbed mixture was acquired. Then, a smaller area (typically 1*1 μm^2) in the middle of the field of vision was scanned by pushing the cantilever very hard, at the highest scan rate (60 Hz). After making this, the scanning was repeated at previous settings and on a larger area. This method is downwards called "scratching", since the cantilever may move the layer or its parts aside and expose the substrate surface. The method allows investigation of adhesion pattern of the adsorbed layer or clusters.

3.3.3.4 Acquirement and evaluation of force-distance curves

The force-distance curves were acquired on every sample, with an emphasis to visualize the difference between areas with different structures' pattern. When "scratching" had been applied, some curves were acquired inside and outside the scratched area. This allows making conclusions about the presence or absence of the polymer and the surfactant on the investigated surface, about the rigidity of the layer, its elasticity and hydration. The force-distance curves are presented without any further processing except "shifting" the curves by means of the Origin 7.0 software package in order to reflect precisely the zero lines and zero positions (elimination of feedback distortions).

CHAPTER 4. RESULTS AND DISCUSSION

The results of our investigations are presented in this Chapter. First, the properties of the SDS / JR400 mixtures of different compositions in bulk solution are described: the ternary phase diagram established during the solubility studies is discussed and a description of the selection procedure of mixtures (samples) for further research is given. Then the results of DLS measurements performed on selected samples are represented. The second part of the chapter shows the results of imaging and characterization of adsorbed polymer-surfactant layers at solid-liquid interfaces with the help of AFM. This part is divided into two sections: the first compares the structure of adsorbed layers at different surfaces and the properties of the corresponding samples in bulk solution. The second section deals with the results of the AFM measurements: the results of two series of "washing-off" experiments are presented consisting of subsequent altering of the polymer-surfactant mixture composition with simultaneous monitoring the properties of the adsorbed layer.

4.1 SDS / JR 400 MIXTURE IN SOLUTION

4.1.1 The ternary phase diagram

The ternary phase diagram was established according to the procedure described in Section 3.2.1. It delivered the general basic picture of interaction between working solutions of both substances and allowed the selection of specific compositions for further investigation.

4.1.1.1 General Description

The ternary phase diagram presented in Figure 4.1 reflects the interactions of the polymer and the surfactant at different compositions. Following regions of the diagram were highlighted and are denoted in Figure 4.1: region 1 exhibits clear solutions with

lower viscosities than that of the pure polymer (see Section 2.3.2). Region 2 indicates the presence of a turbid or precipitated mixture corresponding to phase separation. Region 3 exhibits clear solutions due to resolubilisation and a highly diluted mixture is present in Region 4. Qualitatively, the region of phase separation is in agreement with the literature[11]. Some quantitative differences will be explained in the following sections.

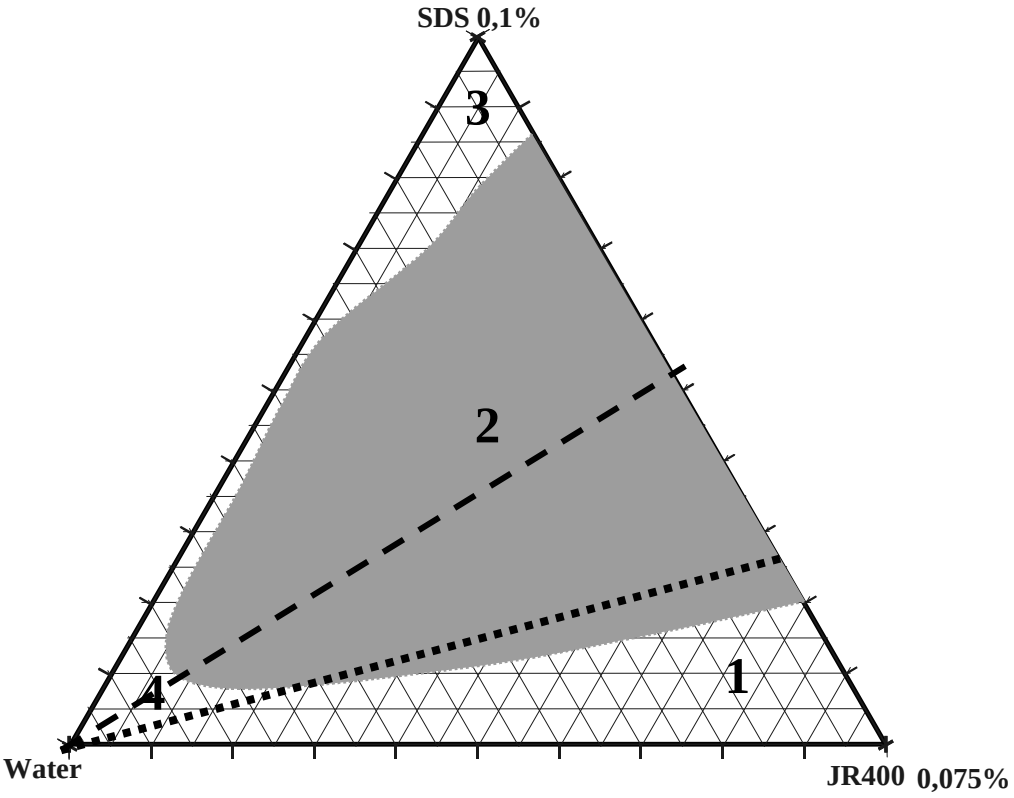

Figure 4.1 – Ternary phase diagram of interaction of the working solutions of SDS and JR400. Dotted line represents the theoretical composition of maximum precipitation, and the dashed line – the composition where this maximum was observed experimentally. The region numbers are explained in text.

All further investigations focused on regions 1, 3 and 4, while no DLS or AFM investigations in the precipitation area itself were possible because of the high turbidity of the samples. To cover a possibly broad range of concentrations and compositions and to highlight the most characteristic properties of the mixtures, a variety of samples was selected for DLS measurements.

4.1.1.2 Important samples

After preliminary measurements, 16 samples were chosen for DLS measurements. They represent all characteristic regions of the phase diagram under different dilutions. The properties of these samples are presented in Table 4.1.

Table 4.1 – List of samples selected for DLS measurements. "Extra water fraction" is a measure of mixture dilution. Samples discussed in this section are shaded.

Sample No.	final concentration / w/w%		stoichiometric ratio* SDS : JR 400	Phase diagram region	Extra Water fraction, wt%,
	SDS	JR400			
8	0,09	0,0075	27,7 : 1	3	0
9	0,085	0,01125	17,4 : 1	3	0
13	0,016	0,003	12,28 : 1	4	80
15	0,01	0,03	0,77 : 1	1	50
20	0,01	0,0525	0,44 : 1	1	20
25	0,057	0,00225	58,17 : 1	4	40
27	0,01	0,0075	3,07 : 1	4	80
45	0,015	0,0563	0,61 : 1	1	10
46	0,01	0,06	0,38 : 1	1	10
47	0,005	0,06375	0,18 : 1	1	10
49	0,08	0,0075	24,58 : 1	3	10
50	0,085	0,00375	52,19 : 1	3	10
66	0,0135	0,0574	0,54 : 1	1	10

For the sake of clearness, the positions of the samples characteristic for discussion of DLS results (shaded in Table 4.1) on the ternary phase diagram are presented in Figure 4.2. The samples are denoted as asterisks.

* Quantitative details of the calculating of stoichiometric ratios are given in the text.

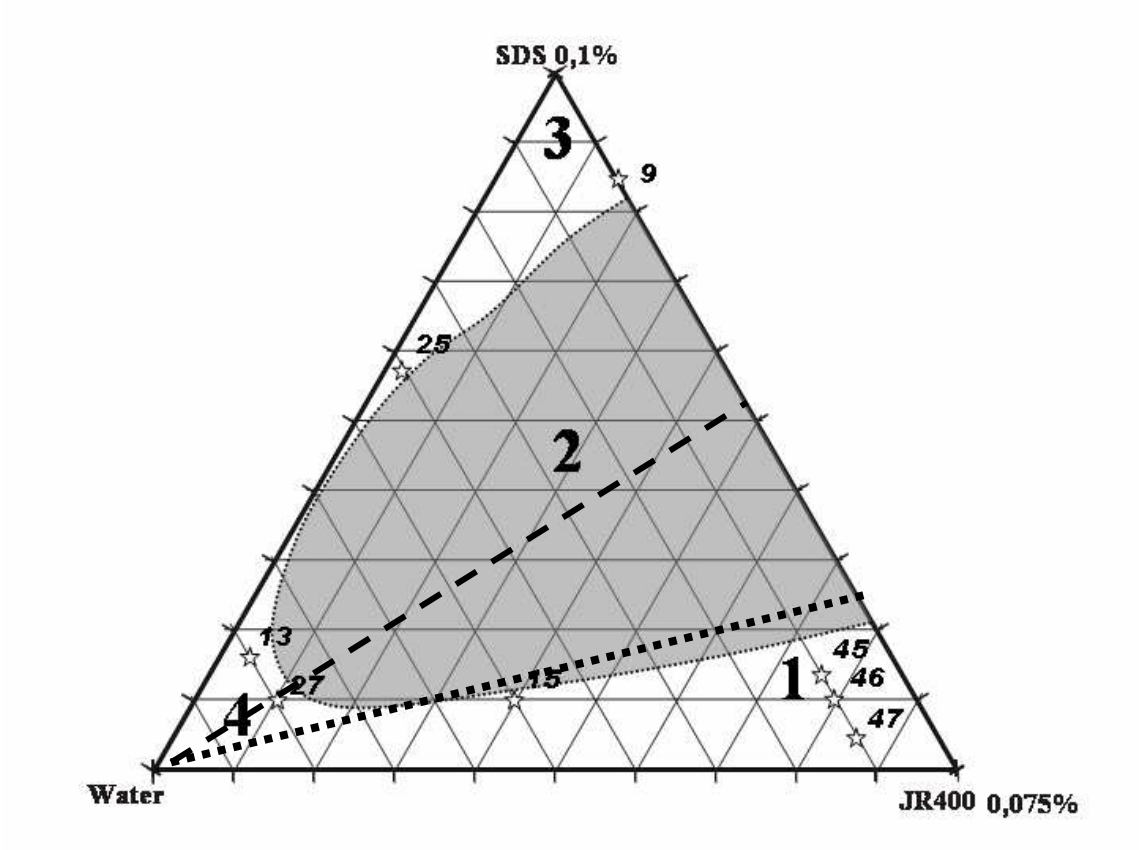

Figure 4.2 – Samples characteristic for the DLS results on the ternary phase diagram. The region of precipitation is shaded. Dotted line represents the theoretical composition of maximum precipitation, and the dashed line – the composition where this maximum was observed experimentally.

4.1.2 Results of particle size measurements with DLS

The size distribution profiles of particles (clusters) obtained with DLS in the SDS-JR400 mixtures are presented in this section. The results are grouped according to the regions of the ternary phase diagram.

4.1.2.1 Region 1 – polymer rich mixtures before precipitation.

Figures 4.3 – 4.5 demonstrate the results of DLS measurements performed on the mixtures with the same dilution in the order of subsequent increase of stoichiometric ratio SDS to JR400 charges. Sample 15 presented in Figure 4.6 is of higher dilution, and

its stoichiometric ratio seems to be the precipitation onset for less diluted samples (see Figure 4.1).

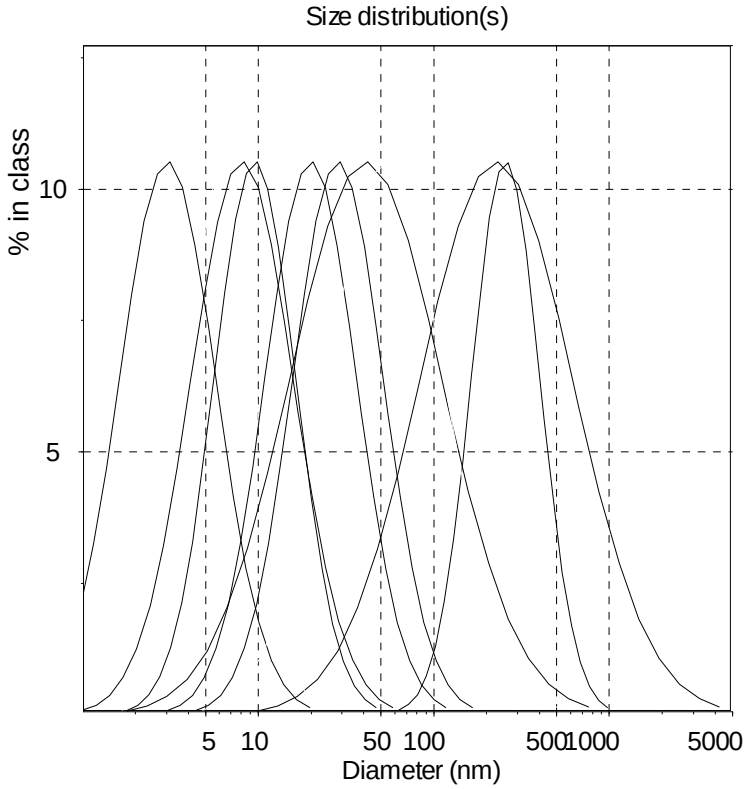

Figure 4.3 – Hydrodynamic diameters of clusters in the mixture of the working solutions of SDS (5%), JR400 polymer (85%) and water (10%), composition point 47 from Fig. 4.2.

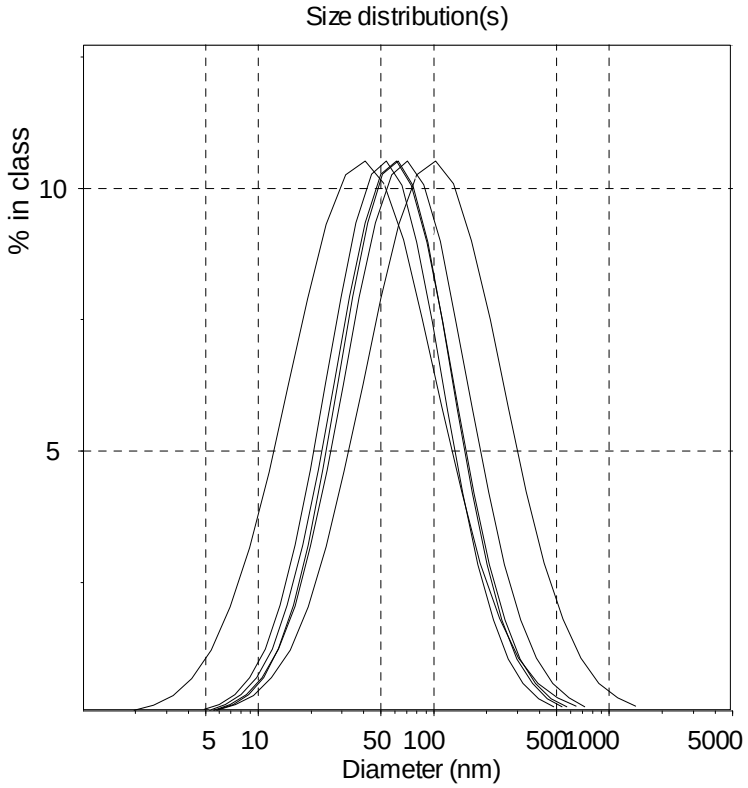

Figure 4.4 – Hydrodynamic diameters of clusters in the mixture of the working solutions of SDS (10%), JR400 polymer (80%) and water (10%), composition point 46 from Fig.4.2.

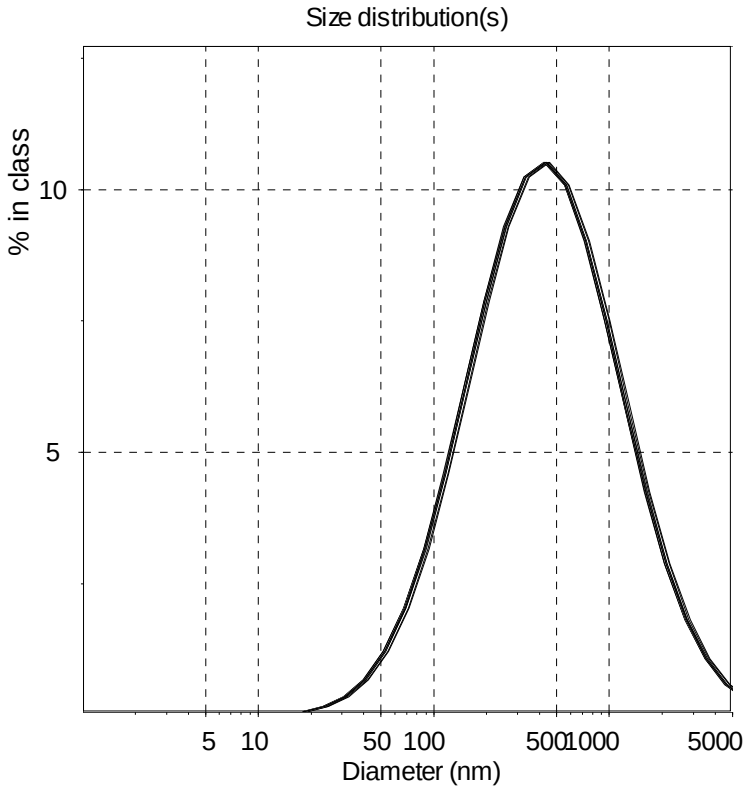

Figure 4.5 – Hydrodynamic diameters of clusters in the mixture of the working solutions of SDS (15%), JR400 polymer (75%) and water (10%), composition point 45 from Fig. 4.2.

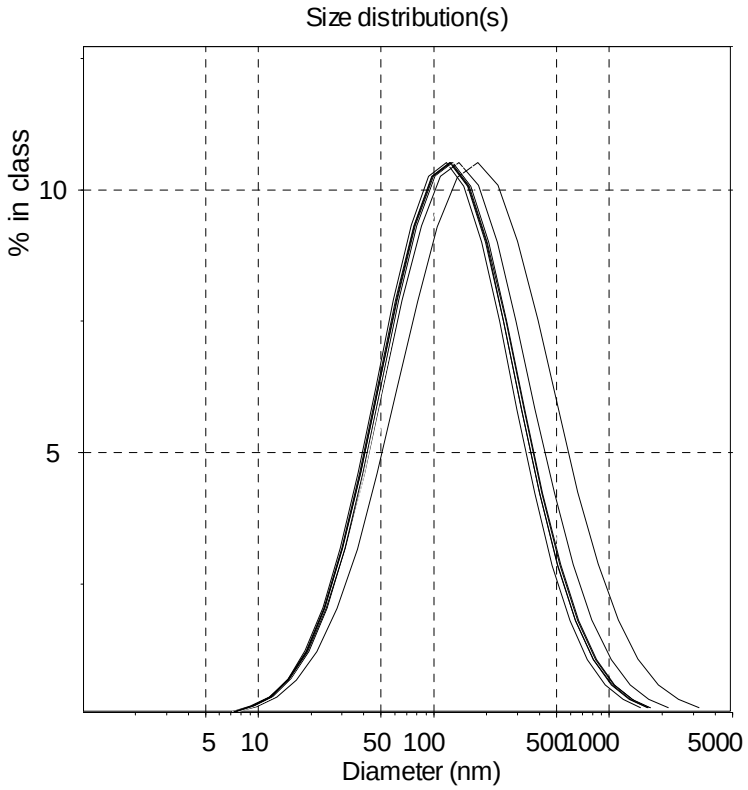

Figure 4.6 – Hydrodynamic diameters of clusters in the mixture of the working solutions of SDS (10%), JR400 polymer (40%) and water (50%), composition point 15 from Fig. 4.2.

We consider the absolute values of hydrodynamic diameters of less significance for characterization of SDS-JR400 system in an "isolated" DLS study, that is, without comparison with other methods. Due to the variability of possible conformations of polymer chains and forms and sizes of micelle-like clusters at different conditions [10, 17] it is hardly possible to draw any conclusions alone from the fact that the mean diameter of polymer-surfactant complexes, for example, in the mixture number 45 is 430 nm. However, the absolute size values are of importance when the DLS results will be compared to the AFM results. This will be presented in next sections.

More important are size relations between the samples of different compositions and the possibility to follow the tendencies shown in the particular region of the phase diagram. For the region 1, it is remarkable how strongly differs the uniformity of cluster sizes depending on the mixture composition. There is approximately one surfactant molecule per 5 polymer binding sites in the sample 47 (under the assumptions made in section 3.1.1.1). The mixture composition here indicates a great amount of free polymer with appropriate loops and curls of polymer chains that are in constant motion. No one of 10 size distribution curves obtained from this sample is similar to another in the same sample. It is important again to mention here that the curves presented have been obtained from the single sample under the *same* conditions – the measurements have been performed subsequently without any changes or stirring of the sample. Also significant that no time-depending tendency can be observed while cooking at the results of subsequent measurements. This means that the correlograms formed during every particular measurement differed from one another, i.e. the particle velocity was sometimes high, sometimes low. As the SDS / JR400 ratio increases in samples 46, less data scattering is observed, and in the sample 45, all distribution curves are superimposed showing a great data uniformity. We observe here a transition from a disordered mixture state to the formation of relatively ordered clusters that can be reproducibly measured with our method. This transition is obviously driven by energetic favourability reasons as the interactions between polymer and surfactant play a more and more important role.

Although the SDS/JR400 ratio in the sample 15 is 0.77:1, i.e. even higher than in the sample 45, the degree of uniformity in the former is obviously less than in the latter

(compare Figures 4.5 and 4.6). The reason could be a higher dilution of sample 15, which means less interaction between forming polymer-surfactant clusters.

4.1.2.2 Region 4 – highly diluted mixtures

Figure 4.7 shows the size distribution for the sample 27 with a composition close to the experimental maximum precipitation line (see section 4.1.3), but highly diluted. Sample 13 in Figure 4.8 has a composition close to the redissolution region and is transparent due to the high dilution.

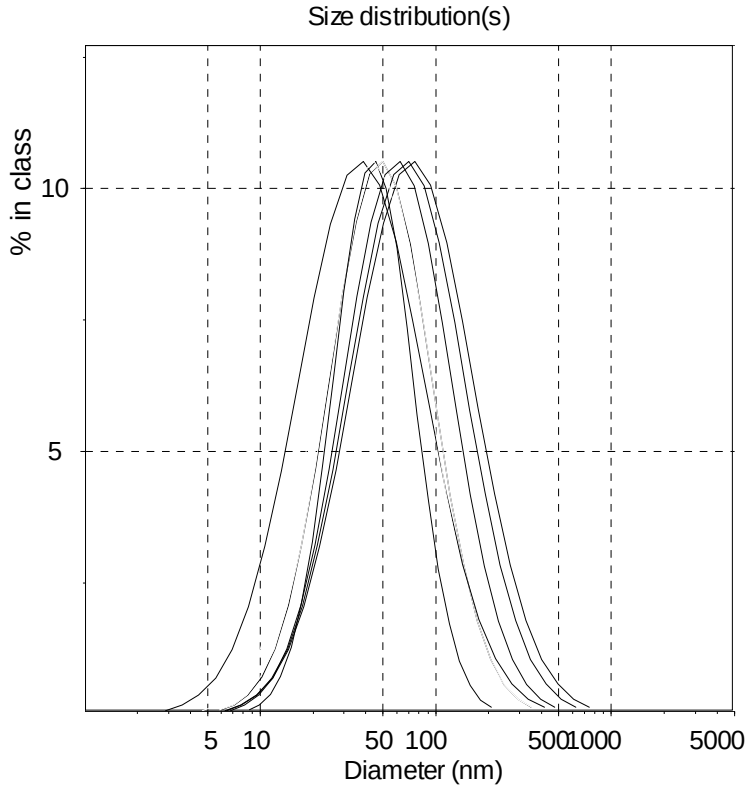

Figure 4.7 – Hydrodynamic diameters of clusters in the mixture of the working solutions of SDS (10%), JR400 polymer (10%) and water (80%), composition point 27 from Fig. 4.2.

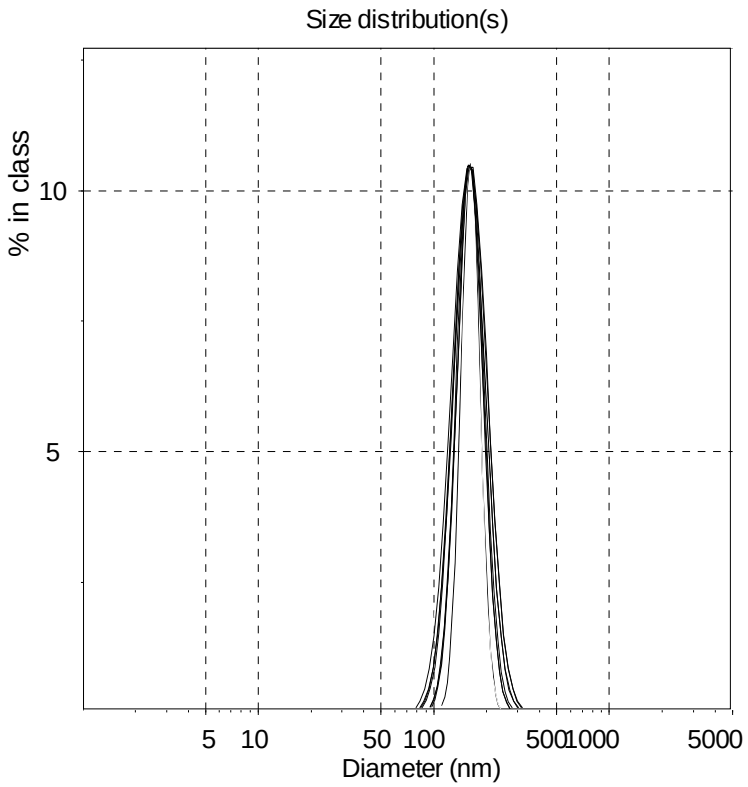

Figure 4.8 – Hydrodynamic diameters of clusters in the mixture of the working solutions of SDS (16%), JR400 polymer (4%) and water (80%), composition point 13 from Fig. 4.2.

Like in the Region 1, we can see here that the reproducibility of the size measurement results increases with the increase of stoichiometric ratio surfactant/polymer. Another remarkable feature seen in the graph in both regions is a parallel increase in the mean cluster size.

4.1.2.3 Region 3 – surfactant rich mixtures in the resolubilisation area

Surfactant rich mixtures in the redissolution area can be considered as most stable ones among all non-precipitated mixtures: Samples 49 and 50 underwent control measurements by DLS and imaging with AFM after 4 months storage at room temperature and demonstrated no significant changes. Mixtures of other compositions, in contrary, changed after this time period, probably due to bacterial contamination that caused precipitation in mixtures of composition close to that of precipitation onset.

An indirect indication of mixture stability is also the high reproducibility of DLS size distribution curves. A comparison of the cluster uniformity will be presented in the next sections.

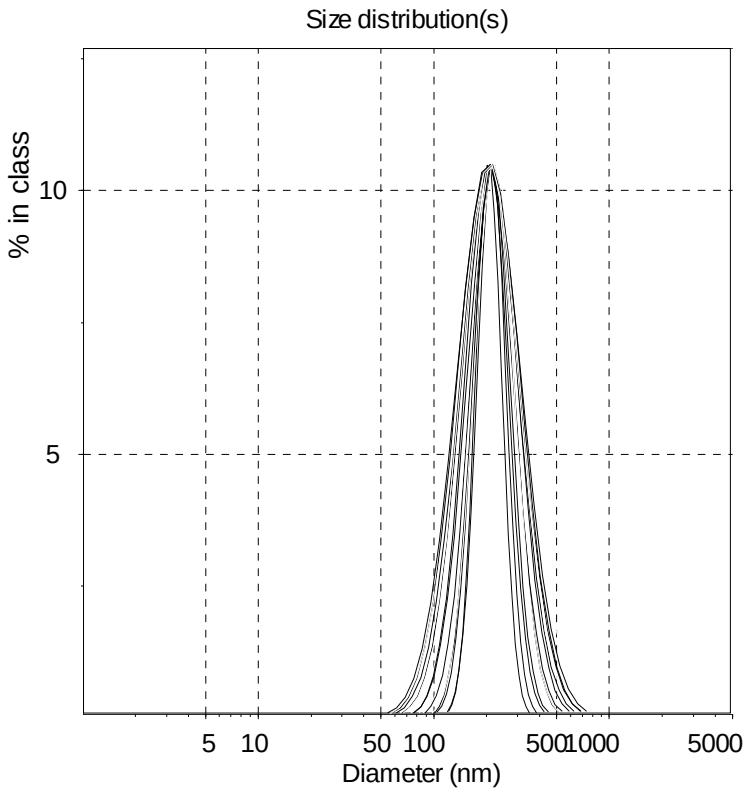

Figure 4.9 – Hydrodynamic diameters of clusters in the mixture of the working solutions of SDS (85%) and JR400 polymer (15%), composition point 9 from Fig. 4.2.

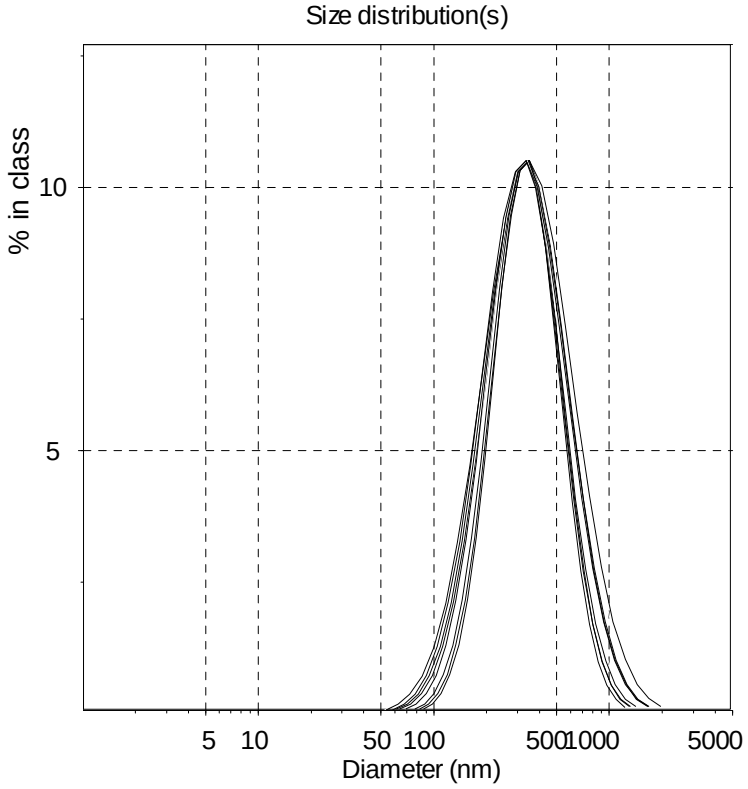

Figure 4.10 – Hydrodynamic diameters of clusters in the mixture of the working solutions of SDS (57%), JR400 polymer (3%) and water (40%), composition point 25 from Fig. 4.2.

4.1.3 Summary and discussion of investigations in the bulk solution

The ternary phase diagram together with the results of light scattering measurements show some quantitative differences when compared with the literature data and the theoretical pictures described in the introduction: the start of phase separation and its maximum seem to occur at substantially higher SDS to JR400 stoichiometric ratios than expected. Indeed, one can see that the mixtures with the ratio close to that at which the maximal precipitation could be expected (e.g. sample 15), are "located" just on the borderline of the phase diagram. The possible explanation for this phenomenon may be the following: since we deal with samples of very high dilution, we may assume that the so-called effect of "ideal gas behaviour" that was referred to in the literature previously [35] is present. That is, no detectable interaction between polymer and surfactant takes place before the T_1 "onset" concentration of interaction is reached. This could also be a plausible explanation for the relatively small slope of the lower borderline of the precipitation region. Contrary to our data, Regismond et al. [11] found that mixtures with composition similar to our samples 15 and 105 show some turbidity or precipitation, and therefore lie just within the turbidity area. A different strictness of the turbidity criteria could be the explanation: we noted that our borderline has been formed by samples *already* demonstrating an initial turbidity, though only under side illumination.

An interesting observation is the demonstration of the transition from "disordered" to the "ordered" cluster pattern with increasing stoichiometric ratio surfactant / polymer in the region 1 when comparing Figures 4.3, 4.4 and 4.5

The mean cluster size tends to change both due to the dilution changes and again, to the changes stoichiometric ratio surfactant / polymer. These changes are of various kinds: in surfactant rich mixtures in region 3 the mean cluster size increases with increasing dilution, and in polymer rich compositions of region 1, on the contrary, the diluted sample 15 has a less mean hydrodynamic diameter of clusters than the sample 45 that is more concentrated. Unfortunately, no possibility is available to compare a sufficient amount of samples with the same stoichiometrical ratio of components and *significantly* different dilution: any "line" representing such a batch of samples on the ternary phase diagram inevitably crosses the precipitation region. Therefore, no tendency couldbe strictly proven.

Nevertheless, it is necessary to remark that a deep discussion concerning the significance of the cluster size in the SDS/JR400 system is not always possible: for example, the term “cluster” itself can not be considered as correct for the region 1 where the polymer-surfactant complexes only start to form. Such a discussion will have a better reason when relatively stable [29] adsorbed structures are involved in it.

4.2 ADSORPTION OF THE SDS / JR 400 MIXTURES ON SURFACES

This section presents the results of AFM investigations of adsorbed layers of SDS-JR400 system of different compositions on different surfaces. In the first subsection, the general pattern of adsorption of mixtures from different regions of the ternary phase diagram is presented. The roles of surface charge and hydrophobicity are highlighted on an example of one sample.

The second subsection compares the structures in the adsorbed layer on freshly cleaved mica and on hydrophobized silica with respect to the properties of the same mixture compositions in bulk.

The third section describes two series of "washing-off" experiments performed by a change of the mixture compositions in the AFM fluid cell. In these experiments mixtures with lower SDS/JR400 ratio were substituted by those with higher polymer-surfactant ratio in order to observe changes in structure and properties of the adsorbed layer.

4.2.1 General adsorption picture

4.2.1.1 Comparison of different mixtures adsorbed on mica

Samples 15, 25 and 27 were selected to represent the results of this study since they are most characteristic for the appropriate regions of the ternary phase diagram due to their composition (see Table 4.1 and Figure 4.2), on the one hand, and brought comparatively clear and well structured images, on the other hand. All samples were AFM imaged with increasing magnification until $1\times1\mu m^2$ scans have been obtained containing different kinds of adsorbed structures: polymer-surfactant aggregates and, if possible, visually aggregate-free substrate surface. Then, force-distance curves were acquired on different parts of the scan area. The curves have been computer-processed with Origin® 7G SR2 software package and are presented in the following pages. For the sake of comprehensiveness, the corresponding scans are presented as well. The spots

where the force-distance curves were acquired are marked. A discussion of the results obtained is presented in the final part of the subsection.

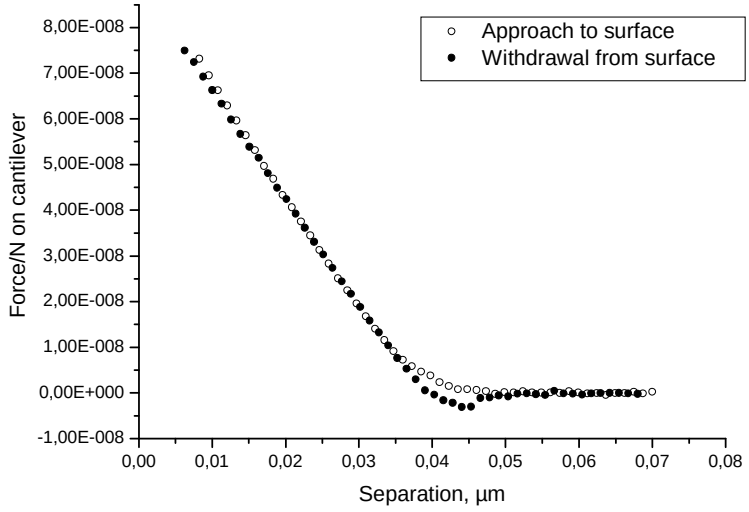

A)

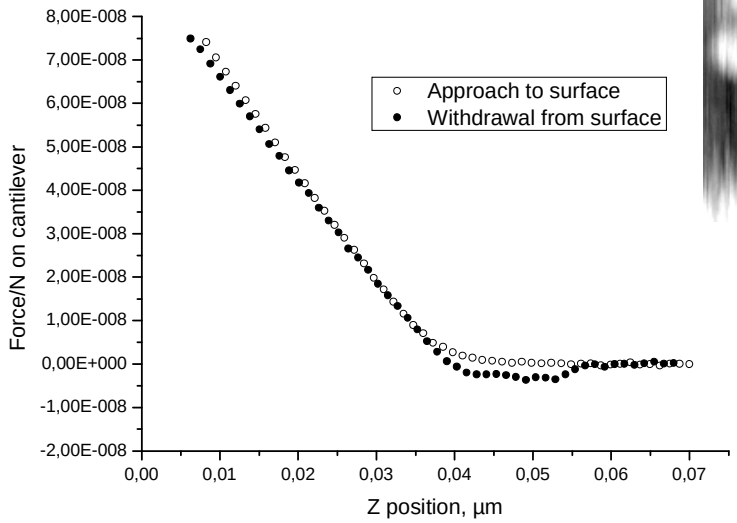

B)

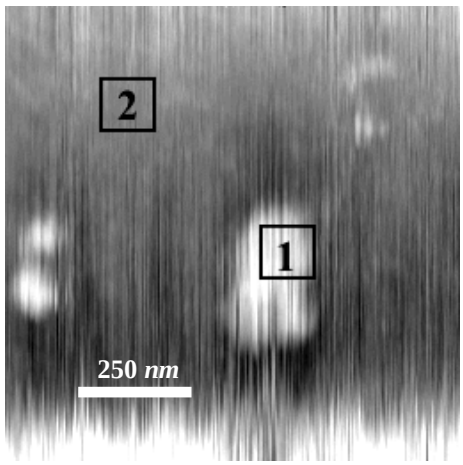

Fig 4.11 – Force-distance curves acquired on the 1×1 µm^2 AFM scan of the adsorbed mixture of the working solutions of SDS (10%), JR400 polymer (40%) and water (50%), composition point 15 from Fig.4.1. The scan is presented on the right hand side. A) Curve acquired on the polymer-surfactant complex marked as spot 1, B) Curve acquired on visually aggregate-free, plane substrate surface marked as spot 2.

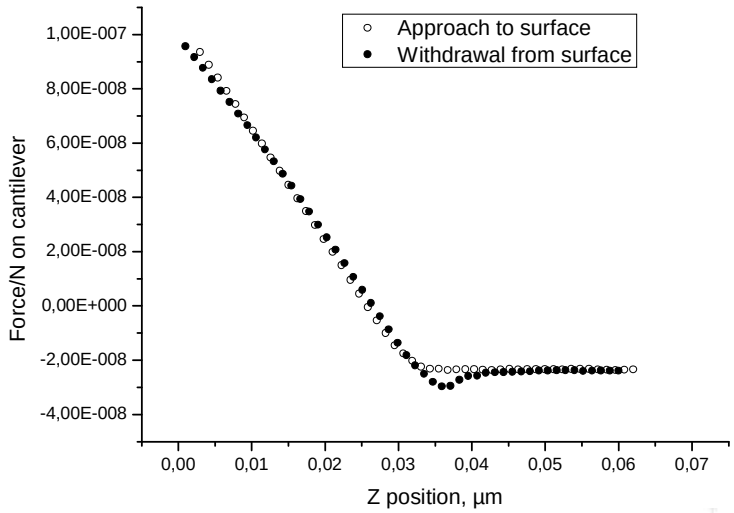

A)

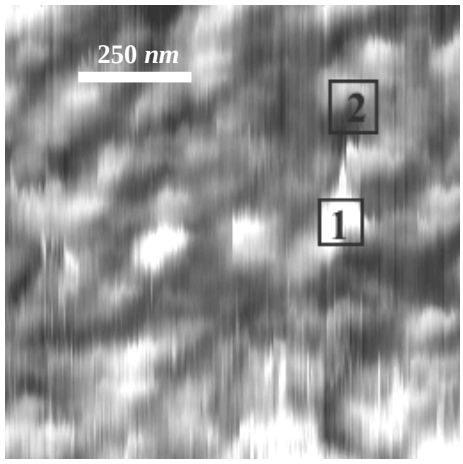

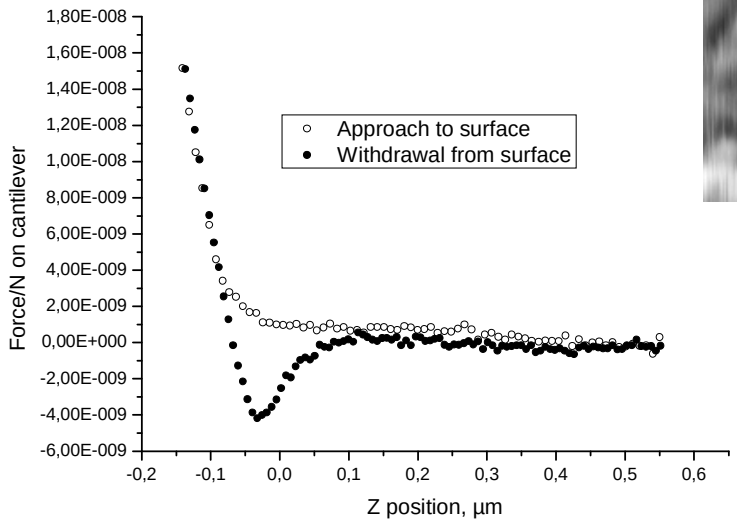

B)

Fig 4.12 – Force-distance curves acquired on the 1×1 µm^2 AFM scan of the adsorbed mixture of the working solutions of SDS (10%), JR400 polymer (10%) and water (80%), composition point 27 from Fig.4.1. The scan is presented on the right hand side. A) Curve acquired on the polymer-surfactant complex marked as spot 1, B) Curve acquired on visually aggregate-free substrate surface between clusters marked as spot 2.

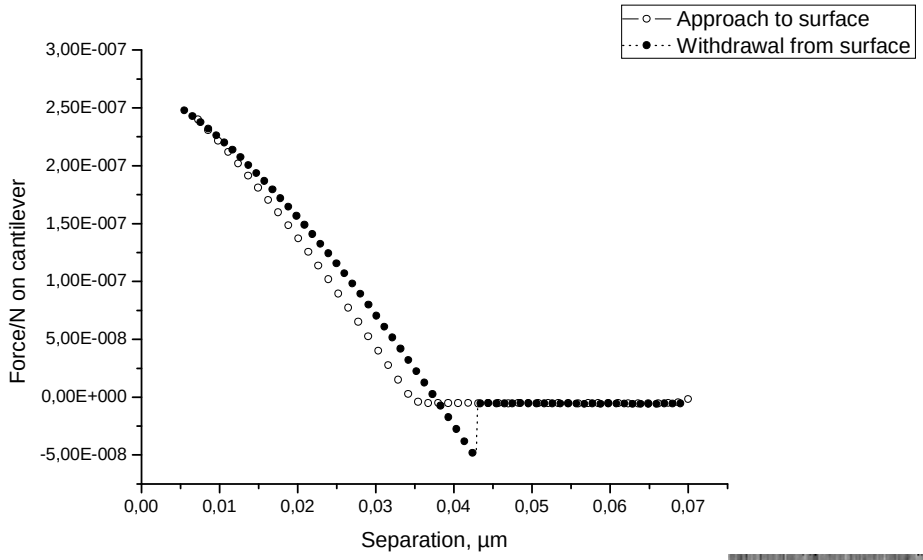

A)

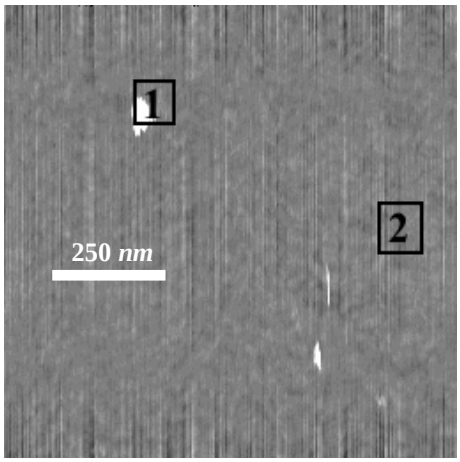

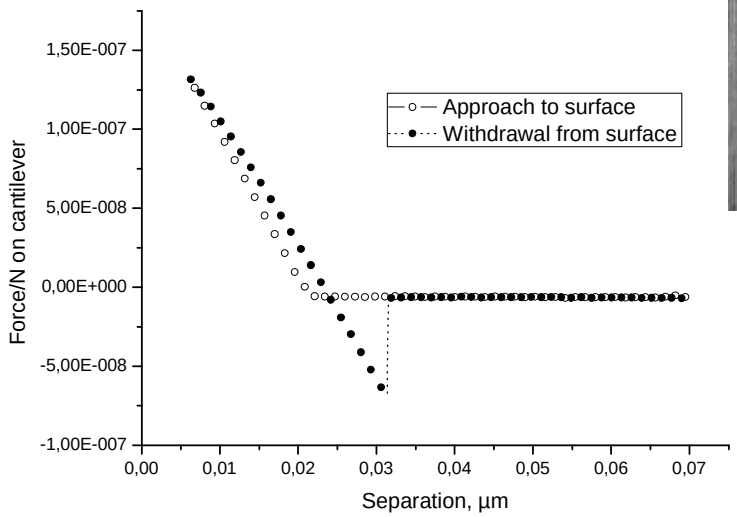

B)

Fig 4.13 – Force-distance curves acquired on the 1×1 µm^2 AFM scan of the adsorbed mixture of the working solutions of SDS (57%), JR400 polymer (3%) and water (40%), composition point 25 from Fig.4.1. The scan is presented on the right hand side. A) Curve acquired on the (eventual) polymer-surfactant complex marked as spot 1, B) Curve acquired on visually aggregate-free substrate surface between clusters marked as spot 2.

Scans and force-distance curves presented in this section suggest that the structure of the adsorbed layer, so far as it can be understood on the basis of the AFM data, logically corresponds to the composition of the particular mixture.

Polymer rich sample 15 demonstrates remarkable elastic properties and viscosity of the adsorbed layer. This conclusion can be drawn from the smooth form of the force-distance curve. It is to mention that high viscosity of the adsorbed layer differs from properties of the same sample in bulk. This was expectable because the total local concentration of both components in the adsorbed layer is by definition [55] higher than in solution. And higher concentration, according to Goddard [17] means a viscosity increase in polymer rich mixtures.

The local composition in the adsorbed layer does not seem to vary principally from one spot to another, which can be seen from the similarity of the curves acquired at different places. This is also in accordance with theory: the composition means that no cluster formation has occurred yet, and the probability to "meet" either polymer or surfactant or both of them in any particular place is similar.

The stoichiometric ratio of components in the sample 27 is close to that of maximum precipitation observed in this study by less dilution. This means that some compartmentalization, i.e. mesoscale separation of surfactant-rich and polymer-rich complexes would occur. It is confirmed by the scan appearance but this will be discussed in section 4.2. After scale correction, the force-distance curves do not show any remarkable difference between different acquisition spots.

The most interesting observation concerns sample 25: the smooth and plane surface seen in the scan means that strongly diluted surfactant rich polymer-surfactant mixtures do not adsorb at mica at all. The force-distance curves confirm this conclusion: they look similar to those acquired on native mica [21, 118]. This is also easy to explain theoretically: anionic surfactant SDS can not adsorb to the negatively charged, hydrophilic mica surface, and all polymer molecules that could adsorb to the surface seem to be bound by highly excessive SDS.

An important remark to this sample: the very first curve acquired on spot 1 looked different and suggested presence of small qualities of polymer (not shown due to poor quality). All further curves were similar to those presented in Figure 4.13 and did not differ from curves acquired on the cluster-free surface. There are only two possible explanations for this phenomenon: either the aggregate in the spot 1 is an artefact, or it existed really but was very weakly adsorbed and desorbed after the first contact with the cantilever.

4.2.1.2 Comparison of the same mixture adsorbed at different surfaces

Sample 27 adsorbed on normal mica, hydrophobized mica and hydrophobized silica surfaces was imaged at the same conditions and underwent "scratching" as described in Section 3.3.3.3. Force-distance curves (more precise, deflection vs. separation curves specific for the Nanoscope III instrument) were acquired before and after scratching. Qualitative differences in the adsorption picture and some force-distance curves are presented in Figures 4.14 – 4.17.

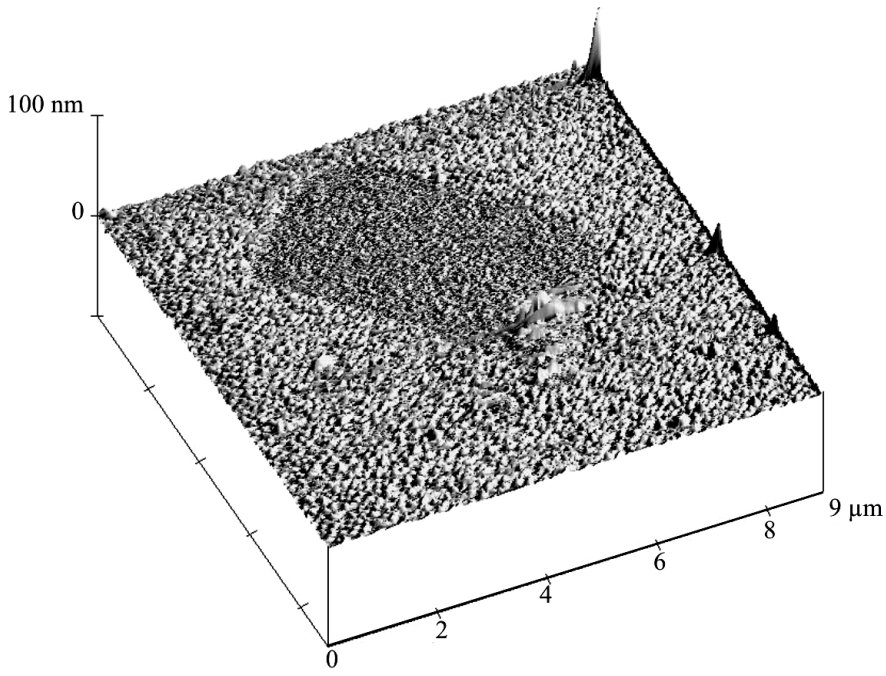

Figure 4.14 – 3-dimensional presentation of 9×9 μm^2 AFM deflection image of the adsorbed mixture of the working solutions of SDS (10%), JR400 polymer (10%) and water (80%), composition point 27 from Figure 4.1 after "scratching" on the hydrophobized silica surface.

Two issues are important in Figure 4.14. First, the scratched area is flat, without any rests of adsorbed structures. Another important observation is that aggregates scratched away from the processed area were not moved aside (almost no aggregates are accumulated on the borders of the scratched area) but obviously desorbed.

Both facts can mean that adsorption of polymer-surfactant aggregates is not very strong at this particular surface due to two possible reasons: the hydrophobized silica surface bears relatively low negative charge, which weakens electrostatic interactions between the surface and the charged groups of the polymer; the hydrophobic adsorption mechanism also can not be fully engaged at this particular mixture composition.

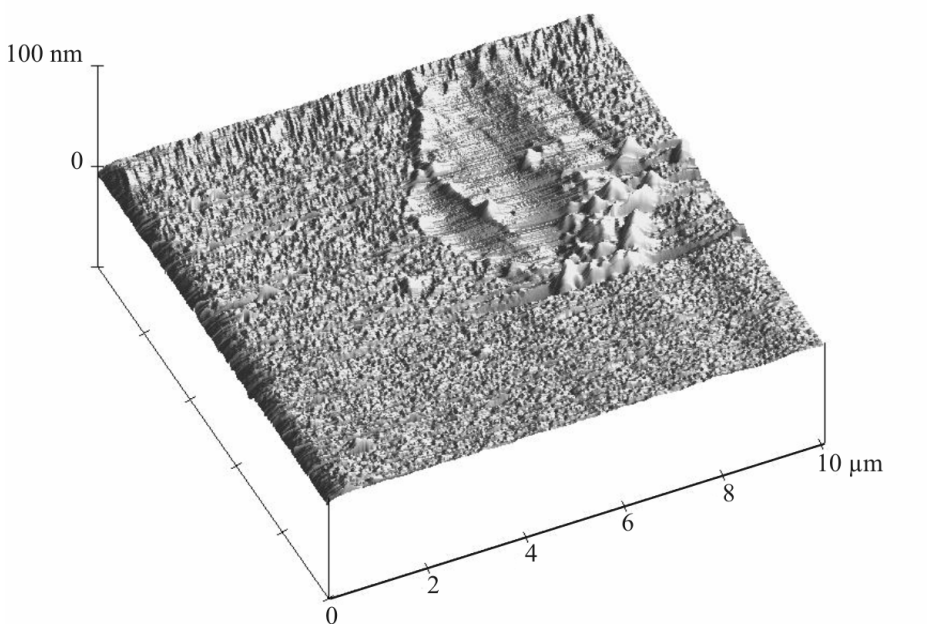

A)

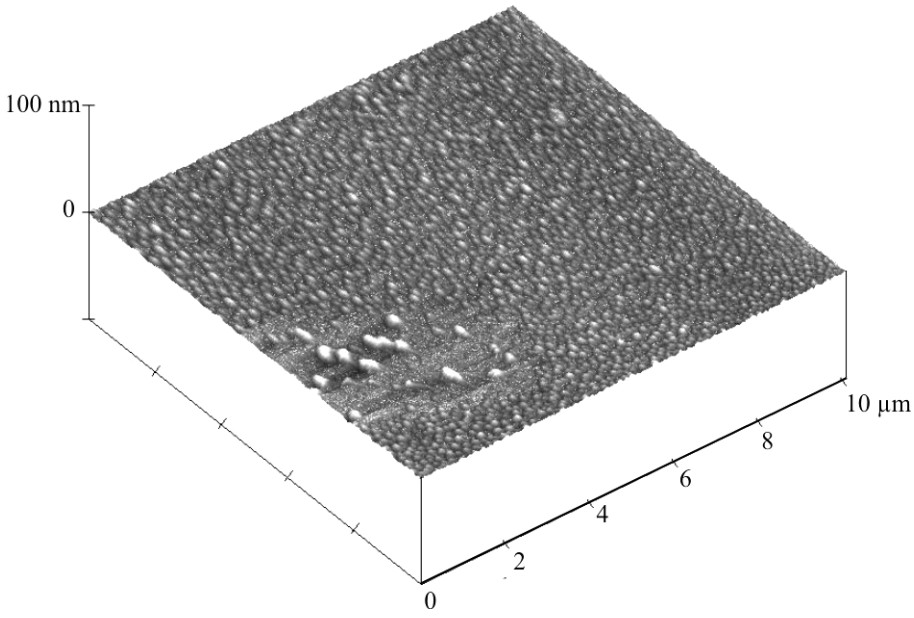

B)

Figure 4.15 – 3-dimensional presentations of 10×10 µm^2 AFM deflection images of the adsorbed SDS-JR400 mixture, composition point 27 from Figure 4.1.
A) after "scratching on the hydrophobized mica surface. The "waved" look of the underlying surface is an artefact.
B) after "scratching" on the freshly cleaved (native) mica surface.

A comparison of Figures 4.14, 4.15 A) and 4.15 B) suggests that the affinity of this polymer-surfactant system to substrates is in the following order: hydrophobized silica < hydrophobized mica < native mica. Contrary to the observations for the silica surface, we see that although most of the aggregates (but not all) could be scratched away from

the hydrophobized mica surface, they did not desorb but were moved aside. On native mica, most of the aggregates remained on the surface, which indicates the strongest adsorption.

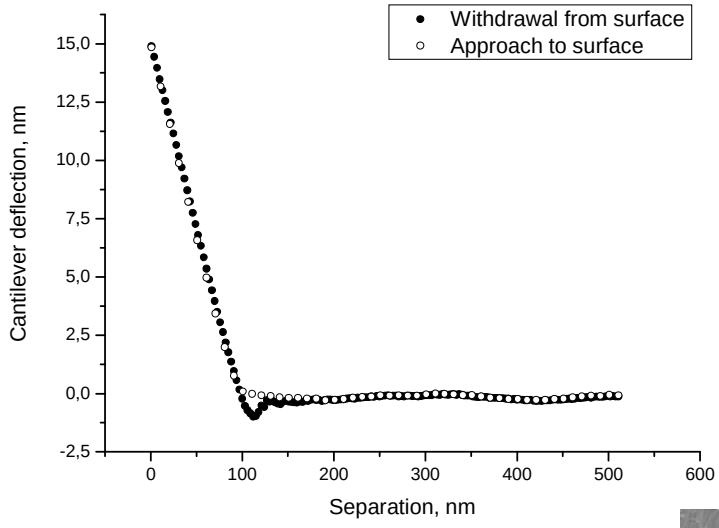

A)

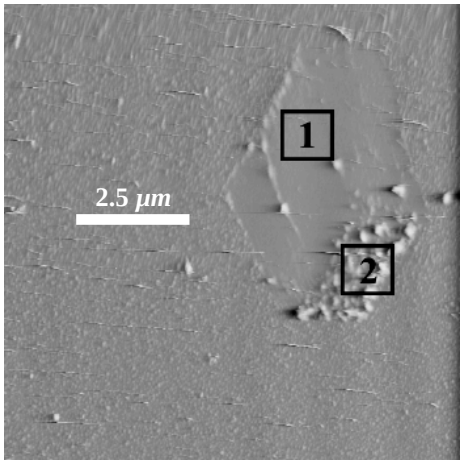

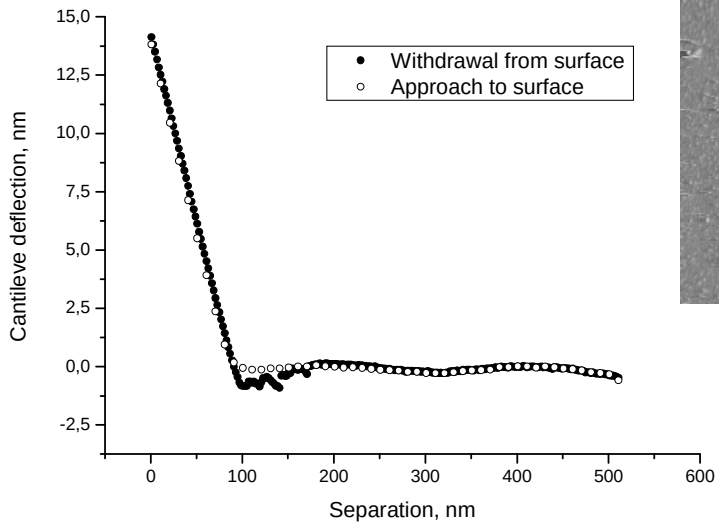

B)

Figure 4.16 - Force-distance curves acquired on the scan presented in Figure 4.15 A) (hydrophobized mica). A) The curve from the flat part of the scratched area (1); B) curve acquired on the "hill" region aside the scratched area (2).

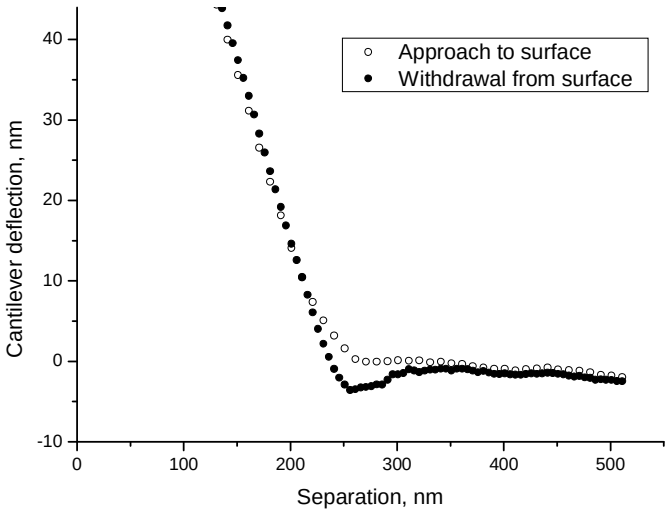

A)

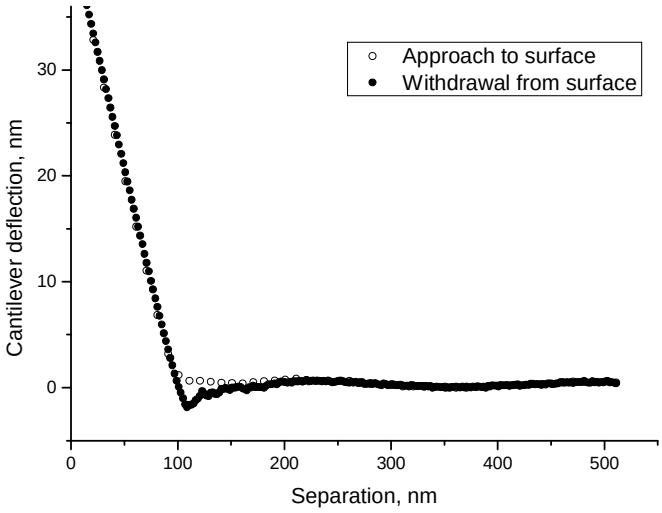

B)

Figure 4.17 - Force-distance curves acquired on the scan presented in Figure 4.14 (hydrophobized silica). A) The curve acquired before scratching; B) curve acquired on the flat part of the scratched area in the middle of the scan.

The comparison of force-distance curves from different surface types, on the one hand, and from scratched or not scratched areas, on the other hand, supports the assumption of different affinity to different surfaces. The curves in Figure 4.16 A) and B) differ from one another (see the thickness of the adsorbed layer indicated by the bottom part of the withdrawal curve, refer section 3.3.2.2), but in both cases strong attractive forces are exerted on the cantilever by the adsorbed layer. Most probably it is

the adsorbed polymer that contributes most significantly to these forces. The layer thickness is less in the scratched area but the layer is also present here.

On the contrary, the curves in Figure 4.17 A) and B) differ from one another dramatically: a soft, thick and elastic layer can be seen on not scratched surface; this layer disappears almost completely after scratching. The curve form resembles the form of curves acquired on surfaces free of any adsorbed layer.

4.2.2 Comparison of structures in the adsorbed layer and in the bulk.

The samples selected for this study are presented in Figure 4.18.

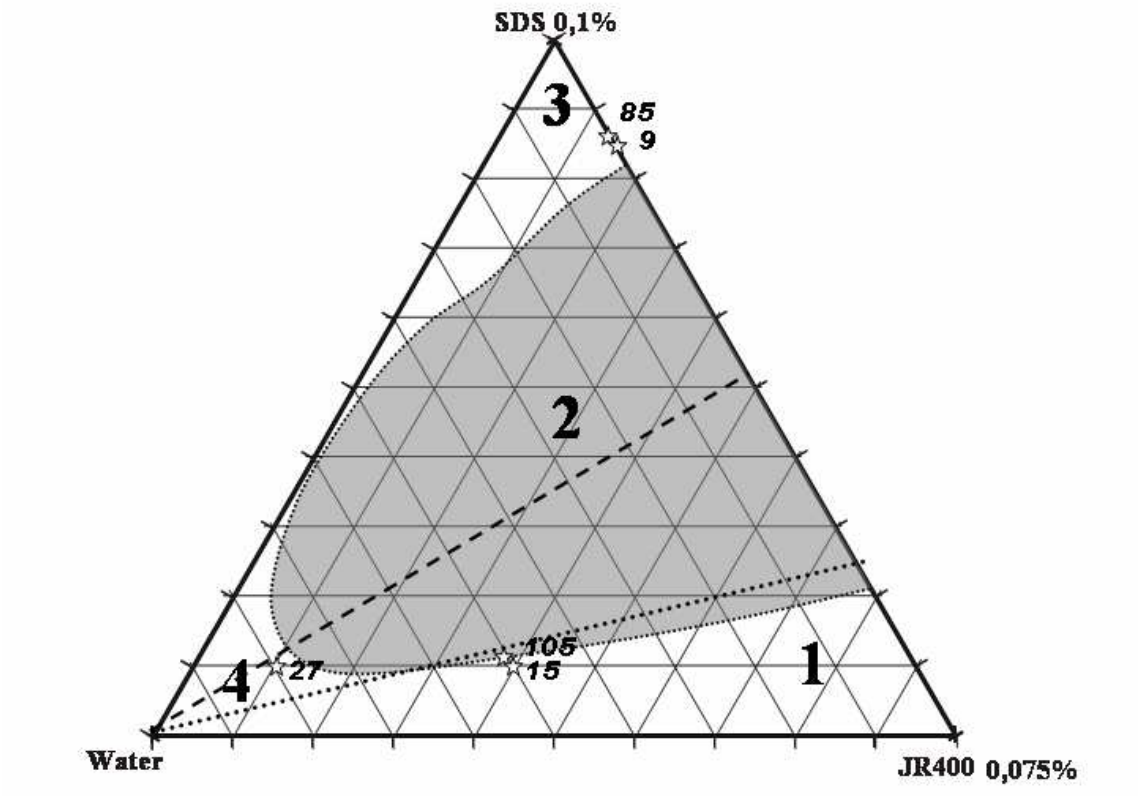

Figure 4.18 – Samples selected for comparison of DLS results with measurements of structures in the adsorbed layer. The region of precipitation is shaded. Dotted line represents the theoretical composition of maximum precipitation, and the dashed line – the composition where this maximum was observed experimentally.

4.2.2.1 Processing of results of DLS measurements

The DLS results obtained on the selected samples and presented in Section 4.1.2 have been processed statistically in order to compare the calculated sizes and volumes to those obtained during AFM measurements (see below). The processing comprised an averaging of size distribution curves in order to obtain a cumulative distribution per sample. This is especially important for sample 15 with broad size distribution and sample 27 with a significant scattering of the DLS results. The results of calculations together with the main characteristics of samples are presented in Table 4.2.

Table 4.2 - Results of DLS measurements of samples from the different regions of the ternary phase diagram. Samples denoted by N/A were only considered for the AFM measurements, not for the DLS measurements.

Sample No.	**final concentration/ w/w%**		**Stoichio-metric ratio SDS / JR 400 unit**	**Phase diagram area**	**mean particle size /nm**	**particle size distribution, nm**		**average particle volume nm^3**
	SDS	JR400				*for at least 85% of counted particles, nm*	*for at least 45% of counted particles, nm*	
15	0.01	0.03	0.77 : 1	1	120.2	30 – 510	60 - 210	300000
105	0.0123	0.0283	1 : 1	1	N/A	N/A	N/A	N/A
27	0.01	0.0075	3.07 : 1	4	43.5	12 - 120	24 - 60	38000
9	0.085	0.01125	17.4 : 1	3	205.8	108 - 324	180 - 300	4560000
85	0.0867	0.01	20 : 1	3	N/A	N/A	N/A	N/A

The volumes of the structures were calculated assuming that they are spherical. Size distribution ranges were used as a measure of particle uniformity. Samples 105 and 85 did not undergo light scattering measurements.

4.2.2.2 AFM Investigations

4.2.2.2.1 Comparison of sample sizes on different surfaces

The AFM investigations of the samples characterized by light scattering, or of those very close in composition (samples 85 and 105, instead of samples 9 and 15, respectively), were performed both on hydrophobized silica and on mica. Investigations included direct imaging of adsorption patterns at various scales and acquisition of force versus distance curves. The following image processing comprised, in particular, height profile analysis in order to compare particle sizes. Height profiles were acquired on the "topography" or "height" images *directly* corresponding to the "deflection" images presented for visual comparison. The deflection images give enhanced contrast of edges and are therefore often more pleasing to the eye in elucidating the form of structures in the x-y plane. Quantitative data in the Z direction is available from the height images. The lines, along which the profiles were acquired, are not indicated.

The images in Fig. 4.19, 4.21, and 4.23, are presented in pairs. This enables a direct visual qualitative comparison of the general adsorption pattern on mica and hydrophobized silica. Although the wetting properties of the substrates vary greatly it can be seen that the adsorption patterns for the pairs are more similar than the adsorption patterns obtained for solutions of different compositions adsorbed on surfaces of the same kind, indicating that the substrate plays a minor role in the adsorption behaviour compared to the role of the initial composition of mixtures.

The height profiles plotted with different image processing programs were coupled and brought to the same scale in both dimensions (errors in precision must be taken into account) using the CorelDRAW® software, version 11.633. On every drawing, the top profile (DI instrument) represents the sample adsorbed on hydrophobized silica, whereas the bottom profile (Park Scientific) characterizes the sample adsorbed on freshly cleaved mica. The peak width information for a number of regions is indicated. The profiles provide further information concerning cluster sizes of adsorbed polymer-surfactant complexes.

Highly diluted area (region 4)

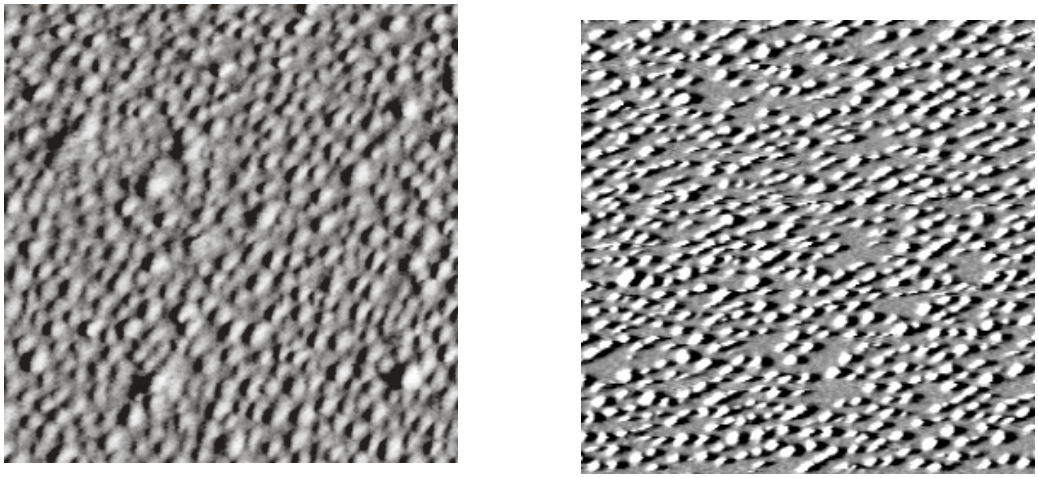

A) B)

Figure 4.19 – 3x3 μm^2 AFM deflection images of the adsorbed mixture of the working solutions of solutions of SDS (10%), JR400 polymer (10%) and water (80%), composition point 27 from Fig.4.18. A) Image of structures adsorbed from the mixture onto a hydrophobized silica substrate): a 3x3 μm^2 section of the 5 x 5 μm^2 image (DI III instrument), B) Image of structures adsorbed from the mixture onto mica (Autoprobe CP instrument)

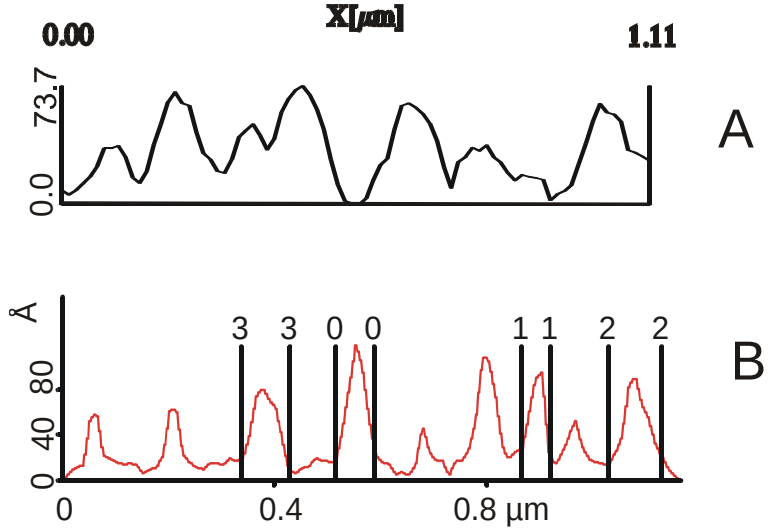

Peak	Peak Width
0:	634 Å
1:	526 Å
2:	1010 Å
3:	970 Å

Figure 4.20 –. Height profiles of adsorbed structures using a working solution of SDS (10%), JR400 polymer (10%) and water (80%). A and B correspond to Fig. 4.19. The peak sizes concern the profile B. For explanation see the text.

Adjacent to the pre-precipitation area (region 1)

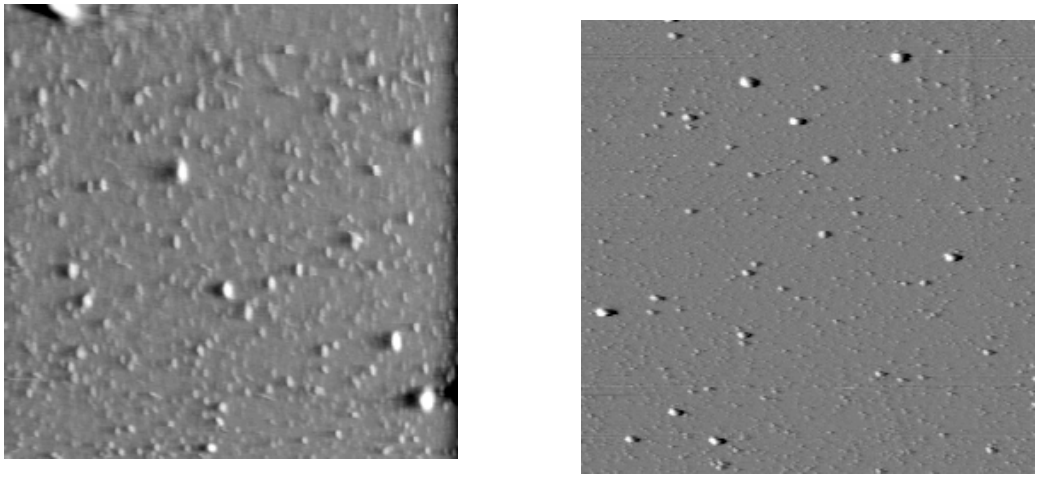

A)

B)

Figure 4.21 – 5x5 μm^2 AFM deflection images of adsorbed structures using a working solution of: A) solution of: A) Sample 105; SDS (12,28%), JR400 polymer (37,72%), water (50%). Composition point 105 from Fig. 4.18. Image of structures adsorbed from the mixture onto hydrophobized silica (DI III instrument), B) Sample 15; SDS (10%), JR400 polymer (40%), water (50%). Composition point 105 from Fig. 4.18. Image of structures adsorbed from the mixture onto mica (Autoprobe CP instrument).

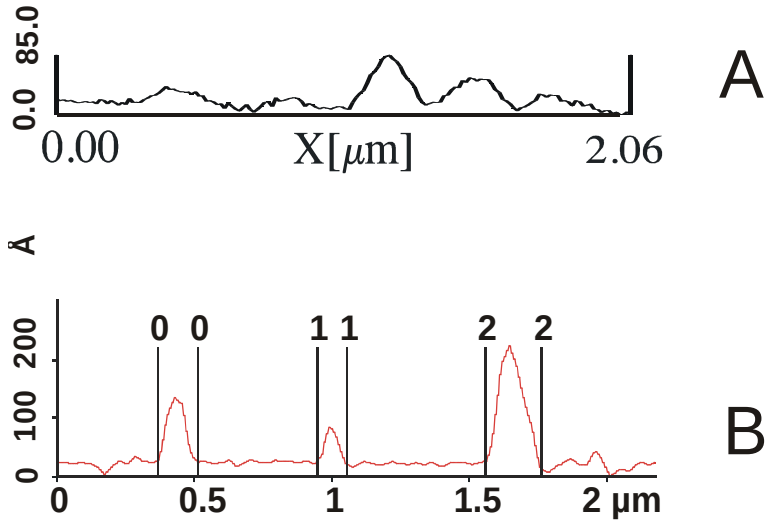

Peak	Peak Width
0:	0.153 um
1:	0.111 um
2:	0.208 um

Figure 4.22 – 5. Height profiles of adsorbed structures using Sample 105 and Sample 15; SDS A and B correspond to Fig. 4.21. The peak sizes concern the profile B. For explanation see the text.

Resolubilisation area (region 3)

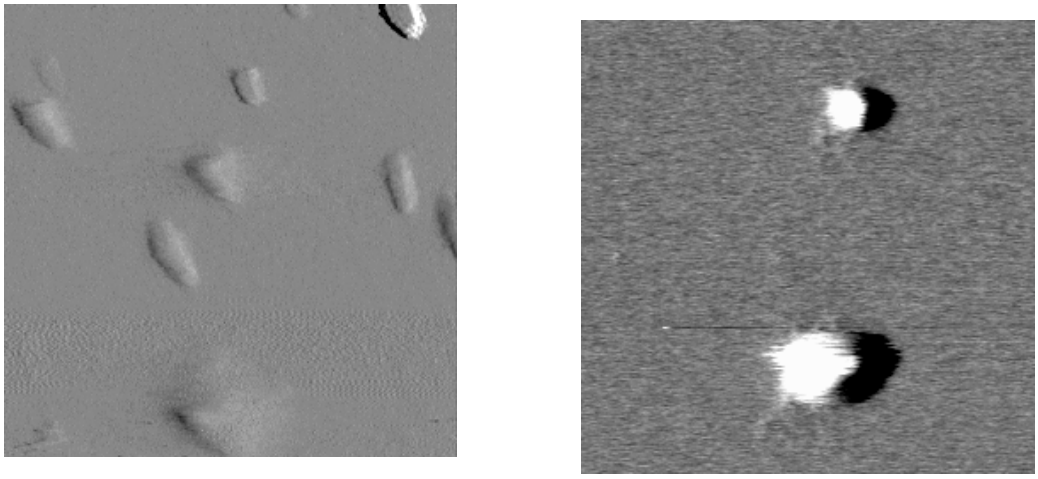

A) B)

Figure 4.23 – 2,5x2,5 μm^2 AFM deflection images of adsorbed structures using the working solutions: A) Sample 85; SDS (86,7%), JR400 polymer (13,3%), water (0%). Composition point 85 from Fig. 4.18. Image of structures adsorbed from the mixture onto hydrophobized silica (DI III Instrument), B) Sample 9; SDS (85%), JR400 polymer (15%), water (0%). Composition point 9 from Fig. 4.18. Image of structures adsorbed from the mixture onto mica (Autoprobe CP instrument).

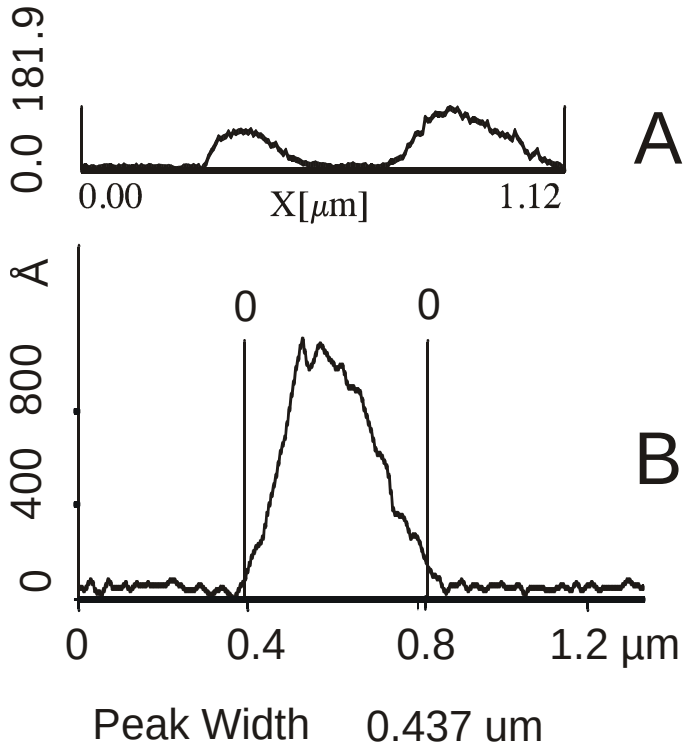

Figure 4.24 – Height profiles of adsorbed structures obtained using Sample 85 and Sample 9. A and B correspond to Fig. 4.23. The peak size concerns the profile B. For explanation see the text.

The light scattering method is, like every other experimental technique, not free of limitations. Those concerning particle size measurements are mentioned above (section 4.1.2) and described, for example, in a recent review by D.Horn et al. [36] and discussed by A. Rawls [37]. Particularly the position of for example a rod-like micelle or a surfactant loop in the laser beam may change the size data. Therefore, only the main trends and the clear differences between samples are discussed here.

When examining the light scattering data in Table 4.2, one can see that the mean particle size is a minimum in the region of high dilution. The mean particle size increases in the region of the precipitation onset, and reaches a maximum in the resolubilisation area. This suggests that the particles in the latter region are not single micelle-like clusters but bigger aggregates formed by surfactants and polymers. A further property revealed by the light scattering results is the change in particle size distribution. At the precipitation onset (sample 15), the particle size distribution is larger than it is for the highly diluted solution (sample 27) and becomes even smaller in the resolubilisation region (sample 9). This trend is revealed by the ratio of largest to smallest particles for 85% of the distribution. Values of 17, 10 and 3 are obtained for samples 15, 27 and 9 respectively. The trend also holds when we consider the central part of the appropriate distribution curves: the ratios are 3.5, 2.5 and 1.67 for the samples 15, 27, and 9, respectively. In both cases, the particles in the resolubilisation region are the most uniform ones, and at the precipitation onset the particle size exhibits the smallest uniformity. The most probable explanation for the interaction pattern observed by the light scattering measurements agrees with the existing model of the interaction between the polymer and surfactant: at the precipitation onset, a very wide range of possible configurations of emerging clusters exist: loopings and coils of the polymer backbone, aggregates of a few SDS molecules, as well as already “mature” micelle-like clusters and their aggregates are present in solution. As the polymer-surfactant ratio approaches that which results in maximum precipitation, most micelle like clusters are established, and, taking into account that we deal here with a very diluted sample, it may be expected that no new loopings, coils or other changes on the polymer backbone occur. The increase in the cluster size and size uniformity observed in the region of resolubilisation may also be explained if we consider the results of Nilsson et al. [38] and their conclusions drawn from these. Nilsson et al. studied the interaction of SDS with ethyl-

hydroxyethylcellulose (EHEC) – a non-ionic polymer – using dye solubilisation and fluorescence quenching. Nilsson et al. found that “in a dilute polymer solution (c<0,05% EHEC) the cluster concentration is fairly constant up to the point where normal micelles begin to form”. This means that no new clusters appear, and an increase in SDS concentration thus may lead to the uptake of “newcoming” SDS molecules by existing micelle-like clusters, which in turn, must lead to an increase in the micellar size. The influence of polymer-surfactant interactions on micelle properties, namely an increase of cluster size with increasing surfactant concentration, has already been reported by Kjøniksen et al. [40]. In our samples that lie in the resolubilisation region, there are more than 15 SDS molecules per one positive charge site on the polymer, even assuming that the relative molecular mass per charge is only 670 (this assumption is close to that of the substitution degree of about 42%, which is relatively high: literature data are between 3 [16, for LM200] and maximally 45% [39], obviously depending on the production batch, see also sections 2 and 3). Therefore, we may presume that electrostatic neutralization has already taken place, and further surfactant binding to polymer is of hydrophobic nature. So, the mentioned conclusions for the non-ionic EHEC may be also relevant for our case of the cationic EHEC in solutions with a large excess of anionic surfactant.

As mentioned previously, the atomic force microscopy images demonstrate more resemblance between the samples of the same or similar solution acquired on different surfaces than between solutions of different compositions obtained using the same surface. A simple visual comparison shows this. Previously, results of some studies [41, 19, 16, 5, 42, 43, 18] suggested a prevalence of interactions between polymer and surfactant over interactions between any component and the surface itself: a change of the concentration of one component in the solution is more important than a modification of the solid surface, and this result is confirmed here.

The analysis of the AFM images reveals that the size and size distribution of the adsorbed particles is in good agreement with those in the bulk. There is also no evidence of any influence of the surface on the bulk structures with respect to their size. When the height profiles of particles adsorbed on hydrophobized silica are compared with those acquired on mica, they show that the particles on mica are “smaller” in the x-y plane and “higher” (i.e. larger in the z dimension) than those obtained from the corresponding mixtures adsorbed on hydrophobized silica. One

possible explanation might be a further flattening of the clusters and networks caused by surface hydrophobicity. The adsorption process in this case is driven essentially by hydrophobic interactions, and the affinity of the complexes to the surface may be stronger than they are in the case of hydrophilic mica. This will favor spreading of the structures over the surface. This explanation, however, looks to be in contradiction to the results presented in section 4.2.1.2 where we have seen that the structures easily desorb from hydrophobized silica. Nevertheless, the latter results are obtained only with sample 27 which shows the least height profile difference on mica compared to hydrophobized silica.

For all samples, particle size data (x axis sizes) from section analysis suggest some squashing, or flattening, of particles. This can be caused both by the cantilever tip compressing the adsorbed layer and (what seems more likely) by spreading of the micelle-like clusters over the surfaces during adsorption.

4.2.2.2.2 Volume analysis

The volumes of particles adsorbed on mica were measured using the image processing software and compared with the volumes of the particles in bulk measured by DLS. However, it should be noted that the statistics is rather poor due to the limited amount of particles in the field of vision of the AFM.

Table 4.3. Average cluster volumes obtained from the AFM and DLS measurements of samples from the different regions of the ternary phase diagram.

Sample No.	stoichiometric ratio SDS : JR 400	Phase diagram area	Average particle volume nm^3	
			AFM	DLS
15	0.77 : 1	1	8000	300000
27	3.07 : 1	4	24000	38000
9	17.4 : 1	3	3700000	4560000

Two examples of direct size comparisons for the samples 9 (redissolution area) and sample 27 (highly diluted area) are represented in Figures 4.25 and 4.26.

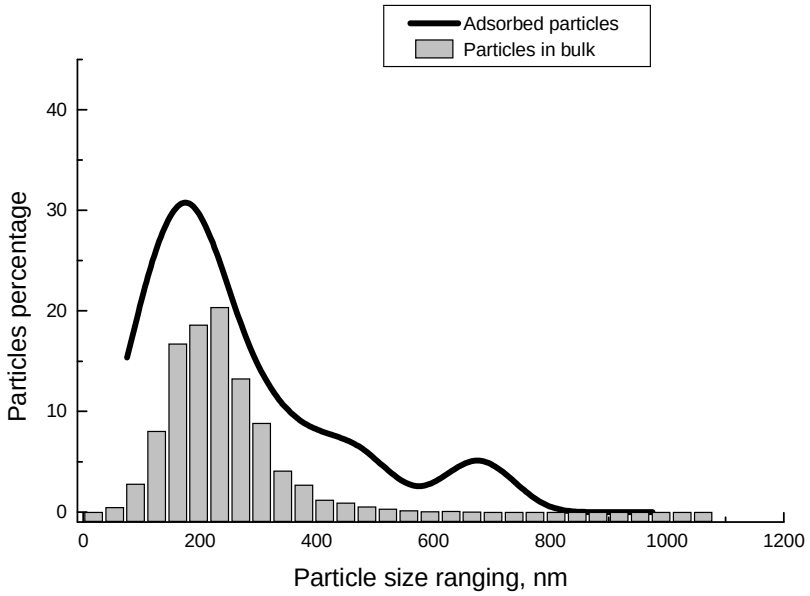

Figure 4.25 – Statistical distribution of cluster sizes in the resolubilisation area of the ternary phase diagram (sample 9) measured by DLS (column graph) and by AFM imaging (line graph, particle diameters are recalculated from the volumes).

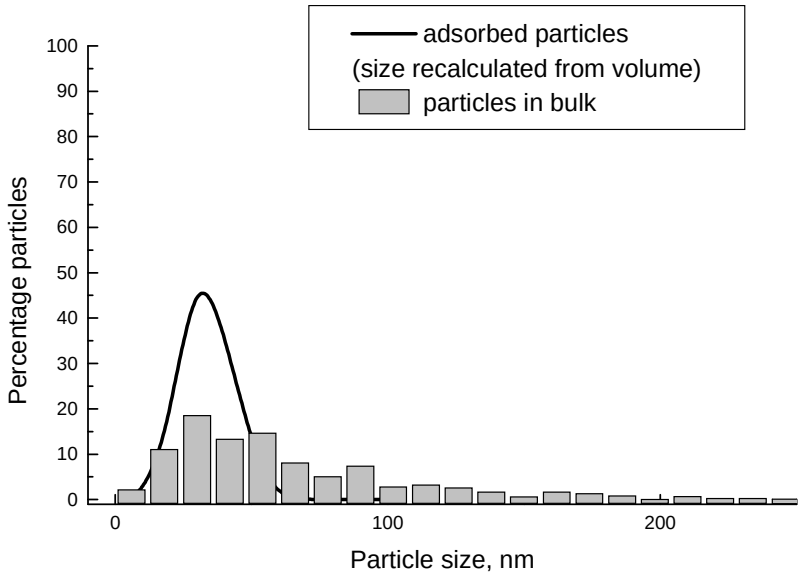

Figure 4.26 – Statistical distribution of cluster sizes in the area of high dilution of the ternary phase diagram (sample 27) measured by DLS (column graph) and by AFM imaging (line graph, particle diameters are recalculated from the volumes).

The differences in the cluster volumes between the mixtures in bulk and adsorbed mixtures vary depending on the mixture composition. As seen from the Table 2, this difference may reach more than one order of magnitude in case of the pre-precipitation area of the ternary phase diagram (sample 15). The most probable explanation for this particular case is that, at low SDS concentrations, a large amount of SDS-free polymer backbone and its loopings is present in the adsorbed mixture. These loose and flexible molecules are not observed in AFM measurements due to their extreme softness and therefore do not contribute to the particle size being imaged, while in DLS these SDS-poor structures are observed.

The particle flattening that occurs during adsorption must be considered, together with the method limitations and the limited statistics when comparing the particle volume data obtained by AFM with the DLS data. Consequently, caution should be exercised when interpreting the particle volumes in quantitative terms.

4.2.3 Changes of the adsorbed mixture as a result of changes in the solution composition

Two series of “washing-off” experiments were performed to investigate possible desorption of adsorbed structures which can be caused by an increase of surfactant/polymer stoichiometric ratio. AFM images were taken and force-distance curves acquired on the hydrophobized silica surface during subsequent change of the composition of solution contained in the fluid cell.

The samples selected for this study are listed in Table 4.4 and presented according to their position on the ternary phase diagram in Figure 4.27. While preparing these experimental series, a special attention was paid to the stoichiometric ratio of components. In addition to these samples, pure working solutions of JR400 Polymer and SDS were used. To demonstrate the desorption of the polymer layer under the influence of relatively high concentrations of SDS a different solution with a 5 times higher SDS concentration was used in the final part of the first series (0.5 wt%, corresponding to approximately 2×cmc of SDS). Such a desorption has been repeatedly reported by many groups [16, 29]. However, no information concerning this desorption phenomenon at high dilutions is available. This is why we investigated how to “wash off” completely or partially the adsorbed layer by increasing polymer-surfactant ratio.

Table 4.4 SDS-JR400 mixtures chosen for washing-off experiments

Sample No.	final concentration, w/w%		Mass portion of working solution, %		stoichiometric ratio SDS : JR 400
	SDS	JR400	SDS	JR400	
97	0.093	0.00535	92.87	7.13	40:1
85	0.0867	0.001	86.7	13.3	20:1
89	0.0245	0.0566	24.55	75.45	1:1
91	0.014	0.0645	14	86	1:2
92	0.00755	0.06933	7.55	92.45	1:4
93	0.0039	0.0721	3.9	96.1	1:8
95	0.002	0.0735	2	98	1:16

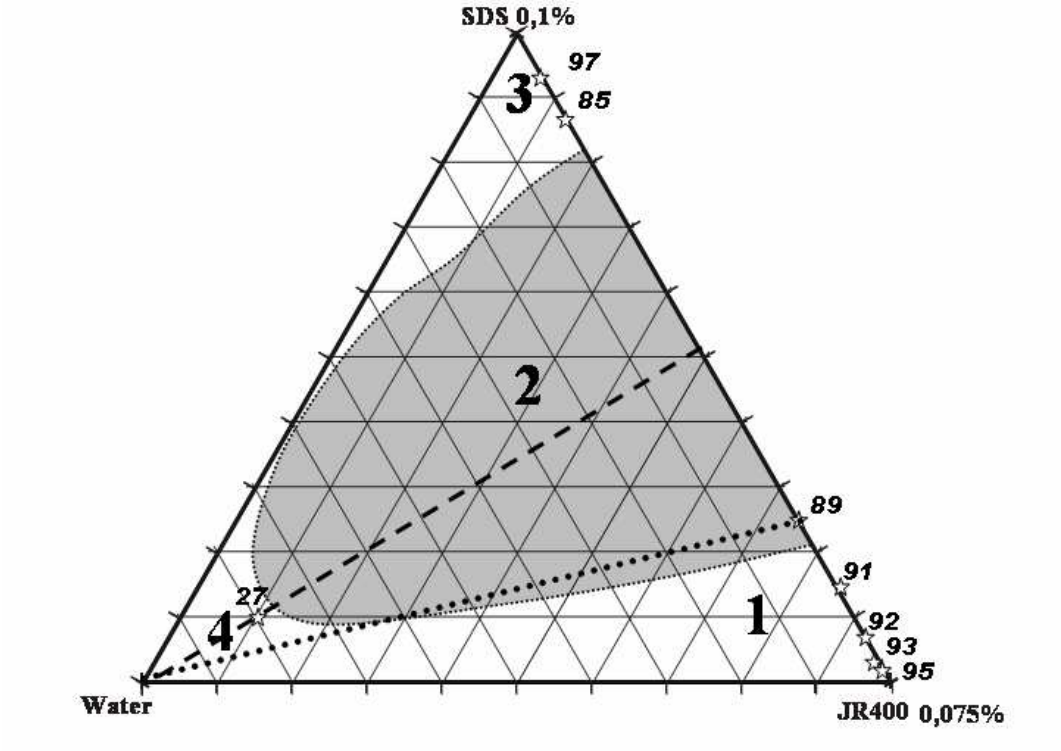

Figure 4.27 – Positions of samples used in the washing-off experiments on the ternary phase diagram.

Schemes of the experimental series are presented in Figure 4.28. The drawings demonstrate the sequence in which the samples with polymer excess were substituted by surfactant-rich samples.

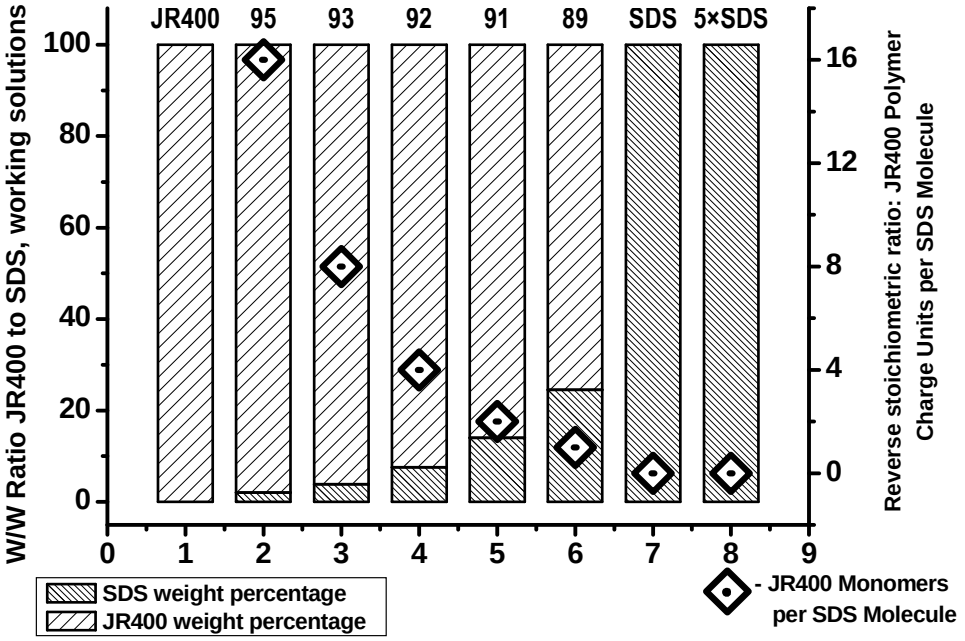

A)

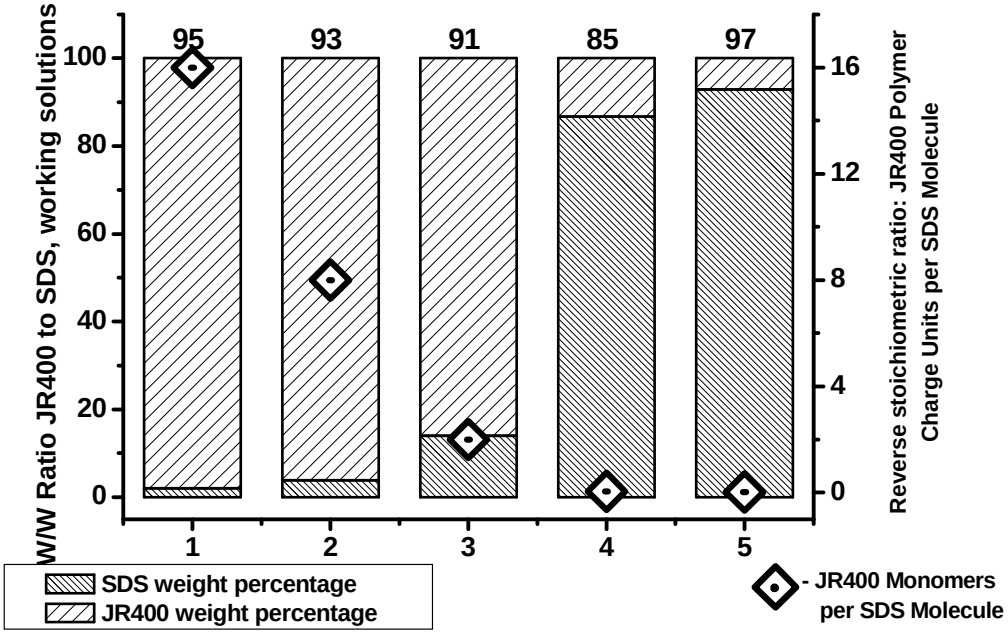

B)

Figure 4.28 – Schematic representation of the order in which sample substitution in "washing-off" experiments occurred. A) in the first series; B) in the second series. The composition of columns reflects the composition of the samples. Diamonds represent the ***reverse*** stoichiometric ratio, i.e. ratio JR400 monomers/SDS.

Injecting a new portion of liquid into the AFM fluid cell causes disturbance and makes it difficult to record a proper image or a meaningful force-distance curve in a reasonable time. It was already noted that sometimes many hours or even days can be needed to reach an equilibrium state in the adsorbed layer [29]. Not every composition could be imaged successfully, and not in every case one can be sure that the results are free of artefacts caused e.g. by repeated withdrawal and engagement of the cantilever tip or by repeated rinsing of the fluid cell in order to eliminate an air bubble. In some cases optical noise was inevitable. Therefore, caution is needed in the interpretation of results and assessment of their relevance. In some cases images or/and force-distance curves will be omitted or presented after additional computer processing performed to eliminate artefacts.

4.2.3.1 First series

The working solution of JR400 Polymer without any additions or dilution was imaged on the hydrophobized mica surface. The adsorbed layer formed on the surface was thin, slightly viscous and homogeneous, i.e. without any structures. Scratching did not cause any remarkable changes for any sufficient time. This characteristic feature is illustrated in Figures 4.29 and 4.30.

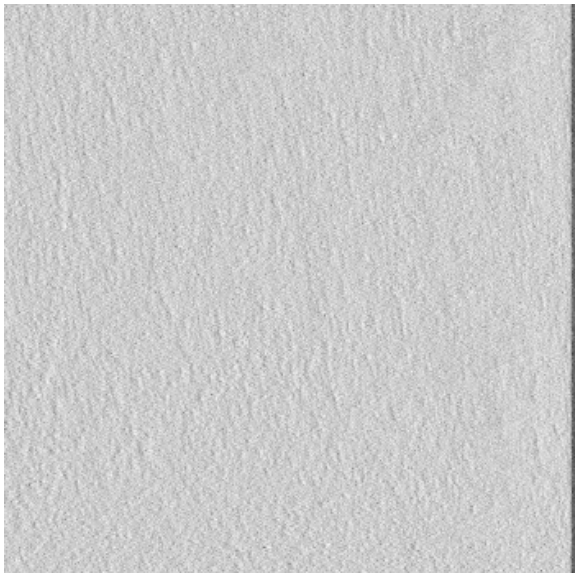

Figure 4.29 – 1×1 μm^2 AFM deflection image of the working solution of JR400 Polymer adsorbed at the hydrophobized silica surface.

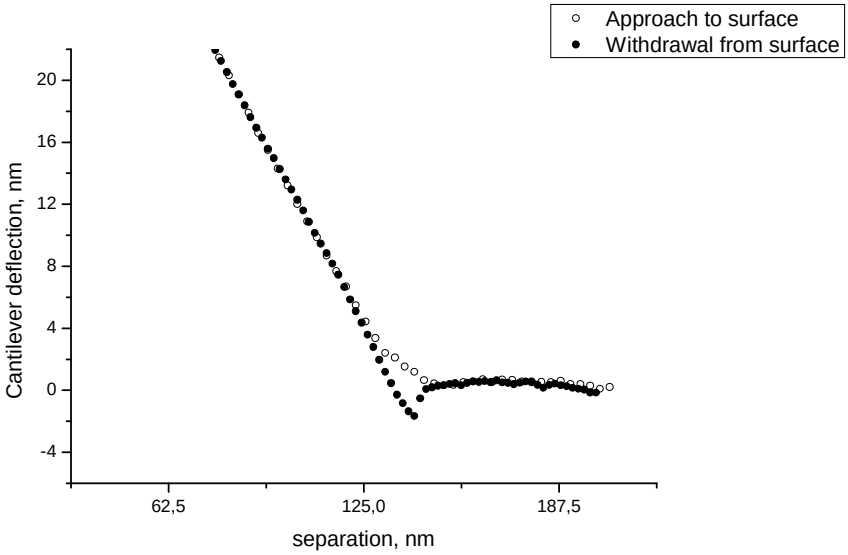

Figure 4.30 – Force-distance curve acquired in the adsorbed layer of the working solution of JR400 Polymer at the hydrophobized silica surface. The right hand part of the curve is omitted due to remarkable optical noise artefacts.

95 → 93

The next sample injected was the Sample 95. No sufficient changes could be observed or distinguished from artefacts. The sample 93 was injected. It is illustrated in Figures 4.31 and 4.32. The image presented was taken immediately after scratching. The scratched area in the right hand bottom part of the image is distinguishable only after a remarkable increase of the image contrast.

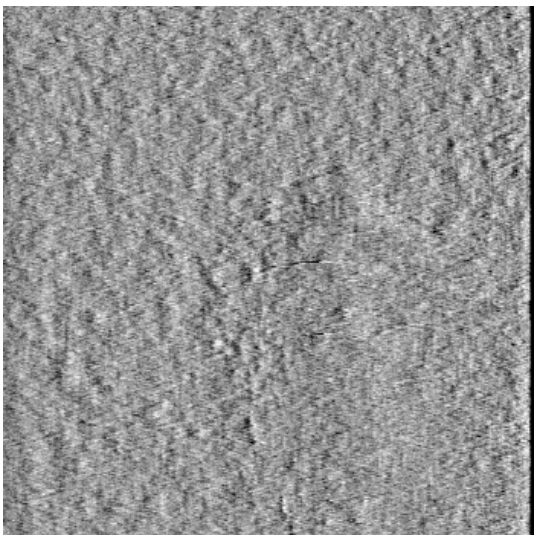

Figure 4.31 – 5×5 μm^2 AFM deflection image of the working solutions of SDS (3,9%) and JR400 Polymer (96,1%), composition point 93 from Figure 4.27 adsorbed at the hydrophobized silica surface in the sequence shown in Figure 4.28 A).

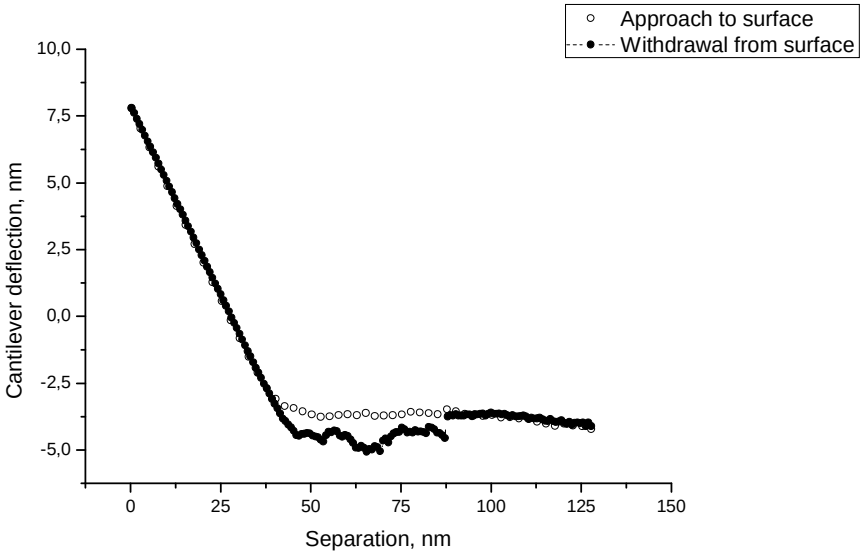

Figure 4.32 – Force-distance curve acquired in the adsorbed layer of the working solutions of SDS (3,9%) and JR400 Polymer (96,1%), composition point 93 from Figure 4.27 adsorbed at the hydrophobized silica surface in the sequence shown in Figure 4.28 A).

After injection of the sample 93, we can see that the adsorbed layer becomes thicker, very viscous and stable against mechanical treating. The first two properties are indicated by the force-distance curve. The curves obtained inside and outside the scratched area were similar. The stability of the layer is seen from the fact that scratching left practically no traces.

93 → 92

Sample 93 was displaced by sample 92. This was the first sample that demonstrated significant difference compared to the previous composition: The adsorbed layer did change during scratching. Nevertheless, the scratching traces were very unstable and disappeared after a few scans. The force-distance curves showed an interesting pattern of multiple deflections, i.e. the cantilever was subject to attractive forces more than one time while withdrawing from the surface. This, together with a further increase of the layer thickness indicates the presence of single polymer chains [138], that is, a beginning structuring of the polymer layer. This description is illustrated in Figures 4.33 and 4.34. Images 4.33 A and B were taken one after another after 5 minutes of scratching with the scan rate of 60 Hz. This made approximately 30 cycles of scratching. Immediately after scratching the image 4.33

A was taken with the scan rate of 5 Hz. This continued 102 seconds and was immediately followed by taking the image 4.33. B.

Figure 4.33 – 5×5 μm^2 AFM deflection images of the working solutions of SDS (7.55%) and JR400 Polymer (92.45%), composition point 92 from Figure 4.27 adsorbed at the hydrophobized silica surface in the sequence shown in Figure 4.28 A).

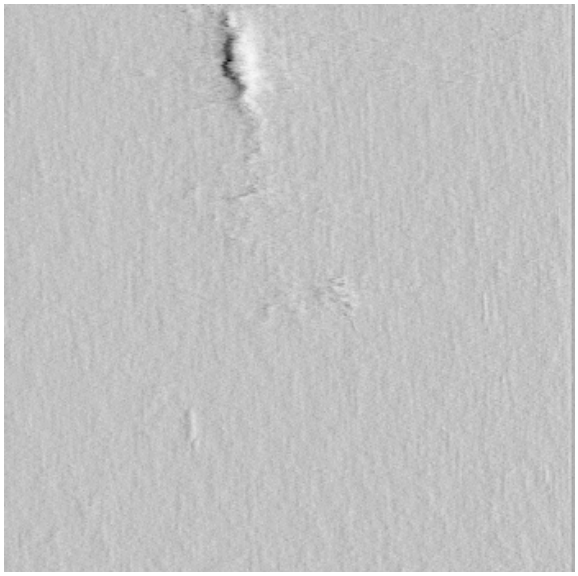

A) Immediately after scratching. The scratching trace (layer gathered to a ”hill”) is seen in the top part of the image.

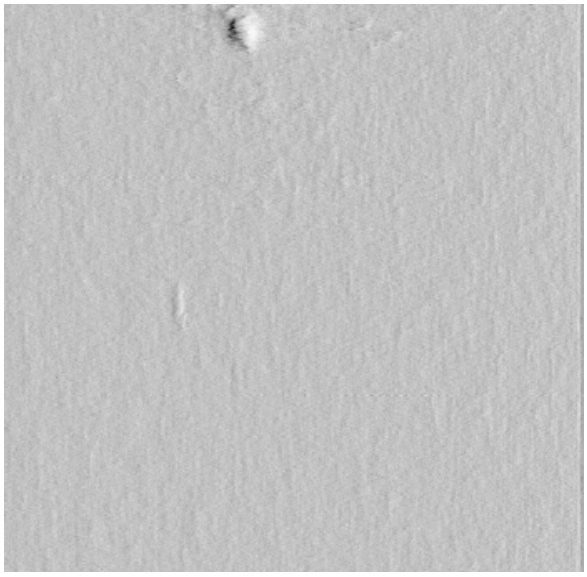

B) After 100 seconds of scanning. The “hill” is significantly smoothed out.

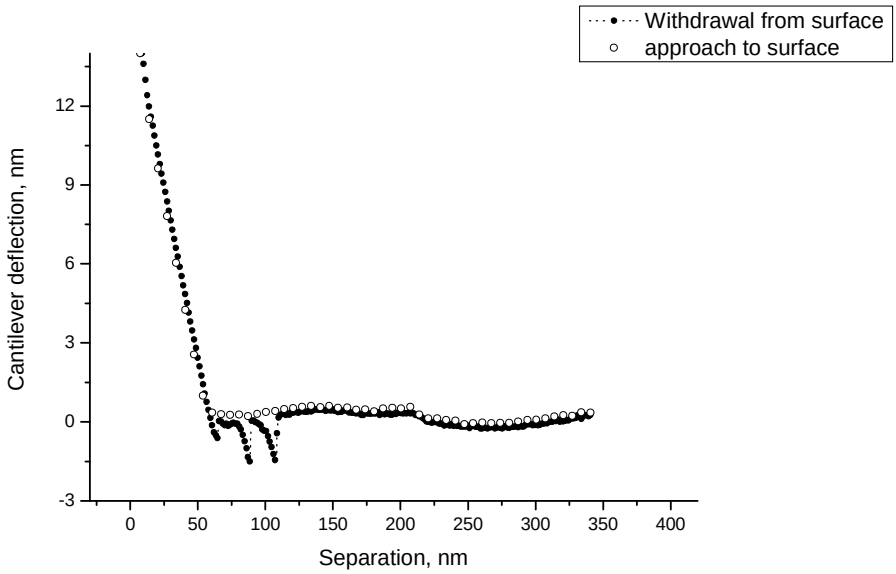

Figure 4.34 – Force-distance curve acquired in the adsorbed layer of the working solutions of SDS (7.55%) and JR400 Polymer (92.45%), composition 92 from Figure 4.27 adsorbed at the hydrophobized silica surface in the sequence shown in Figure 4.28 A). For explanation of the multiple cantilever deflections see the text.

92 → 91

After sample 91 with stoichiometric ratio SDS/JR400 of 1:2 was injected, some indications of structure formation in the adsorbed layer could be observed. This is illustrated in Figure 4.35.

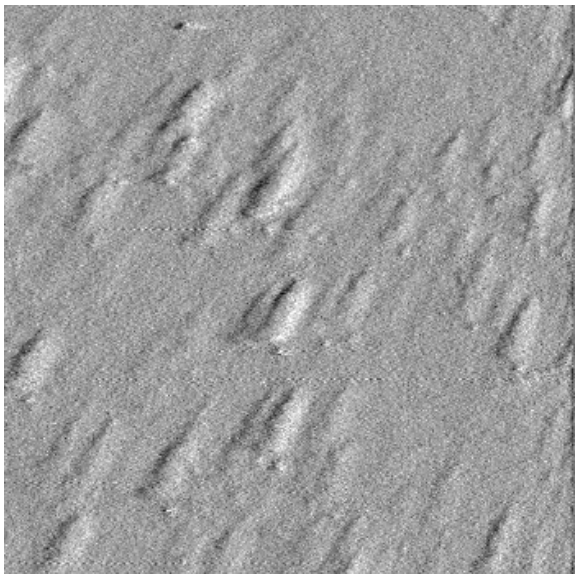

Figure 4.35 – 1×1 μm^2 AFM deflection image of the working solutions of SDS (14%) and JR400 Polymer (86%), composition 91 from Figure 4.27 adsorbed at the hydrophobized silica surface in the sequence shown in Figure 4.28 A). The elongated form of structures is an artefact.

After scratching, the substance seems to be much more stable than in mixtures with higher polymer-surfactant ratios. The structures formed by scratching cannot be smoothed out so easy as in previous images.

Figure 4.36 – 5×5 μm^2 AFM deflection images of the working solutions of SDS (14%) and JR400 Polymer (86%), composition 91 from Figure 4.27 adsorbed at the hydrophobized silica surface in the sequence shown in Figure 4.28 A). Images A and B were taken with an interval of 3 minutes one after another after 5 minutes of scratching.

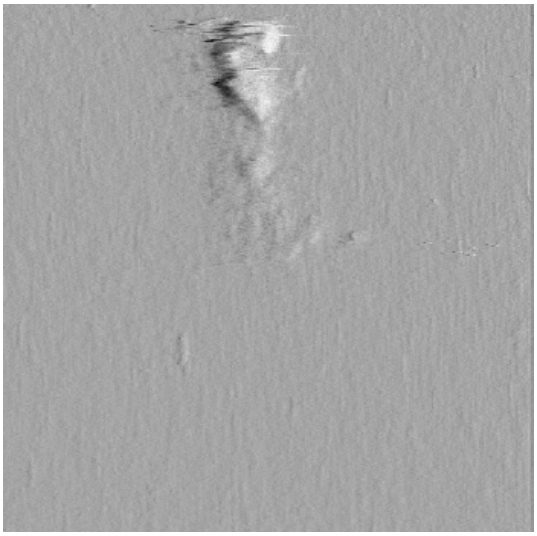

A) Immediately after scratching. The scratching trace (layer gathered to ”hills”) is seen in the top part of the image.

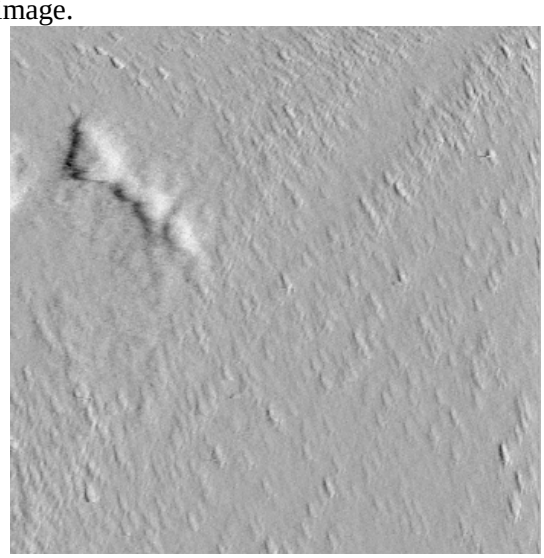

B) After 200 seconds of scanning. Image acquired in 45^o rotated position to verify the structure truth. The elongated form of structures is an artefact.

The force-distance curve shows some decrease in layer thickness and viscosity. Furthermore, the layer acquired some homogeneity, in contrast to the previous

sample. This, together with other features described above, can be indicative of a beginning transition to the formation of dense aggregates that could lead to an onset of precipitation in the bulk solution. This assumption can be supported by the DLS data from measurements performed on sample 45 with a stoichiometric ratio of the components very similar to sample 91(section 4.1.2.1). That mixture shows transition accomplishment from “disordered” state to “ordered”, which again suggests the similar transition in the present sample.

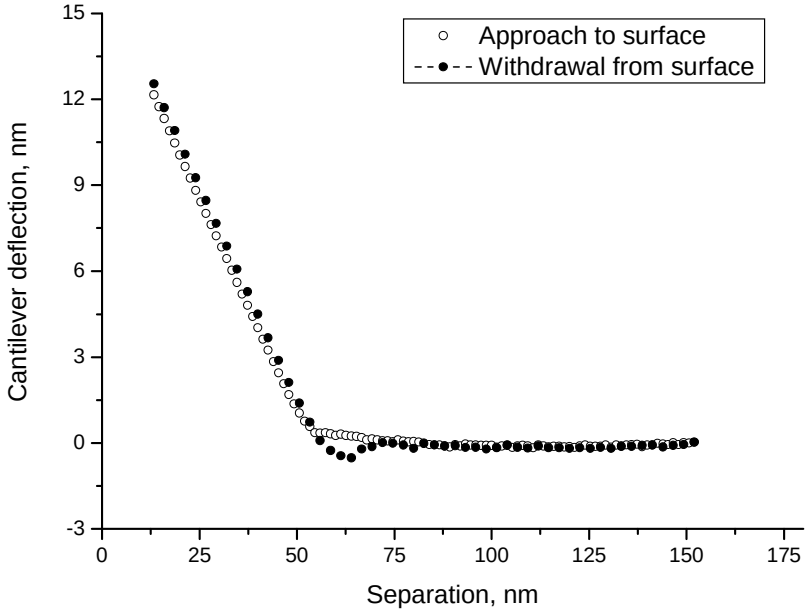

Figure 4.37 – Force-distance curve acquired in the adsorbed layer of the working solutions of SDS (14%) and JR400 Polymer (86%), composition 91 from Figure 4.27 adsorbed at the hydrophobized silica surface in the sequence shown in Figure 4.28 A).

91 → 89

The transition to the mixture with components stoichiometric ratio of theoretical maximum precipitation brought too much artefacts in images: the solution injected into the fluid cell was simply turbid. This caused increased difficulty of taking the images and finally prevented capturing of any artefact-free images of this sample. Nevertheless, informative force-distance curves could be obtained, like those shown in Figure 4.38. one of the curves acquired immediately after mixture injection suggest the further indications of single polymer chain extension. This could mean a further structuring of the adsorbed layer: the aggregates become separated from one another, the tip contact to the single chains becomes more frequent.

Figure 4.38 – Force-distance curves acquired in the adsorbed layer of the working solutions of SDS (24,55%) and JR400 Polymer (75,45%), composition 89 from Figure 4.27 adsorbed at the hydrophobized silica surface in the sequence shown in Figure 4.28 A).

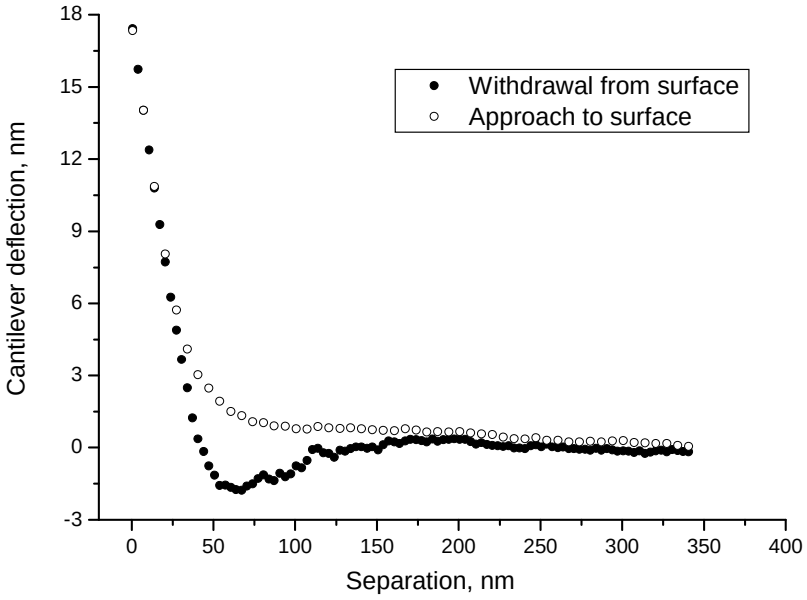

A) Typical view of force-distance curve for this composition

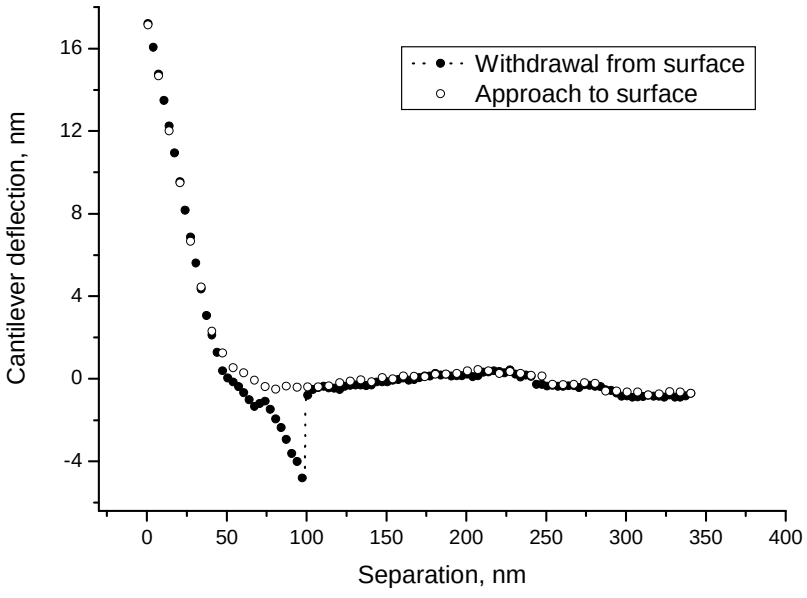

B) single polymer chain extension. “Waves” in the right hand part of the curve are and artefact.

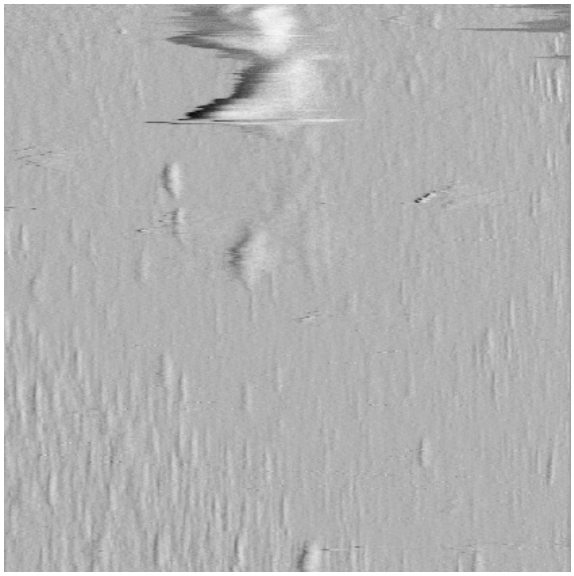

Figure 4.39 – 5×5 μm^2 AFM deflection image of the working solutions of SDS (24,55%) and JR400 Polymer (75,45%), composition 89 from Figure 4.27 adsorbed at the hydrophobized silica surface in the sequence shown in Figure 4.28 A). The elongated form of structures as well as (partially) spreading of the gathered "hill" in the top part of image are artefacts.

In general, the mixture No. 89 injected in the fluid cell exerts a moderate influence on the adsorbed layer. Multiple clusters begin to form, although this process takes a very long time. The image acquired after "scratching" and presented in Figure 4.39 shows only a small increase in cluster size and amount.

89→ SDS→ 5SDS

Injection of pure SDS solution caused dramatic changes in the cell especially multiple artefacts and a very long equilibration time. After 2 hours of equilibration some changes could be observed, like remarkable softness of the polymer film: even "holes" could be easily "dug" in the adsorbed layer by simple "scratching". Unfortunately, the changes were not very pronounced and seen only in a few cases.

Really significant changes occurred after rinsing of the fluid cell with the 5 times more concentrated working solution of SDS (0,5 wt%). The scan in Figure 4.40 and

the force-distance curve in Figure 4.41 show interesting features: A scratched area is clearly seen in the top part of the scan. The clusters adsorbed at the surface are well formed, well distinguishable and rigid. The thickness of the adsorbed layer assessed with the help of the force-distance curve became almost negligibly small although no "jump in contact" with the underlying surface could be observed as a rule. In brief, the adsorbed layer became similar to those of mixtures of much higher stoichiometric ratio surfactant/polymer on the hydrophobized silica surface. This could be interpreted like a gradual displacement of polymer by surfactant and formation of micelle-like clusters in the adsorbed layer.

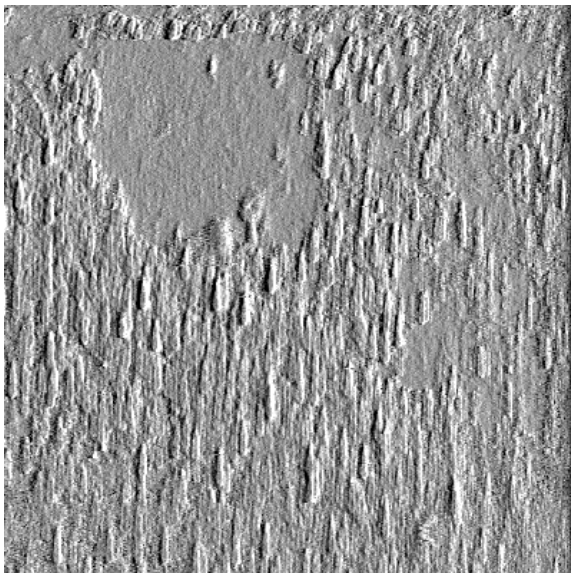

Figure 4.40 – 5×5 μm^2 AFM deflection image of a polymer-surfactant layer adsorbed at the hydrophobized silica surface in the sequence shown in Figure 4.28 A) after repeated rinsing with 0,5 wt% solution of SDS. The elongated form of structures in the bottom half of the image is an artefact – only transversal size is relevant. The plane scratched area is clearly seen in the top part of the image.

It is interesting that the structures presented in Figure 4.40 are of large size resembling complexes adsorbed from surfactant rich mixtures (compare Figure 4.23 A).

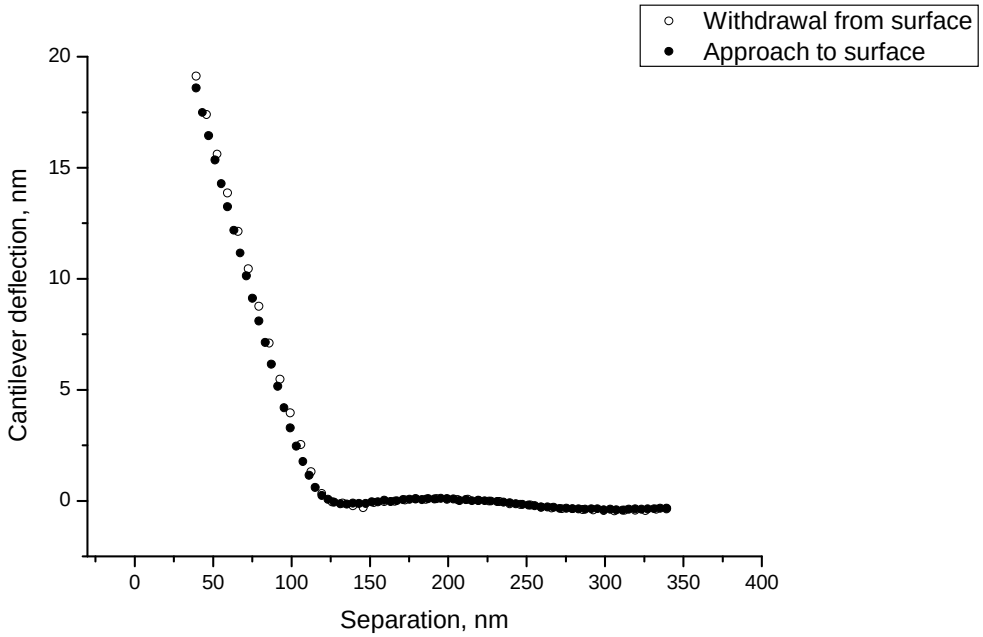

Figure 4.41 – Force-distance curve acquired in the polymer-surfactant layer adsorbed at the hydrophobized silica surface in the sequence shown in Figure 4.28 A) after repeated rinsing with 0,5 wt% solution of SDS.

4.2.3.2 Second series

The second series of "washing-off" investigations was performed to obtain some additional information concerning especially the processes occurring at compositions very close to the precipitation – in the pre-precipitation and (more important) in resolubilisation the area. It was attempted to avoid turbidity, artefacts, and distortions occurred in the first series of measurements. Two surfactant rich mixtures were applied in the second series. They deliver some more interesting features presented here.

The second difference as compared to the first series was that no pure polymer solution was injected at the very beginning. This could explain slower equilibration and less expressed structures in the surfactant-rich samples: no preadsorbed polymer layer is present that could act as a sort of "lubricant" between adsorbing polymer-surfactant complexes and the underlying surface, thus facilitating transformations. The order of the sample substitution in this series is presented in Figure 4.28, B. The data acquired at imaging of samples 95, 93 and 91 did not significantly differ from

those obtained in the first series of substitution experiments. Therefore, only the results from the surfactant-rich mixtures are presented I this section.

Figure 4.42 – 5×5 μm^2 AFM deflection image of the working solutions of SDS (86,7%) and JR400 Polymer (13,3%), composition 85 from Figure 4.27 adsorbed at the hydrophobized silica surface in the sequence shown in Figure 4.28 B).

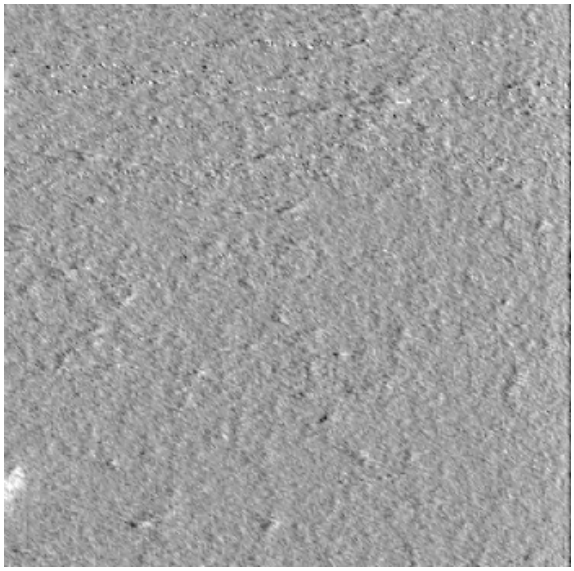

A) Image obtained immediately after sample injection. No structures are seen

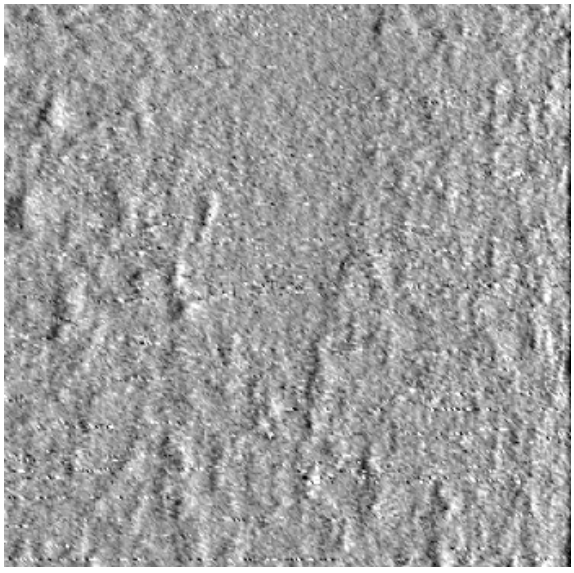

B) Image scanned after 45 min of equilibration and 5 minutes of scratching. The scratched area is seen in the upper part of the scan. Some structures are suggested in the adsorbed layer.

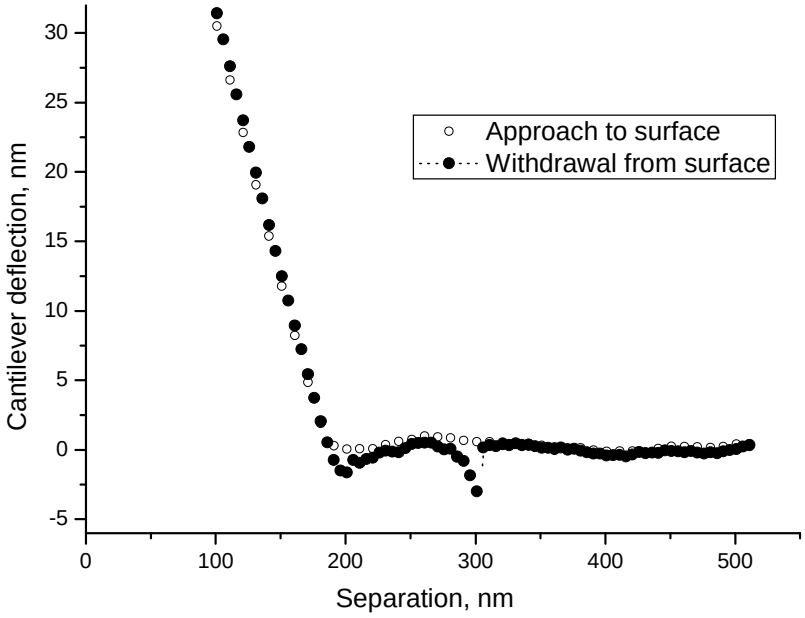

Figure 4.43 – Force-distance curve acquired in the adsorbed layer of the working solutions of SDS (86,7%) and JR400 Polymer (13,3%), composition 85 from Figure 4.27 adsorbed at the hydrophobized silica surface in the sequence shown in Figure 4.28 B).

Both images and the force-distance curve indicate the presence of a thick (up to 100 nm), soft adsorbed layer containing both polymer and surfactant.

85 → 97

The sample 97 added into the fluid cell causes changes in the adsorbed layer similar to those caused by SDS in the first series of washing-off measurements (compare images 4.45 and 4.40). This influence, however, is moderate. Just after injection, as well as after scratching, the situations are similar to that with sample 85: thick and relatively homogeneous layer immediately after injection, and increasing stiffness and evidence of structures after some equilibration time.

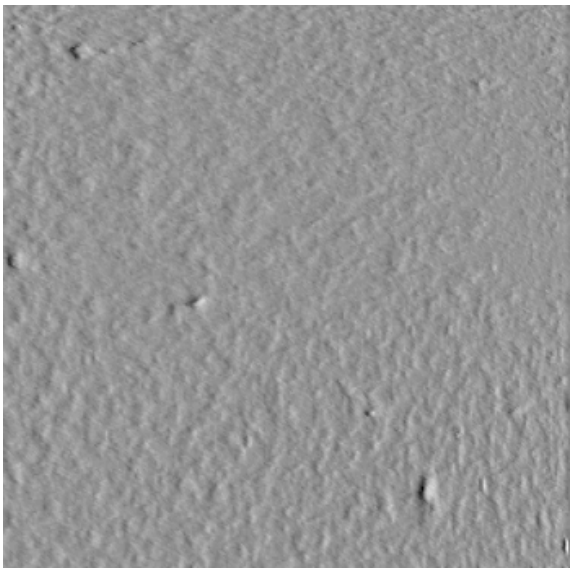

Figure 4.44 – 10×10 μm^2 AFM deflection image of the working solutions of SDS (92,87%) and JR400 Polymer (7,13%), composition 97 from Figure 4.27 adsorbed at the hydrophobized silica surface in the sequence shown in Figure 4.28 B). Image acquired before scratching.

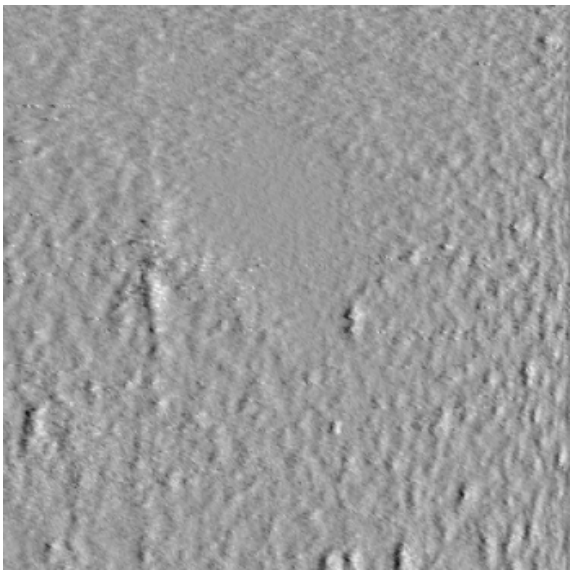

Figure 4.45 – 8×8 μm^2 AFM deflection image of the working solutions of SDS (92,87%) and JR400 Polymer (7,13%), composition 97 from Figure 4.27 adsorbed at the hydrophobized silica surface in the sequence shown in Figure 4.28 B). Image acquired immediately after 5 minutes of scratching.

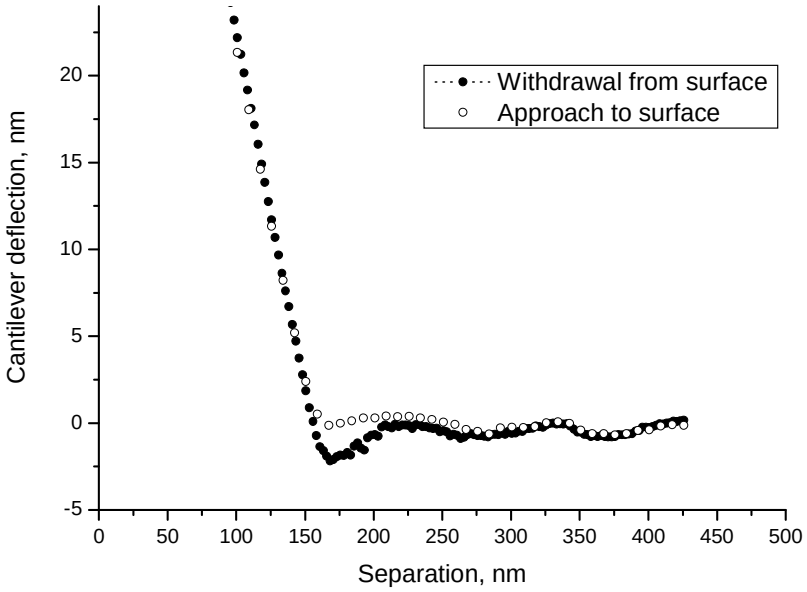

Figure 4.46 – Force-distance curve acquired in the adsorbed layer of the working solutions of SDS (92,87%) and JR400 Polymer (7,13%), composition 97 from Figure 4.27 adsorbed at the hydrophobized silica surface in the sequence shown in Figure 4.28 B). The "wave" form of the right hand part of the curve is an artefact.

A brief summary of washing-off investigations can be presented as follows. If the solution composition changes, the adsorbed layer undergoes changes similar to those in bulk, but with a remarkable time gap. These processes in adsorbed layer have been investigated and reported by Shubin, Horn, Goddard, Holmberg [16, 17, 36, 136] and many other researchers at different conditions and mostly at higher polymer or, more often, surfactant, concentrations [48-50]. Our results suggest that similar polymer-surfactant arrangements take place at low concentrations, too.

CHAPTER 5. SUMMARY AND CONCLUSIONS

The properties of structures formed by polymer-surfactant mixtures containing the anionic surfactant SDS and the cationic polymer JR400 were studied in the bulk solution using DLS and during adsorption at solid-liquid interfaces using AFM. The mixtures were studied in a broad range of the component concentrations: the surfactant concentration to 0,4 × CMC of the pure surfactant, the polymer concentration did not exceed 0,075 wt/wt%. The mixed system was studied both below and above the CAC and the PSP. The range of theoretical stoichiometric ratios between surfactant molecules and polymer charge units was from 0.18 to 58.17.

The ternary phase diagram was established exhibiting three most interesting regions: pre-precipitation area of modified viscosity (polymer excess, below the CAC), post-precipitation area (resolubilisation at surfactant excess, above the PSP), and highly diluted samples with stoichiometrical surfactant-polymer ratio close to that of maximum precipitation. DLS measurements were performed in mixtures representing all three regions of the diagram.

Soft-contact AFM imaging was used to visualize the structure of the adsorbed layer, while acquirement of the force-distance curves together with the special scratching treatment brought information about the mechanical properties of the layer. AFM studies included:

Investigation of the composition (indirect data) of the adsorbed layer formed on the same substrate by mixtures of different compositions prepared prior to adsorption.

Investigation of the mechanical and adhesive properties of the adsorbed layer formed by the mixtures of the same composition, prepared prior to adsorption, at different substrates: native mica, hydrophobized mica and hydrophobized silica.

Investigation of the changes in the adsorbed layer caused by changes in the bulk solution.

Investigation of the visual picture of the adsorbed layer formed by the systems of the same or similar composition, prepared prior to adsorption, at different substrates: native mica and hydrophobized silica.

Comparison of the sizes of the micelle-like clusters in the bulk solution, obtained during the DLS measurements, with the sizes of the clusters observed on the AFM images of the adsorbed layer from the solutions of mixtures with corresponding compositions.

The micelle-like clusters in the mixtures of different compositions showed different sizes and, more important, different size uniformity increasing with the increasing polymer-surfactant ratio.

Polymer-rich mixtures adsorbed readily at all kinds of surfaces used in this work. The adsorption of highly diluted mixtures with the polymer-surfactant ratio close to that of experimentally observed precipitation maximum depended significantly on the surface properties: the higher the negative charge and hydrophilicity of the surface, the stronger the adsorption. Surfactant-rich mixtures hardly adsorbed to mica and moderately – to the hydrophobized silica.

During the "washing-off", or substitution, experiments performed on the hydrophobized silica surface a dependence between the structure of the adsorbed layer and the composition of the bulk phase could be observed. An increase of SDS/JR400 ratio lead first to the thickening of the adsorbed layer together with its structuring and formation of the micelle-like clusters in it, and then to the partial desorption from the surface with the further layer structuring.

Following conclusions could be drawn from the investigations:

1. The adsorption of the SDS-JR400 system at the negatively charged interfaces is driven mostly by the polymer affinity to the surface. SDS molecules adsorb together with the polymer chains to which they are bound.
2. In the SDS-JR400 system prepared prior to adsorption the size of micelle-like clusters measured in the bulk is comparable to the size of adsorbed structures. The clusters seem to undergo only minor or no changes during adsorption of polymer-surfactant mixtures at mica and silica.
3. If the polymer and the surfactant have been mixed prior to adsorption the visual adsorption pattern does not depend on the surface properties: it is the same at freshly cleaved mica and at hydrophobized silica.
4. However, the surface has an influence on the properties of the adsorbed mixture: its adhesion to freshly cleaved mica is stronger than to the hydrophobized mica, and the adsorption to the hydrophobized mica surface is in turn stronger than to hydrophobized silica. A possible explanation could be the role of the electrostatic attraction and the thickness of the hydrophobizing layer.
5. The properties of adsorbed layer are prone to changes following those in the composition in the bulk solution. This occurs also at low polymer and surfactant concentrations. The changes are slow and can be visualized only under special treatment of the adsorbed layer.

6. The role of the adsorption substrate is, therefore, to form the adsorbed layer – the space with the increased concentration of both components. Most of the properties of this layer are, however, governed by the mixture composition in the bulk solution.

This study brings a further contribution to the understanding of properties of the mixtures of cationic polymers and anionic surfactants both in the bulk solution and in adsorbed state. It shows the prevalence of solution composition in defining the adsorption pattern of the pre-mixed systems. The correctness of the model of co-operative adsorption of S^-P^+ systems is confirmed for the broad range of stoichiometric ratios and especially for high dilutions. The reasons of the role played by the order of addition of components that was highlighted by previous studies [29, 137] is shown.

LITERATURE

(1) Maruta, I. *Nippon Kagaku Zasshi* **1962**, *83*, 782.
(2) Verezhnikov, V.N., Vlasova, L.V., Neiman, R.E. *Kolloidn. Zh.* **1966**, *28*, 328.
(3) Holmberg, C., Nilsson, S., Sundeloef, L.-O. *Langmuir* **1997,** *13*, 1392.
(4) Ridell, A., Evertsson, H., Nilsson, S. *J. Colloid Interface Sci.* **2002**, *247*, 381.
(5) Cosgrove, T., Mears, S.J., Obey, T., Thompson, L., Wesley, R.D. *Colloids Surf. A* **1999**, *149*, 329.
(6) Lindman, B. In *Handbook of Applied Surface and Colloid Chemistry*; Holmberg, K., Ed., John Wiley & Sons Ltd., Chichester, UK, 2002, Vol. 1.
(7) Groot, R.D., *Langmuir* **2000,** *16*, 7493.
(8) Goddard, E.D., Hannan, R.B, *J. Colloid Interface Sci.* **1976**, *55*, 73.
(9) Yamaguchi, Y., Inaba, Y., Uchiyama, H., Kunieda, H. *Colloid Polymer Sci.* **1999**, *277*, 1117.
(10) Chronakis, I.S., Alexandridis, P. *Macromolecules* **2001**, *34*, 5005.
(11) Regismond, S.T.A., Winnik, F.M., Goddard, E.D. *Colloids Surf. A: Physicochem. Eng. Aspects* **1996**, *119*, 221.
(12) Regismond, S.T.A., Winnik, F.M., Goddard, E.D. *Colloids Surf. A: Physicochem. Eng. Aspects* **1998**, *141*, 165.
(13) Regismond, S.T.A., Gracie, K.D., Winnik, F.M., Goddard, E.D. *Langmuir* **1997,** *13*, 5558.
(14) Regismond, S.T.A., Heng, Y.-M., Goddard, E.D., Winnik, F.M. *Langmuir* **1999,** *15*, 3007.
(15) Shubin, V., Petrov, P., Lindman, B. *Colloid Polymer Sci.* **1994**, *272*, 1590.
(16) Shubin, V. *Langmuir* **1994,** *10*, 1093.
(17) Goddard, E.D. *Colloids Surf.* **1986**, *19*, 301.
(18) Arnold, G.B., Breuer, M.M. *Colloids Surf.* **1985**, *13*, 103.
(19) Agrillier, J.F., Ramachandran, R., Harris, W.C., Tirrell, M. *J. Colloid Interface Sci.* **1991**, *146*, 242.
(20) Karaman, M.E., Meagher, L., Pashley, R.M. *Langmuir* **1993,** *9*, 1220.
(21) Senden, T.J., Drummond, C.J., Kékicheff, P. *Langmuir* **1994,** *10*, 358.
(22) Biggs, S., Mulvaney, P. ACS Symp. Ser. **1995**, *615*, 255.
(23) Patrick, H.N., Warr, G.G., Manne, S.A., Aksay, J.A. *Langmuir* **1997,** *13*, 4349.
(24) Schmitt, R.L., Goddard, E.D. *Cosmetics & Toiletries* **1994**, *109*, 83, 86-88, 93.
(25) Lam, S., Hellgren, A.C., Sjoberg, M., Holmberg, K., Schoonbrood, H.A.S., Unzue, M.J., Asua, J.M., Tauer, K., Sherrington, D.C., Goni, A.M. *J. Appl. Polymer Sci.* **1997**, *66*, 187.
(26) Zou, S., Zhang, W., Zhang, X., Jiang, B. *Langmuir* **2001,** *17*, 4799.
(27) Fleming, B.D., Wanless, E.J., Biggs, S. *Langmuir* **1999,** *15*, 8719.
(28) Fleming, B.D., Wanless, E.J. *Microscopy and Microanalysis* **2000**, *6.* 104.
(29) Dedinate, A., Claesson, P.M., Bergstroem, M. *Langmuir* **2000,** *16*, 5257.
(30) Sakai, K., Yoshimura, T., Esumi; K. *Langmuir* **2003,** *19*, 1203.
(31) Braem, A.D., Biggs, S., Prieve, D.C., Tilton, R.D. *Langmuir* **2003,** *19*, 2736.
(32) Hair, M.L., Hertl, W. *J. Phys. Chem.* **1969**, *73*, 2372.
(33) Hair, M.L., Tripp, C.P. *Colloids Surf. A* **1995**, *105*, 95.
(34) Sherman, R., Hirt, D., Vane, R. *Journal of Vac. Sci. & Tech. A* **1994**, *12*, 1876.
(35) Chari, K. *J. Phys. (Paris) II* **1995**, *5*, 1421.

(36) Horn, D., Klingler, J., Schorf, W., Graf, K. *Progress in Colloid & Polymer Science* **1998**, *111*, 27.
(37) Rawl, A. *Basic Principles of Particle Size Analysis*, www.malvern.co.uk
(38) Nilsson, S., Holmberg, C., Sundeloef, L.-O. *Colloid Polymer Sci.* **1995**, *273*, 83.
(39) Sjostrom, J., Piculell, L. *Colloids Surf. A* **2001**, *183-185*, 429.
(40) Kjoniksen, A.-L., Nystroem, B., Lindman, B. *Langmuir* **1998,** *14,* 5039.
(41) Somasundaran, P., Cleverdon, J. *Colloids Surf.* **1985**, *13*, 73.
(42) Joabsson, F., Lindman, B. *Progress in Colloid & Polymer Science* **2000**, *116*, 74.
(43) Cosgrove, T., Mears, S.J; Thompson, L., Howell, I. *ACS Symp. Ser.* **1995**, *615*, 196.
(44) Adamson, A.W., *Physical Chemistry of Surfaces*; 5th ed., John Wiley & Sons: New York, 1990.
(45) Hüttl, G., Heger, K., Klemm, V., Theissig, J., Wagner, W., Müller, E. *Fresenius J. Anal. Chem.* **1999**, *363*, 206.
(46) Bremmel, K.E., Jameson, G.J., Biggs, S. *Colloids Surf. A* **1999,** *155*, 1.
(47) Cleveland, J.P., Schaffer, T.E., Hansma, P.K *Phys. Rev. B* **1995**, *52*, 8692.
(48) Fielden, M.L., Claesson, P.M., Schillen, K. *Langmuir* **1998,** *14*, 5366.
(49) Kjellin, U. R. M., Claesson, P. M., Audebert, R. *J. Colloid Interface Sci.* **1997**, *190*, 476.
(50) Furst, E. M., Pagac, E. S., Tilton, R. D. *Ind. Eng. Chem. Res.* **1996**, *35*, 1566.
(51) Zana, R. *Curr. Opin. Colloid Interface Sci.***1996**, 1, 566.
(52) Rosen, M. J. *CHEMTECH* **1993**, 30-33.
(53) Yang, Ch., Rathman, J.F. *Polymer* **1996**, *37*, 4621.
(54) Manne, S., Schäffer, T. E., Huo, Q., Hansma, P. K., Morse, D. E., Stucky, G. D., Aksay I. A. *Langmuir* **1997,** *13*, 6382.
(55) Big Soviet Encyclopedy, online edition, http://encycl.yandex.ru/, Yandex: Moscow, 2001-2003.
(56) Mushkambarov, N.N. *Physical and colloid chemistry*, Geotar-Med: Moscow, 2000.
(57) Derjaguin, B.V., Landau, L. *Acta Phys. Chim. U.R.S.S.* **1941**, *14*, 633.
(58) Verwey, E.G.W., Overbeek, J.T.G. *Theory of the Stability of Lyophobic Colloids;* Elsevier: New York, 1948.
(59) Israelachvili, J.N. *Intermolecular & Surface Forces*; 2nd ed., Academic Press: London, 1992.
(60) Tanford, C. *The Hydrophobic Effect*; John Wiley & Sons: New York, 1980.
(61) Israelachvili, J.N., Mitchell, D.J., Ninham, B.W. *J. Chem. Soc. Faraday Trans. 2* **1976**, *72*, 1525.
(62) Israelachvili, J.N., Mitchell, D.J., Ninham, B.W. *Biochim. Biophys. Acta* **1977**, *470*, 185.
(63) Mitchell, D.J., Ninham, B.W. *J. Chem. Soc. Faraday Trans. 2* **1981**, *77*, 601.
(64) Magid, L.J., Han, Z., Warr, G.G., Cassidy, M.A., Butler, P.D, Hamilton, W.A. *J. Phys. Chem. B* **1997**, *101*, 7919.
(65) Lee, E.M., Thomas, R.K., Cummins, P.G., Staples, E.J., Penfold, J., Rennie, A.R. *Chem. Phys. Lett.* **1989**, *162*, 196.
(66) Grant, L.M., Tiberg, F., Ducker, W. *J. Phys. Chem. B* **1998**, *102*, 4288.
(67) Wolgemuth, J. L., Workman, R.K., Manne, S. *Langmuir* **2000,** *16*, 3077.
(68) Tadros, T.F. *Surfactants*; Academic Press: London, 1984.
(69) Corkill, J. M., Goodman, J. F., Walker, T., Wyer, J. A. *Proc. Roy. Soc. A* **1969**, *312*, 243.

(70) Rassing, J., Sams, P.J., Wyn-Jones, E. *J. Chem. Soc., Faraday Trans. 2* **1974**, *70*, 1247.
(71) Aniansson, E.A.G., Wall, S.N. *J.Phys.Chem.* **1975**, *79*, 857.
(72) Aniansson, E.A.G., Wall, S.N., Amren, M., Hoffmann, H., Kielmann, I., Ulbricht, W., Zana, R., Lang, J., Tondre, C. *J.Phys.Chem.* **1976**, *80*, 905.
(73) Okubo, T., Kitano, H., Ishiwatari, T., Ise, N. *Proc. Roy. Soc. A* **1979**, *366*, 81.
(74) Aveyard, R. In *Surfactants*; Tadros, T.F., Academic Press: London, 1984, p. 2.
(75) Aveyard, R. In *Surfactants*; Tadros, T.F., Academic Press: London, 1984, p. 153.
(76) Hartley, G.S., *Aqueous solutions of Paraffin Chain Salts;* Hermann and Cie: Paris, 1936.
(77) Shah, S.S., Jamroz, N.U., Sharif, Q.M., : *Colloids Surf. A* **2001,** *178*, 199.
(78) Matsuoka, K., Moroi, Y., Saito, M. *J. Phys. Chem.* **1993**, *97*,13006.
(79) Lindman, B. In *Surfactants*; Tadros, T.F., Academic Press: London, 1984, p. 91.
(80) Missel, P.J., Mazer, N.A., Carey, M.C., Benedek, G.B., in *Solution Behaviour of Surfactants - Theoretical and Applied Aspects, Vol. 2.* Mittal, K. L., Fendler, E. J., Plenum Press: New York, 1982, p.373.
(81) Tamamushi, B., Tamaki, K. Proc. Intern. Congr. Surface Activity, 2nd, London, **1957**, *3*, 449.
(82) Kiraly, Z., Findenegg, G.H. *J. Phys. Chem. B* **1998**, 102, 1203.
(83) Green, R.J., Tasker, S., Davies, J., Davies, M.C., Roberts, C.J., Tendler, S.J.B. *Langmuir* **1997,** *13*, 6510.
(84) Levchenko, A.A., Argo, B.P., Vidu, R., Talroze, R.V., Stroeve, P. *Langmuir* **2002,** *18*, 8464.
(85) Tilberg, F., Landgren, M. *Langmuir* **1993,** *9*, 927.
(86) Levitz, P., Damme, H.V., Keravis, D. *J. Phys. Chem.* **1984**, *88*, 2228.
(87) Singh, P.K., Adler, J.J., Rabinovich, Y.I, Moudgil, B.M. *Langmuir* **2001,** *17*, 468.
(88) Quist, P.-O., Sonderland, E. *J.Colloid Interface Sci.* **1995**, *172*, 510.
(89) Manne, S., Cleveland, J.P., Gaub, H.E., Stucky, G.D., Hansma, P.K. *Langmuir* **1994**, *10*, 4409.
(90) Leung, P.S., Goddard, E.D., Han, C., Glinka, C.J. *Colloids Surf* **1985**, *13*, 47.
(91) Dong, J., Mao, G. *Langmuir* **2000**, *16*, 6641.
(92) Burgess, I., Jeffrey, C. A., Cai, X., Szymanski, G., Galus, Z., Lipkowski, J. *Langmuir* **1999**, *15*, 2607.
(93) Fleer, G. J., Cohen-Stuart, M. A., Scheutjens, J. M. H. M., Cosgrove, T., Vincent, B. *Polymers at Interfaces*; Chapman & Hall: London, 1993.
(94) Jones, R.A.L., Richards, R.W. *Polymers at Surfaces and Interfaces*; Cambridge University Press: Cambridge, 1999.
(95) Kamath, Y.K., Dansizer, C.J., Weigmann, H.D. *J. Appl. Polymer Sci.* **1985**, *30*, 937.
(96) Somasundaran, P., Zhang, L. *Surfactant Science Series* **2000**, *90*, 441.
(97) Harrison, I.M., Meadows, J. Robb, I.D., Williams, P.A. *J. Chem. Soc. Faraday Trans.* **1995**, *91*, 3919.
(98) Howse, J.R., Steitz, R., Pannek, M., Simon, P., Schubert, D. W., Findenegg, G. H. *Phys. Chem. Chem. Phys.* **2001**, *3*, 4044.
(99) Parker, J.L., Claesson, P.M., Cho, D.L., Ahlberg, A., Tidblad, J., Blomberg, E. *J. Colloid Interface Sci.* **1990**, *134*, 449.
(100) Binnig, G., Rohrer, H., *et al.*, *Phys. Rev. Lett.*, **1982** *49*, 57.

(101) Howland, R., Benatar, L. *A Practical Guide to Scanning Probe Microscopy*. TM Microscopes, Sunnyvale , 2000.
(102) Binnig, G., Quate, C.F., Gerber, Ch. *Phys. Rev. Let.t* **1986** *56*, 930.
(103) Butt, H.J., Jaschke, M., Ducker, W. *Bioelectrochem. Bioenerg*. **1995,** *38*, 191.
(104) Shimabayashi, S., Uno, T., Nakagaki, M. *Colloids Surf. A* **1997**, *123-124*, 283.
(105) Vermohlen, K., Lewandowski, H., Narres, H.-D., Schwuger, M. J. *Colloids Surf. A* **2000**, *163*, 45.
(106) Avranas, A., Retter, U., Malasidou, E. *J. Colloid Interface Sci.* **2002**, *248*, 347.
(107) Ducker, W.A., Senden, T.J., Pashley, R.M. *Langmuir* **1992**, *8*, 1831.
(108) Cullen, D.C., Lowe, C.R. *J. Colloid Interface Sci.* **1994**, *166*, 102.
(109) Stipp, S.L.S. *Langmuir* **1996**, *12*, 1884.
(110) Klein, J. *Nature* **1980**, *288*, 248.
(111) Klein, J., Luckham, P. *Nature* **1982**, *300*, 429.
(112) Klein, J. *J. Chem. Soc. Faraday Trans. 1* **1983**, *79*, 99.
(113) Luckham, P., Klein, J. *J. Chem. Soc. Faraday Trans. 1* **1990**, *86*, 1363.
(114) Manne, S; Gaub, H.E. *Science* **1995**, *270*, 1480.
(115) Burgess, I., Zamlynny, V., Szymanski, G., Lipkowski, J., Majewski, J., Smith, G., Satija, S., Ivkov, R. *NIST Special Publication* **2002**, *977* 32-33.
(116) Fadnavis, N., Engberts, J. B. F. N. *J. Am. Chem. Soc.* **1984**, *106*, 2636.
(117) Manne, S., Warr, G.G. In *Supramolecular Structure in Confined Geometries*; Manne, S., Warr, G.G., Ed., ACS: Washington, 1999.
(118) Schnell, E. *Rasterkraftmikroskopie als Methode zur Charakterisierung amphiphiler Strukturen*, PhD Thesis; Regensburg University: Regensburg, 2002
(119) Wanless, E.J., Ducker, W.A. *J. Phys. Chem. B* **1996**, *100*, 3207.
(120) Liu, J.-F., Ducker, W.A. *J. Phys. Chem. B* **1999**, *103*, 8558.
(121) Anguillo, R. A., Thau, P. (Warner-Lambert Co.). U.S. (1974), Patent Application: US 71-203457.
(122) Lindman, B, Thalberg, K. In *Interactions of Surfactants with Polymers and Proteins*, Goddard, E.D. and Ananthapadmanabhan, K.P., Ed., CRC Press: Boca Raton, 1992.
(123) Goddard, E. D. *J. Colloid Interface Sci.* **2002**, *256*, 228.
(124) Wanless, E.J., Davey, T.W., Ducker, W.A. *Langmuir* **1997**, *13*, 4223.
(125) De Clermont-Gallerande, H., Doucet, O., Marsande, E., Fouchard, D., Orcet, A. M., Zastrow, L. *Internat. J. Cosm. Sci*. **2001**, *23*, 15.
(126) Goddard, E.D., Phillips, T.S., Hannan, R.B. *J. Soc. Cosm. Chem.* **1975**, *26*, 461.
(127) Goddard, E.D., Faucher, J.A., Scott, R.J., Turney, M.E. *J. Soc. Cosm. Chem.***1975**, *26*, 539.
(128) Marques, E. F., Regev, O., Khan, A., Miguel, M. D., Lindman, B. *Macromolecules* **1999**, *32*, 6626.
(129) Robb, I.D. *Annual Surfactants Review* (**2000**), *3*, 97.
(130) Aleksandrovskaya, S. A., Tret'yakova, A. Ya., Barabanov, V. P. *Vysokomol. Soedin., Ser. B* **1984**, *26*, 280.
(131) Harada, A., Nozakura, S. *Polym. Bull.* **1984**, *11*, 175.
(132) Moudgil, B.M. Somasundaran, P. in *Fundam. Adsorpt., Proc. Eng. Found. Conf.*, Myers, a.L., Belfort, G.: Eds. Eng. Found.: New York, 1984.
(133) Moudgil, B.M. Somasundaran, P. *Colloids Surf.* **1985**, *13*, 87.
(134) Nagarajan, R. *Polymeric Materials Sci. Eng.* **2001**, *85* 65.

(135) Lunkenheimer, K., Miller, R., Tutschke, G. *Patent application* Ger. (East) 1986 DD 84-270230.
(136) Holmberg, K. *Surfactants and polymers in aqueous solution;* 2nd ed., John Wiley & Sons: New York, 2003.
(137) Fleming, B.D. *The Adsorption of Surfactants and Polymers at the Solid/Solution Interface*; Ph.D. Thesis; The University of Newcastle Callaghan, Australia, 2001.
(138) Ortiz, C., Hadziioannou, G. *Macromolecules* **1999**, *32*, 780.